Degree project in Pharmaceutical Formulation – KLGM06

Spray-dried powders for inhalation

Faculty of Engineering, Department of Process and Life Science Engineering, Lund University

Author: Jiapei Su & Qianru Zhu

Date: May 2025

Supervisors: Kyrre Thalberg, Anna Fureby, Hugo Öhrneman

Examiner: Marie Wahlgren

LUNDS UNIVERSITET

LTH

LUNDS TEKNISKA HÖGSKOLA

POPULAR SUMMARY

Tiny Powders for Better Lung Treatments

Imagine inhaling medicine that fights lung diseases right where it's needed—without pills or injections. In this project, we explored how to turn a protein-based solution into a dry powder suitable for inhalation, using a method called spray-drying. By carefully adjusting the recipe, including the addition of a natural amino acid called L-leucine, we aimed to improve how well the powder handles moisture and how efficiently it reaches the deeper parts of the lungs.

Lung diseases like asthma and chronic obstructive pulmonary disease (COPD) affect millions of people. Traditional inhalers often fail because moisture clogs the powder, wasting doses. We spray-dried a model protein (BSA), combined with a sugar (trehalose), and varying amounts of L-leucine, to form particles under 3.5 µm in size, small enough to be carried deep into the lungs.

We found that using 20% L-leucine helped the powder resist moisture compared with 10% or without L-leucine, improving flowability and reducing clumping in humid conditions. In a test setup simulating inhalation, these powders delivered about 60% of their content to the deeper lung regions. Additionally, the process yielded over 75% of the intended powder, which is promising from a manufacturing standpoint.

Why does this matter? In hot and humid climates, current inhalers sometimes fail to deliver consistent doses. Our findings suggest that this kind of formulation might improve performance in those environments. Under the microscope, the particles look like tiny, wrinkled raisins—shapes that help them float smoothly into airways rather than sticking to each other.

Although this study used a model protein, the same approach might one day be adapted for other drugs, including vaccines or antibiotics. The next steps include refining the technique and exploring how it could be scaled up in collaboration with the pharmaceutical industry.

ACKNOWLEDGEMENTS

This master´s thesis has been performed by two students at the Department of Food and Pharma Technology and the Department of Design Science, in collaboration with Emmace consulting AB.

We would like to express our sincere gratitude to our supervisors Kyrre Thalberg, Anna Fureby and Hugo Öhrneman, all of whom have offered invaluable support, time and guidance throughout the project of this diploma work. Our thanks also go to Marie Wahlgren for kindly agreeing to be our examiner and for her support and availability when needed.

We are especially grateful to Emmace Consulting AB for their extensive experimental support, including the provision of essential materials and assistance with HPLC analysis for the NGI experiments. Our sincere thanks go to Jackie, Ann, and Peter for their practical help and continuous support throughout the project. We also appreciate the Aerosol Technology Laboratory, one of the most advanced facilities in the world, for providing access to equipment that was critical for our experimental work. We further thank Daniel Madsen at nCHREM, for his valuable assistance with SEM analysis. We are grateful to Hans and Olexander for their kindness and generous support at the department, assisting us with both the equipment and materials needed for our experiments.

We are deeply thankful to our families and friends for their encouragement and unwavering support throughout all our years of study. Our heartfelt thanks to our friend Wenyan for the mutual support and joyful companionship during the lab work, especially when things got challenging. And lastly, a sincere thank you to ourselves for the strong teamwork, cooperation, and dedication we brought to this journey.

ABSTRACT

The pulmonary route has emerged as a promising strategy for delivering protein therapeutics, particularly for patients suffering from respiratory diseases such as asthma, chronic obstructive pulmonary disease (COPD), and pulmonary infections.

This project investigated the effect of operating parameters of a laboratory spray dryer on the characteristics of powders composed of Bovine Serum Albumin (BSA), L-leucine, and Trehalose Dihydrate, with the aim of optimizing their production for inhalation applications. The pre-study focused on optimizing spray-drying process parameters, including feed concentration (solid content), inlet temperature, nozzle diameter, spray gas flow rate, and feed solution flow rate. The main study used the optimized parameters from the pre-study to produce the final formulations. These powders were analyzed to determine their size, morphology, moisture content, and aerodynamic properties using light microscopy, laser diffraction, Scanning Electron Microscopy, bulk density measurements, water content measurements, Next Generation Impactor analysis, and Aerodynamic Particle Sizing.

The chosen spray drying conditions from the pre-study had an inlet temperature of 120 °C, an outlet temperature of 65 °C, a spray gas flow rate of 2.3 m^3/h, and a feed rate of 1.7 ml/min. In the main study, formulations containing BSA or L-leucine were produced with high yields, above 75%. The d(0.5) of the particles are below 3.5 μm, with corrugated and raisin-like shape.

Among our tested formulations, 10BSA_20Leu performed best, with low residual moisture (2.6%), high bulk density (0.35 g/cm^3), and Mass Median Aerodynamic Diameter (MMAD) between 2.5–2.9 μm, suitable for pulmonary administration. Trehalose-based powders with high leucine content showed better moisture resistance and dispersibility compared to pure trehalose, which had the lowest humidity resistance. Particle morphology and flowability were strongly related to the excipient type: leucine and BSA formed a corrugated surface that enhanced aerosolization but also increased bounce during NGI analysis. Samples enriched with 20% leucine displayed flake-like surface textures, attributed to crystalline excipient migration during drying. The effect of leucine was dose-dependent, indicating the importance of fine-tuning the excipient ratio for optimal inhalation performance.

Table of Contents

LIST OF ABBREVIATIONS

AD: Aerodynamic Diameter
API: Active Pharmaceutical Ingredient
APS: Aerodynamic Particle Sizing
BSA: Bovine Serum Albumin
DPI: Dry Powder Inhaler
FPD: Fine Particle Dose
FPF: Fine Particle Fraction
GSD: Geometric Standard Deviation
HPMC: Hydroxypropyl Methylcellulose
MMAD: Mass Median Aerodynamic Diameter
MOC: Micro Orifice Collector
NGI: Next Generation Impactor
SEM: Scanning Electron Microscopy

1 INTRODUCTION

Local administration to the lungs allows for high drug concentrations at the target site while minimizing systemic exposure and associated side effects (Patton & Byron, 2007, n.d.). Furthermore, pulmonary delivery bypasses first-pass hepatic metabolism, making it especially advantageous for proteins that are otherwise unstable or rapidly degraded in the gastrointestinal tract (Shoyele & Slowey, 2006, n.d.). Among the various formulation technologies available, spray-drying has gained considerable attention for the development of inhalable protein pharmaceuticals.

1.1 Spray-dried protein pharmaceuticals

Spray drying is a technology that atomizes liquid materials into fine droplets, rapidly evaporates water in a fast, high-temperature airflow, and ultimately obtains dry powder (Figure 1). The spray drying process can generally be divided into four consecutive stages: atomization, spray contact with hot air flow, drying, and particle separation. First, in the atomization stage, the drug solution or suspension is atomized into tiny droplets through a nozzle. Subsequently, these droplets quickly come into contact with the high-temperature dry air flow during the spray-air contact stage and begin to evaporate water rapidly. After entering the drying stage, the solvent in the droplets continues to evaporate, causing a solid shell structure to gradually form on the surface of the droplets and eventually transform into dry particles. Finally, in the separation stage, the dried powder particles are separated from the air flow by a cyclone separator and collected in a receiving tank, while the exhaust gas is filtered and discharged from the system.

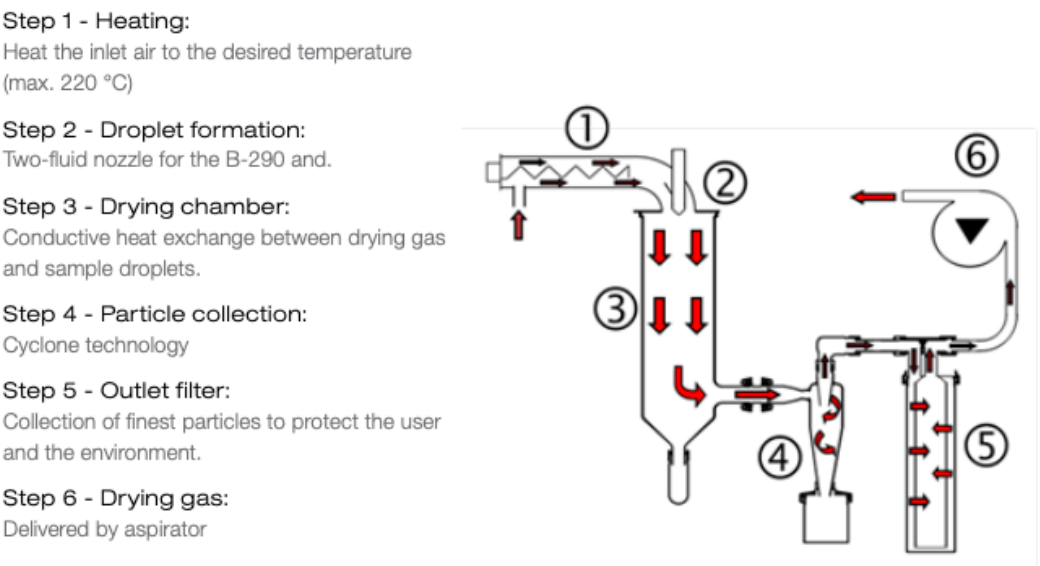

Figure 1: Spray drying process flow chart (Source: Büchi product manual). This figure shows the basic process of spray drying.

This technique offers several advantages, including the ability to produce dry powders with controlled particle size, morphology, and aerodynamic properties suitable for deep lung

deposition. In addition, spray drying enhances the stability and shelf life of protein-based drugs, addressing a critical challenge in protein formulation (Pilcer & Amighi, 2010; Price et al., 2019). These attributes position spray drying as a highly versatile and scalable method for producing inhalable protein therapeutics.

1.2 Dry powder formulation and inhaler device

Dry powder formulations for inhaled medicines typically consist of an active pharmaceutical ingredient (API), usually a protein or peptide, combined with a sugar-based carrier such as lactose or mannitol to facilitate drug dispersion and flowability (Pilcer & Amighi, 2010).

Three commonly used pharmaceutical aerosol systems are nebulizers, metered dose inhalers (MDIs), and dry powder inhalers (DPIs). Dry powder inhalation (DPI) is a very popular pulmonary drug delivery strategy because it is breath-actuated and does not require the use of any propellants. Combined with spray drying technology, DPI formulations can be designed to have optimal aerodynamic properties such as particle size, density, and surface morphology, which are critical for deep lung deposition. Despite these advantages, formulating dry powders for inhalation remains challenging, especially in maintaining protein stability and achieving dose consistency (Douafer et al., 2020; Pilcer & Amighi, 2010; Price et al., 2019; Li et al., 2020). Figure 2 below explains how to inhale dry powder using an inhaler device.

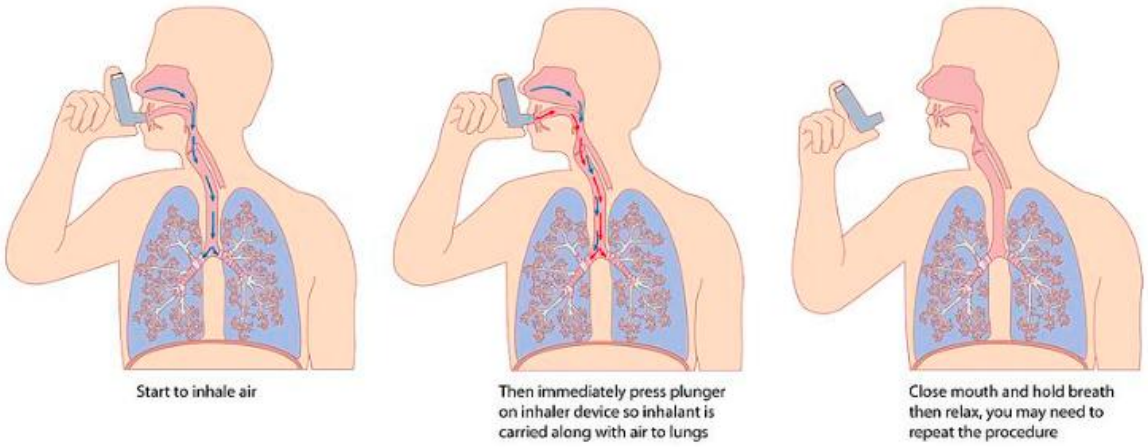

Figure 2: Proper use of a inhaler: activate the device, inhale, and hold breath to allow drug delivery to the lungs. Source: Science Photo Library.

1.3 Formulation and excipients in spray drying

BSA is often used as a model protein in studies since the active pharmaceutical ingredient (API) may be very expensive. BSA is also a flexible globular protein, which tends to partially unfold at the air–liquid interface upon adsorption due to its conformationally labile domains, leading to potential aggregation during drying (Landström, 2000; Andrade et al., 1990). In order to overcome the agglomeration problem caused by strong cohesion between particles, DPI often adds various functional excipients such as lactose, mannitol, trehalose, leucine or surfactants to the API to preserve the protein structure and activity and also adjust the surface energy and

structural morphology of the particles, improve the dispersibility, stability and lung deposition efficiency of the powder (Alhajj et al., 2021; Douafer et al., 2020; Pilcer & Amighi, 2010; Price et al., 2019; Vehring, 2008). For protein drugs, amino acids or surfactants are often added to prevent interface-induced denaturation or aggregation. Reasonable excipients such as leucine can promote surface migration and form a protective layer during spray drying, thereby enhancing powder hydrophobicity, flowability, and dispersibility, which together facilitate more efficient pulmonary delivery (Vehring, 2008; Ordoubadi et al., 2023).

Trehalose is a hydrophilic excipient commonly used in dry powder inhalation preparations of protein drugs. It is widely used in the spray drying process due to its excellent stability protection effect. Research in recent years has further revealed the specific mechanism of excipients in particle surface migration and structural regulation. As a surface-active component, leucine tends to be enriched on the surface of droplets, and the same is true for BSA. However, due to the low solubility of leucine and its easy crystallization, a crystal shell is also formed on the surface of droplets. Although the diffusion rates of trehalose and leucine are very similar (both are small molecules), their surface activity and crystallization rates are different, resulting in leucine being more easily enriched on the surface. Ordoubadi et al systematically evaluated the performance of different concentrations of leucine during the spray drying process and found that leucine can form a hydrophobic protective layer on the particle surface, significantly reducing hygroscopicity and preventing agglomeration (Ordoubadi et al., 2023). Some studies state that because leucine has a higher Peclet number behavior than trehalose (its diffusion rate is lower than the solvent evaporation rate), this causes it to deposit on the droplet surface and form a "shell structure". As shown in Figure 3 below, BSA, as a protein, has a higher Péclet number than leucine and is prone to forming wrinkled and collapsed structures (Lechanteur & Evrard, 2020; Osman et al., 2017).

The Péclet number for the drying of droplets containing suspended particles can be defined as:

$$Pe = R^2/DT_{dry} \qquad (1)$$

Where R is the radius of the droplet, T_{dry} is the time of drying, and D is the collective diffusion coefficient of the suspended particles (Tsapis et al., 2002).

Further stability testing showed that the high leucine formulation maintained good dispersibility and pulmonary delivery performance even in a high humidity condition (RH 60%), indicating that it has important value in improving the physical stability of DPI preparations. And studies have shown that there are significant differences in the deposition behavior of different leucine contents on the particle surface. At low concentrations (such as 10%), leucine covers a limited surface of the particles, and the improvement effect on hygroscopicity and is weak; when the leucine content is increased to 20% or above, it can form a continuous shell structure on the particle surface, effectively inhibiting water adsorption and structural collapse, and significantly improving the physical stability and aerosol performance of the powder in a high humidity condition (Ordoubadi et al., 2023). Therefore, optimizing the addition ratio of leucine is an important strategy to improve the performance of protein DPI preparations.

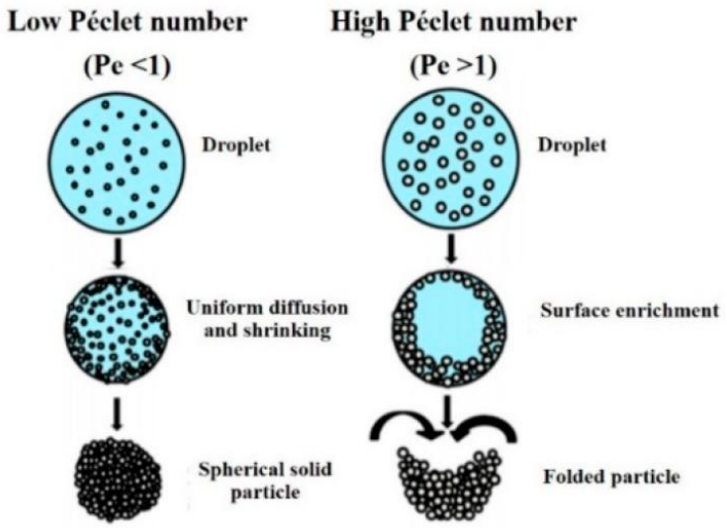

Figure 3: Different drying processes of droplets containing excipients with low Péclet numbers (Pe < 1, left) or high Péclet numbers (Pe > 1, right) are shown.(Lechanteur & Evrard, 2020; Osman et al., 2017)

1.4 Spray-drying conditions

The key process parameters in the spray drying process mainly include inlet air temperature, atomization method, atomization airflow rate, feed rate, and solid content. These factors jointly determine the particle size distribution, water residue, hollow structure, powder density, and fluidity of the final particles. Higher inlet air temperature can improve drying efficiency, but protein denaturation should be avoided; atomization gas velocity and feed concentration affect particle size and atomization quality.

Figure 4 shown below explains the effects of different parameters in the spray drying process on the experimental scenario and the final product. Too high a temperature may destroy the stability of the biological agent, so drying at a lower temperature can improve the applicability of the formulation to a variety of biological molecules. In addition, the difference in evaporation rate caused by changing the drying temperature will also affect the morphology of the particles. Finding the drying conditions to achieve the ideal particle size is a very important experimental goal. The humidity of the dried product affects the stability and aerodynamic properties of the particles. The yield has a very important economic value in practical applications.

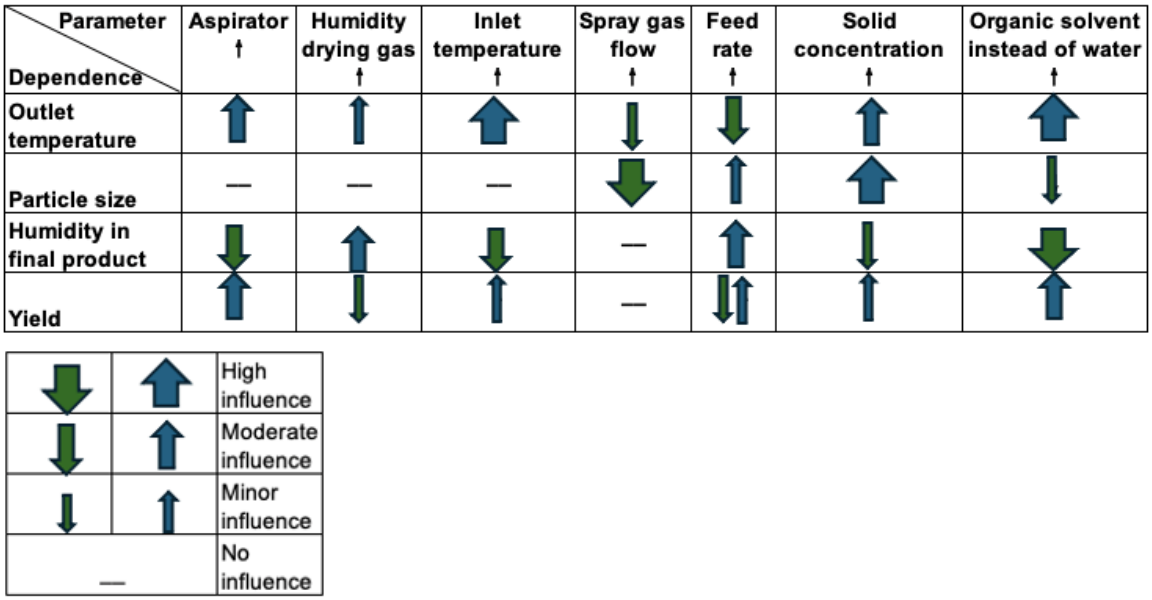

Figure 4: Effects of key spray drying parameters on product outcomes. Arrows (↑ / ↓) indicate whether increasing a parameter leads to an increase or decrease in the variable. Arrow colors reflect influence strength: dark blue (high), blue (moderate), green (minor). A dash (–) means no effect. Adapted from Büchi process guidelines.

1.5 Characteristics of inhalation powders

Inhaled powders for pulmonary delivery need to possess a series of physicochemical properties to ensure that they can be effectively dispersed and deposited in the lower respiratory tract. First, particle size is an important parameter that determines whether the powder can reach the lungs. It is generally believed that the mass median aerodynamic diameter (MMAD) of the particles should be controlled within the range of 1–5 μm to avoid deposition in the throat area and smoothly enter the bronchioles and even the alveolar area (Pilcer & Amighi, 2010; Heyder, 2004).

In addition to the particle size, the uniformity of the particle size distribution is also critical. The geometric standard deviation (GSD) is used to reflect the degree of dispersion of the particle size distribution. The smaller the value, the more concentrated the particles are, which helps to improve the consistency of the dose and the efficiency of lung deposition. It is generally believed that a GSD value below 2.0 helps ensure reproducibility and consistency in targeted therapeutic delivery of inhaled powders (Garcia-Contreras et al., 2015).

On top of that, the surface morphology and structure of particles also directly affect their behavior during inhalation. Particles with rough surfaces, hollow or porous surfaces are generally easier to disperse than particles with smooth surfaces because the contact area between them is smaller, thereby reducing the agglomeration of particles caused by van der Waals forces (Crowder et al., 2002; Vehring, 2008). In addition, particles with low density and loose structure are more easily carried by the airflow in the inhalation device and show better aerosolization performance.

Flowability and dispersibility are another key indicator of the performance of inhalation powders. Good flowability not only helps the stable operation of powders during production and filling but also reduces the agglomeration between particles and improves their release efficiency in the inhalation device (Crowder et al., 2002; Pilcer & Amighi, 2010; Sou et al., 2011). Dispersibility determines the aerosolization performance of the powder during inhalation, affecting the consistency and efficiency of lung deposition. Studies have shown that the addition of surfactant excipients such as leucine can effectively improve the surface structure of particles and reduce the adhesion between particles, thereby significantly improving the dispersibility of powders (Sou et al., 2011). The flowability of powders is usually evaluated by parameters such as bulk density, angle of repose or compression. Dispersibility is typically assessed by analyzing particle size distribution and aerodynamic performance, with particle morphology observed through scanning electron microscopy (SEM) providing additional insights into the surface characteristics and structural stability of the particles (Crowder et al., 2002; Garcia-Contreras et al., 2015).

Moisture content and humidity resistance are also key factors affecting the performance of inhalation powders. Dry powder inhalers are highly sensitive to environmental humidity. If the hygroscopicity is too high, the powder may agglomerate or collapse, reducing its dispersibility (Vehring, 2008). Some excipients, such as trehalose, can stabilize bioactive ingredients in a dry state, but they are prone to absorb water and agglomerate under high humidity conditions, thus affecting drug delivery performance (Sou et al., 2011). The evaluation of moisture stability usually includes moisture content determination, humidity exposure experiments, and analysis of the particle size or morphology changes of the powder under different humidity conditions to comprehensively judge its humidity resistance (Garcia-Contreras et al., 2015).

1.6 Project layout and aim

The project was divided into two parts: the pre-study and the main study. The pre-study focused on optimizing spray drying conditions to produce inhalable particles. Bovine serum albumin, Trehalose Dihydrate and L-leucine were used in the formulations, and the resulting particles were analyzed using light microscopy and laser diffraction to assess their morphology and size. The primary aim of this phase was to optimize spray drying conditions to produce powders suitable for inhalation.

The main study applied the optimal spray drying conditions identified in the pre-study and further characterized the particles. This includes evaluations of bulk density, water content, and particle morphology via light microscopy and Scanning Electron Microscopy (SEM), while aerodynamic performance was assessed using both a Next Generation Impactor (NGI) and an Aerodynamic Particle Sizer (APS). This phase aimed to explore the physical performance and aerodynamic properties of spray-dried powders with different ratios of excipients (BSA, L-leucine and Trehalose).

2 MATERIALS AND METHODS

The experimental work for the master's thesis was carried out at the Department of Process and Life Science Engineering, Division of Food and Pharma, from January to May 2025.

2.1 Materials

The materials used in this study were provided by the Division of Food and Pharma and are listed in Table 1.

Table 1: Materials used for the production and characterization of dry powders for inhalation.

Materials	**Supplier**	**Grade**
Bovine serum albumin (BSA)	Sigma-Aldrich	Analytical
Trehalose Dihydrate	Sigma-Aldrich	EP / Ph. Eur.
L-leucine	Sigma-Aldrich	EP / Ph. Eur.
Lamp oil	Petromax Alkan	Analytical
Sorbitan Monolaurate (Span20)	Sigma-Aldrich	Laboratory
Brij/glycerol mixture	Made by Emmace Consulting AB	Laboratory

2.2 Preparation of powder formulations

2.2.1 Pre-study

In the first stage of this study, spray drying conditions were optimized to produce powders with particle sizes suitable for inhalation (below 5 μm, with a target size of approximately 3 μm). Spray drying was performed using a Büchi Mini B-290 Spray Dryer equipped with a narrow cyclone to improve particle collection efficiency.

The spray drying conditions for all pre-study formulations, including combinations of Trehalose Dihydrate, L-leucine, and BSA, are presented in Tables 2–5. Comprehensive conversion tables for the spray dryer settings are provided in Appendix 6.1. The feed solutions were prepared by dissolving Trehalose Dihydrate, L-leucine, and BSA in distilled water under magnetic stirring. Prior to addition, BSA was equilibrated to room temperature after removal from the refrigerator to ensure proper dissolution.

Table 2: Spray Drying conditions for Trehalose Dihydrate formulations in the pre-study.

Batch	Solid content (%)	Tin (°C)	Tout (°C)	Aspirator rate (%)	Feed rate (mL/min)	Nozzle size (mm)	Spray gas flow rate (m^3/h)
Tre_01	10	90	55	100	3.2	1.5	1.4
Tre_02	10	120	67	85	3.2	1.5	1.4
Tre_03	5	120	65	70	3.2	1.4	0.8
Tre_04	5	90	52	90	3.2	1.4	0.8
Tre_05	5	120	64	85	3.2	1.5	1.4
Tre_06	5	90	50	80	3.2	1.5	1.4
Tre_07	5	120	64	95	3.2	1.5	2.3
Tre_08	5	90	50	85	3.2	1.5	2.3

Table 3: Spray Drying conditions for L-leucine with Trehalose Dihydrate formulations in the pre-study.

Batch	Solid content (%)	Tin (°C)	Tout (°C)	Aspirator rate (%)	Feed rate (%)	Nozzle size (mm)	Spray gas flow rate (m^3/h)
10Leu_01	10	90	52	80	3.2	1.5	1.4
10Leu_02	5	90	54	80	3.2	1.5	1.4
10Leu_03	10	120	68	75	3.2	1.5	1.4
10Leu_04	5	120	67	70	3.2	1.5	1.4
20Leu_01	5	90	56	80	3.2	1.5	1.4

Table 4: Spray Drying conditions for BSA with Trehalose Dihydrate formulations in the pre-study.

Batch	Solid content (%)	Tin (°C)	Tout (°C)	Aspirator rate (%)	Feed rate (%)	Nozzle size (mm)	Spray gas flow rate (m^3/h)
10BSA_01	5	90	53	75	3.2	1.5	1.4
10BSA_02	5	90	56	70	1.7	1.5	1.4

Table 5:Spray Drying conditions for BSA, L-leucine with Trehalose Dihydrate formulations in the pre-study.

Batch	Solid content (%)	Tin (°C)	Tout (°C)	Aspirator rate (%)	Feed rate (%)	Nozzle size (mm)	Spray gas flow rate (m^3/h)
10BSA_10Leu_01	5	90	52	75	3.2	1.5	1.4
10BSA_10Leu_02	5	90	59	70	1.7	1.5	1.4
10BSA_10Leu_03	5	120	60	85	3.2	1.5	2.3
10BSA_10Leu_04	5	120	66	70	1.7	1.5	2.3
10BSA_10Leu_05	5	90	50	90	3.2	1.5	2.3
10BSA_10Leu_06	5	90	56	90	1.7	1.5	2.3

2.2.2 Main study

Based on the optimized parameters from the pre-study, Table 6 outlines the spray drying settings used for BSA, L-leucine, and Trehalose Dihydrate formulations in the main study. 10BSA refers to a formulation containing 10% BSA and 90% Trehalose dihydrate. 10Leu indicates a mixture of 10% L-leucine and 90% Trehalose Dihydrate. 10BSA_10Leu represents a three-component formulation comprising 10% BSA, 10% L-leucine and 80% Trehalose Dihydrate. Tre refers to pure Trehalose (100%). 10BSA_20Leu represents a three-component formulation comprising 10% BSA, 20% L-leucine and 70% Trehalose Dihydrate.

Table 6: Spray Drying conditions for BSA, L-leucine, Trehalose Dihydrate formulations in the main study.

Batch	Solid content (%)	Tin (°C)	Tout (°C)	Aspirator rate (%)	Feed rate (%)	Nozzle size (mm)	Spray gas flow rate (m^3/h)
10BSA	5	120	64	75	1.7	1.5	2.3
10Leu	5	120	65	72	1.7	1.5	2.3
10BSA_10Leu	5	120	68	80	1.7	1.5	2.3
Tre	5	120	63	75	1.7	1.5	2.3
10BSA_20Leu	5	120	66	88	1.7	1.5	2.3

2.3 Characterization of powders

The dry powder characteristics were analyzed using light microscopy, laser diffraction, scanning electron microscopy, water content tests and bulk density measurements. Their suitability for aerosol delivery via inhalation devices was assessed using a Next Generation Impactor and an Aerodynamic Particle Sizer.

2.3.1 Light microscopy

Particle morphology and shape were analyzed using light microscopy with an Olympus Microscope BX50, equipped with a ×10 ocular lens. Dispersion was achieved using a Branson Sonifier B-12 ultrasonic probe in an ice bath. Approximately 50 mg of powder was dispersed in 1mL of Span20 and 4 mL of lamp oil, using a Branson Sonifier B-12 ultrasonic probe in an ice bath. A drop of the resulting suspension was placed on a glass slide and covered with a cover slip. Images were captured using ×20 and ×50 objective lenses. Additionally, images of a calibration scale (1 mm in length with 100 divisions of 0.01 mm, manufactured by Graticules Ltd.) were taken to enable particle size comparison.

2.3.2 Laser diffraction

The particle size distribution of the dry powders was determined using laser diffraction with a Malvern Mastersizer 2000. A He-Ne laser was used as the light source, and both Mie and Fraunhofer theories were applied. Mie theory, suitable for smaller particles, considers optical properties but may introduce bias if refractive indices are unknown (Gréhan et al., 1992). Fraunhofer theory assumes spherical particles much larger than the light wavelength and does not require optical inputs, though it is less accurate for small particles (Darder et al., 2021).

For sample preparation, 50 mg of powder was dispersed in 1mL of Span20 and 4 mL of lamp oil. Dispersion was achieved using a Branson Sonifier B-12 ultrasonic probe in an ice bath. The resulting suspension was added dropwise to the oil dispersion unit of the Mastersizer 2000 until the desired obscuration level (5%, 10%, or 15%) was reached. The refractive indexes applied in the measurements were 1.53 for the sugars and 1.43 for the lamp oil, with an absorption coefficient of 0.01. The reported particle size corresponds to d(0.5), the median of the volume-based particle size distribution. This value was obtained by averaging results from triplicate measurements performed under different obscuration conditions. The span of the volume distribution, which indicates the width of the distribution relative to the median diameter, was determined using the following equation by Mastersizer 2000 software. The polydispersity of the particles was expressed by the span. Span is a commonly used metric to describe the relative width of a unimodal particle size distribution (Tan & Nakajima, 2005).

$$Span = (d_{0.9} - d_{0.1})/d_{0.5} \quad (2)$$

Where $d_{0.1}$ is the particle diameter below which 10% of the total particle volume exists, $d_{0.5}$ (also called the median diameter) is the particle diameter below which 50% of the total particle volume exists, $d_{0.9}$ is the particle diameter below which 90% of the total particle volume exists.

2.3.3 Scanning Electron Microscopy (SEM)

Scanning Electron Microscopy (SEM) was employed to analyze particle shape and surface morphology, and to compare differences between powder batches. SEM offers high versatility in imaging, enabling not only particle size characterization but also the evaluation of surface features. It provides a practical balance between imaging resolution and acquisition time, making it a valuable tool for detailed powder characterization (Moon et al., 2025).

SEM imaging was conducted using a JEOL JSM-6700F scanning electron microscope operated at an accelerating voltage of 10 kV and an emission current of 10 μA. Images were captured at magnifications of ×250, ×1000, and ×10,000. For sample preparation, a thin layer of each powder was spread onto a brass mount affixed with adhesive tape. The mounts were then coated with a 15 nm conductive layer of gold/palladium (Au/Pd) using a sputter coater. The coating was performed under argon gas at a working pressure of 0.05 mbar, a sputtering current of 15 mA, and a sputtering time of 180 seconds to enhance image quality by improving secondary electron emission.

2.3.4 Water content measurements

Water content of the spray-dried powders was determined by assessing the weight loss upon drying at 105 °C. Approximately 0.5 g of each powder sample was accurately weighed into pre-weighed aluminum foil containers. The samples were placed in a drying oven set to 105 °C and dried for specified time intervals: 1 hour and 2 hours. After each drying period, the containers were removed, cooled in a desiccator, and reweighed. All measurements were performed in triplicate, and results were reported as the mean values.

2.3.5 Bulk density measurements

Bulk density measurements were performed following the established protocol (Healy et al., 2008). This aspect is especially important in the capsule filling process, where powder bulk density significantly influences both the fill weight and the consistency of the final product (Stranzinger et al., 2019). Exactly 5.2 cm^3 of each powder sample was gently filled into a pre-weighed graduated cylinder, ensuring no compression. Excess powder was leveled with a spatula, and the total mass was recorded using an analytical balance. All measurements were performed in triplicate, and results were reported as the average values.

2.3.6 Humidity Study

Five formulation replicates were placed in a 75% RH desiccator at room temperature for a certain period. The humidity of the desiccator was adjusted by an over-saturated solution of 50 g NaCl and 100 g water. 15-20 mg of powder was weighed and placed in capsules. All capsules were placed in the desiccator for 1 hour, 3 hours, and overnight to observe whether the powder hardened and clogged.

2.3.7 Next Generation Impactor (NGI)

The aerosol performance of spray-dried powders was evaluated using a Next Generation Impactor (NGI, Copley, Nottingham, UK) with a pre-separator (Figure 5A). Although NGI

cannot directly measure the aerodynamic diameter of individual particles, it can determine the aerodynamic particle size distribution through staged collection and subsequent analysis. Fine particle dose (FPD), fine particle fraction (FPF), MMAD, GSD, and delivered rate were used as evaluation indicators.

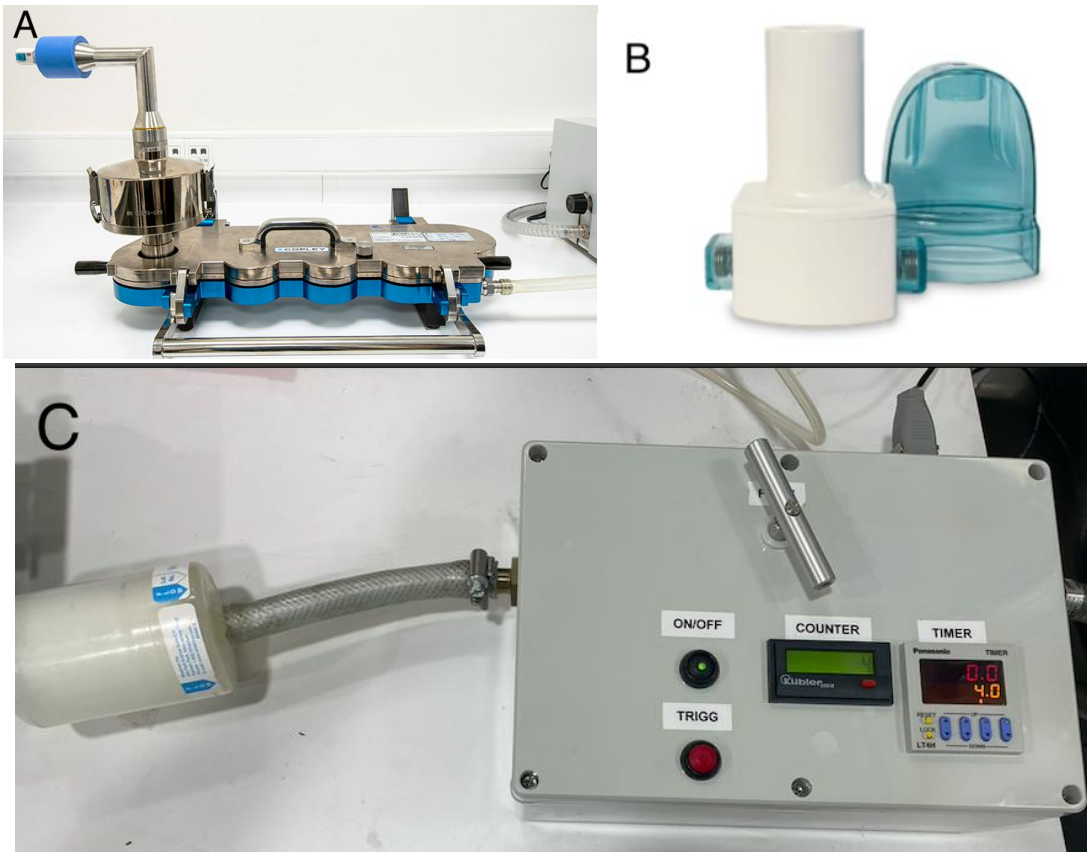

Figure 5: A. Next Generation Impactor (NGI) by Copley (http://www.arimedilac.com/en/Uretim-Tesisi), B. RS01 monodose dry powder inhaler with high resistance by Plastiape (www.berryglobal.com). C. Trigger Box by AB FIA Odarslövs mölla

The NGI experiments were performed in a climatic chamber (Figure 6) with humidity maintained at 30% RH and 50% RH and temperature maintained at 25°C. In the aerodynamic performance experiment (NGI and APS), the capsules filled with powder were placed in the environment for 45 minutes. Considering that the time the capsules were exposed to air in actual applications usually does not exceed this time, we believe that this setting has fully simulated its air exposure stability and has representative and practical reference value.

19-25 mg of lyophilized powder was filled in HPMC (hydroxypropyl methylcellulose) capsules and kept in a desiccator. Two filled capsules were used for each NGI run for each formulation, and triplicate samples were used for each NGI run to minimize variation. A layer of Brij/glycerol mixture was coated on the NGI plate to minimize particle bouncing and secondary entrainment. 15 ml of distilled water was added to the pre-separator for the same purpose. The Brij/glycerol

mixture was provided by Emmace Consulting AB and was prepared by dissolving 15 g of Brij in 100 mL of ethanol and then mixing 10 mL of this solution with 40 mL of glycerol (85%).

In each measurement, two capsules containing the sample were dispersed sequentially through a low-resistance Plastiape (Figure 5B) RS01 DPI device (Plastiape, SpA, Osnago, Italy). The inspiratory flow rate of the vacuum pump was adjusted by adjusting the Trigger Box (Figure 5C) to simulate the required dose reaching the designated area of the lung in vitro. The TriggerBox was adjusted and monitored by a flow meter until the flow rate was adjusted to 62 L/min, and the pressure in the device was measured by a manometer to be 4 kPa. During the measurements, each run was performed for 4 seconds.

Figure 6: Climate Chamber: FITOCLIMA 27.000 PH, ARLAB, Portugal.

The dispersed powders in the capsule, pre-separator, NGI throat, and all 7 stages of NGI and MOC (Micro Orifice Collector) were dissolved in distilled water and quantitatively analyzed using HPLC analysis. HPLC testing was performed with the assistance of Emmace Consulting AB. Only three formulations, 10BSA, 10BSA_10Leu and 10BSA_20Leu, were characterized by NGI because our HPLC method requires the presence of BSA in the formulation and formulations without BSA could not be tested. The aerodynamic diameter distribution is inferred by calculating the weight of the particles at different levels of deposition. The FPD was defined as the amount of drug with an aerodynamic diameter less than 5 μm, representing the respirable dose likely to deposit in the lower respiratory tract. The FPF was expressed as the percentage of the total dose corresponding to the FPD. The delivered fraction was calculated as the percentage of the recovered dose emitted from the capsule relative to the total dose. GSD indicates the

variation range of particle size. It describes the standard deviation of particle size distribution under the assumption of log-normal distribution.

2.3.8 Aerodynamic Particle Sizing (APS)

Another method of measuring aerodynamic particle size is to use an Aerodynamic Particle Sizer® (APS™) spectrometer model 3321 (Figure 7A) modified by Emmace Consulting AB with the addition of a 5L tube to reach the required volume, in combination with an Aerosol diluter 3302 (Figure 7B) (for 100:1 diluting the powder to the optimal concentration range for the APS device) and a trigger box to simulate the required dose reaching the designated area of the lung in vitro. As shown in Figure 7B, a computer program with the Aerodynamic Particle Sizer® enabled the test conditions to be monitored in real time.

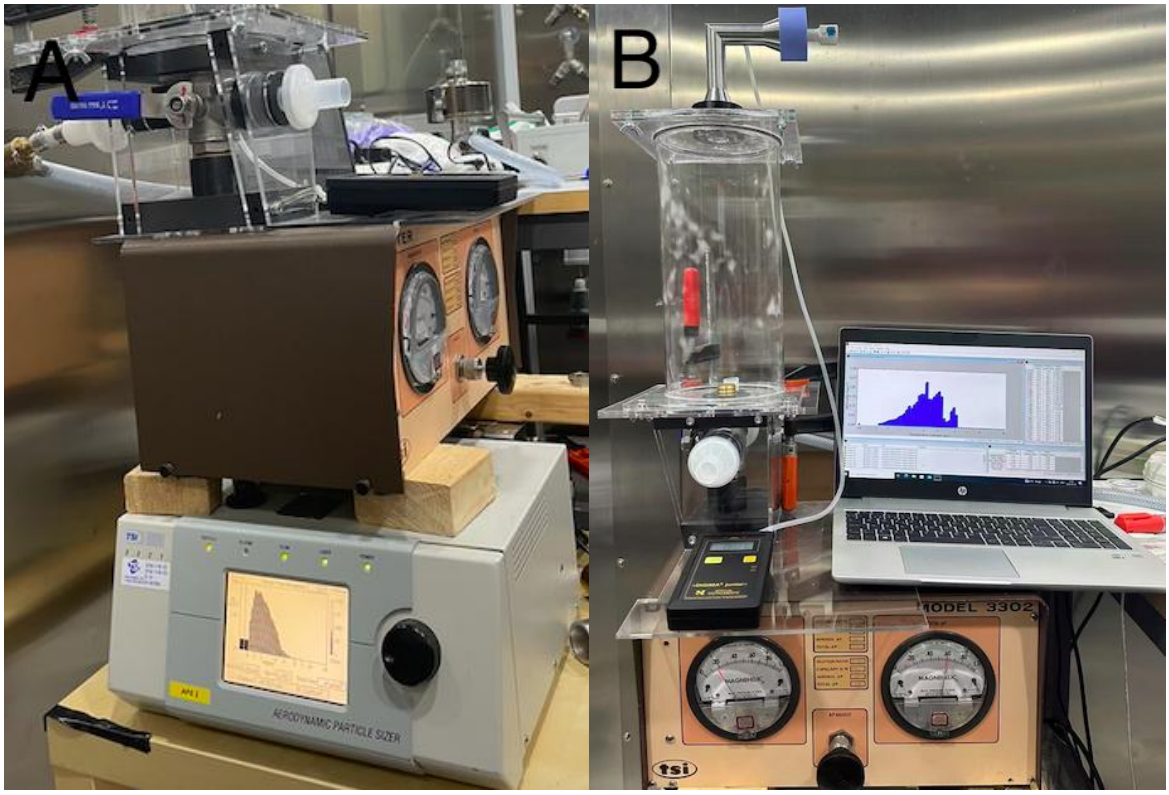

Figure 7: A. Aerodynamic Particle Sizer® (APS™) spectrometer model 3321 connected to Aerosol diluter 3302. B. Aerosol diluter 3302 is connected to a 5L tube. The throat on the tube is connected to a pressure meter to monitor the internal pressure of the tube in real time.

Like NGI, the Trigger Box was adjusted to a gas flow rate of 62 L/min with the help of a pressure gauge and a flow meter, at which time the pressure was 4.3 kPa. In another experimental condition, the flow rate was measured to be 48 L/min under a pressure of 2 kPa.

Capsules were weighed and equilibrated in the same way as in the NGI experiment, with triplicate samples of each sample set up. The weight of the powder to be weighed is given in Appendix 6.4.1. Each run was performed for 2 seconds, and one capsule was used for each APS run. The same inhaler for NGI was applied here. Each measurement lasted for 30 seconds, and

each sample was performed for 5 minutes, which means 10 measurements for each sample. Five Formulations were performed at 30% RH, 50% RH, and 60% RH.

3 RESULTS & DISCUSSION

In the pre-study, spray drying yield was not the primary focus and therefore was not consistently recorded. However, it was evident that the yields for pure trehalose dihydrate formulations were the lowest, likely due to strong electrostatic interactions causing powder adhesion to the spray dryer surfaces. In contrast, other formulations containing L-leucine and/or BSA demonstrated visibly higher yields. In the main study, spray-drying yields were carefully measured and summarized in Table 7. Consistent with earlier observations, pure trehalose formulations again showed the lowest yield, whereas all other formulations achieved yields exceeding 75%, indicating high process efficiency and improved powder recovery when leucine and/or BSA were included (Sosnik & Seremeta, 2015).

Table 7: Spray-drying yields for BSA, L-leucine, Trehalose Dihydrate formulations in the main study.

Batch	Yield (%)
10BSA	77.9
10Leu	80.2
10BSA_10Leu	82.3
Tre	54.8
10BSA_20Leu	81.3

3.1 Pre-study

3.1.1 Particle morphology by light microscopy

Images of the spray-dried powders in the pre-study captured at different magnifications (×20 and ×50) are provided in the Appendix 6.2. Under light microscopy, spray-dried Trehalose Dihydrate powders displayed spherical particles and very few internal vacuoles. Some degree of agglomeration was observed, likely due to incomplete dispersion in the oil mixture. The proportion of Span20 in the lamp oil may require optimization to improve the dispersion efficiency. The addition of L-leucine led to noticeable morphological changes, some of the spray-dried L-leucine with Trehalose Dihydrate particles became raisin-like. The spray-dried BSA with Trehalose Dihydrate formulations also produced raisin-like particles of varying sizes. Spray-dried BSA, L-leucine with Trehalose Dihydrate formulations exhibited the most complex morphology, with significant agglomeration and more vacuoles.

3.1.2 Particle size distribution by laser diffraction

When particle size was calculated using Fraunhofer theory in laser diffraction analysis, the resulting sizes were consistently smaller than those obtained with Mie theory. Moreover, the Fraunhofer model yielded lower weighted residuals, suggesting a better overall fit to the

measurement data. The particle size distribution and results of each formulation in the pre-study using Fraunhofer theory are shown in Appendix 6.3. The proportion of Span20 in lamp oil appears to be suboptimal, as pure trehalose cannot be fully dispersed.

Initially, a comparison was made between 10Leu_01 (10% solid content) and 10Leu_02 (5% solid content). The formulation with 5% solid content (10Leu_02) exhibited a smaller mass median diameter (4.3 μm) compared to that with 10% solid content (4.8 μm), leading to the decision to proceed with 5% solid content in subsequent experiments. At lower solid content, the droplets formed during atomization contain less solute, which typically leads to smaller dried particles after solvent evaporation.

Secondly, the effect of inlet temperature on particle size was evaluated. Powders produced at a higher inlet temperature (120 °C), including Tre_02, 10Leu_03, and 10Leu_04, exhibited smaller particle sizes compared to those produced at a lower inlet temperature (90 °C), such as Tre_01, 10Leu_01, and 10Leu_02. At higher inlet temperature, the solvent evaporates more rapidly, leading to quicker shell formation and shrinkage of the droplets, which can result in smaller particles. Thirdly, the influence of feed rate on particle size was investigated. Formulations spray-dried at a lower feed rate of 1.7 mL/min (10BSA_10Leu_02 and 10BSA_02), showed smaller particle sizes compared to those processed at a higher feed rate of 3.2 mL/min (10BSA_10Leu_01 and 10BSA_01). Similarly, a lower feed rate introduces less liquid into the drying chamber per unit time, allowing more efficient heat transfer and more complete drying of each droplet.

Additionally, to rapidly determine the optimal spray-drying parameters, pure trehalose was used to evaluate the effects of nozzle diameter, inlet temperature, and spray gas flow rate. Among the tested conditions, the smallest particle size was observed for Tre_07, which used a 1.5 mm nozzle, an inlet temperature of 120 °C, and a flow rate of 2.3 m^3/h. Lastly, we investigated whether the same trend applied to the BSA and leucine formulations with trehalose. The smallest particle size (3.46 μm) was observed for 10BSA_10Leu_06, which was spray-dried at 90 °C with a feed rate of 1.7 ml/min. However, for the main study, we chose an inlet temperature of 120 °C (as used in 10BSA_10Leu_04, particle size 3.54 μm), because higher inlet temperatures generally promote better drying efficiency, reduce residual moisture, and improve powder flowability, without significantly increasing particle size.

3.1.3 Water content

For the water content measurements in the pre-study, small glass vials were used instead of aluminum pans. This may have influenced the drying process, as the powder could not be spread evenly in the vials. Additionally, unlike the main study where measurements were taken after 1 and 2 hours of drying, the pre-study only included a 30-minute drying period. Therefore, it is uncertain whether the powders were completely dried. However, the results still reveal observable trends in water content across the samples. Some of the results are shown in Table 8, with values representing averages from triplicate measurements. Compared with 10BSA_10Leu_03, 10BSA_10Leu_04, 10BSA_10Leu_05, and 10BSA_10Leu_06, the results indicate that a higher inlet temperature (10BSA_10Leu_03, 10BSA_10Leu_04) leads to lower water content. Additionally, at the same inlet temperature, a lower pump rate (10BSA_10Leu_04, 10BSA_10Leu_06) also results in reduced water content.

Table 8: Water content (mean of triplicates) of spray-dried powders in the pre-study.

Samples	Water content after drying 0.5h (%)
10BSA_10Leu_03	4.8
10BSA_10Leu_04	3.9
10BSA_10Leu_05	5.4
10BSA_10Leu_06	4.1

3.1.4 Bulk density

Selected results from the bulk density measurements conducted in the pre-study are presented in Table 9, with values representing averages from triplicate measurements. The standard deviation for each sample was also calculated to assess the variability in the measurements. Comparing 10BSA_10Leu_03 and 10BSA_10Leu_04, both prepared under higher inlet temperature, the bulk density values are relatively lower than those at lower temperatures (10BSA_10Leu_05 and 10BSA_10Leu_06). This suggests that faster drying at higher temperature condition may lead to surface roughness or irregular shapes, which may hinder tight packing, resulting in lower bulk density. Comparing samples with the same inlet temperature, the bulk density values show some variation, but no consistent trend can be clearly attributed to the feed rate. This suggests that feed rate may not have a significant or consistent impact on bulk density in this case.

Table 9: Bulk density (mean of triplicates) and standard deviation of spray-dried powders in the pre-study.

Samples	Average Bulk Density (g/cm^3)	STDEV
10BSA_10Leu_03	0.29	0.002
10BSA_10Leu_04	0.30	0.003
10BSA_10Leu_05	0.33	0.008
10BSA_10Leu_06	0.32	0.010

3.2 Main study

3.2.1 Particle morphology by light microscopy and scanning electron microscopy (SEM)

Below are the light microscopy images illustrating the particles's morphologies (Figure 8-Figure 12). The raisin-like morphology observed in 10BSA and 10BSA_10Leu formulations, along with the presence of internal vacuoles, is consistent with the behavior expected for protein-rich systems with high Péclet numbers. The limited diffusion of BSA compared to the evaporation rate promotes its accumulation at the droplet surface, resulting in wrinkled and collapsed structures upon drying. BSA is a multi-domain protein, and its least stable domain has been reported to undergo partial unfolding upon adsorption at the air–water interface (Andrade et al., 1990). This conformational change exposes additional hydrophobic regions, enhancing its surface activity. The exposed hydrophobic regions can promote intermolecular interactions, increasing the likelihood of protein aggregation.

In contrast, 10Leu particles showed spherical shapes with multiple vacuoles, reflecting the surface activity of L-leucine, which tends to migrate to the droplet-air interface and form a shell; also the rapid precipitation and crystallization of leucine during drying due to its low solubility. 10BSA_20Leu showed more rounded vacuoles and reduced agglomeration compared to 10BSA_10Leu, supporting the findings by Ordoubadi et al. (2023), who reported that leucine contents above 20% facilitate the formation of a more uniform and protective outer layer. This shell likely stabilizes the particles and mitigates collapse or sticking, resulting in improved morphology and dispersibility. The observed spherical morphology and partial agglomeration of Tre are characteristic of amorphous saccharides with low glass transition temperatures. As described by Vehring (2008), such materials are susceptible to moisture uptake during or after drying, which can lead to reduced physical stability and particle coalescence.

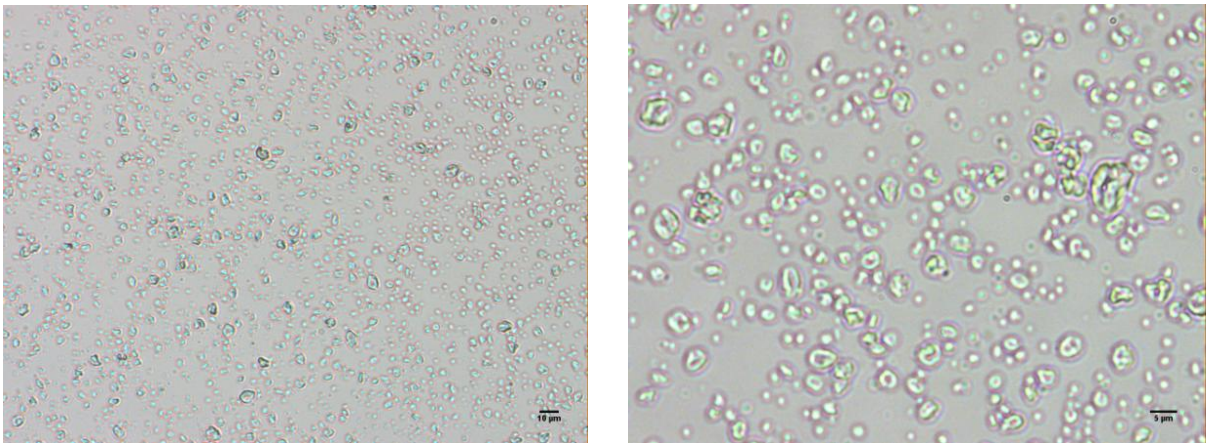

Figure 8: Light microscopy image of spray-dried 10BSA at magnification x20 (left) and x50 (right).

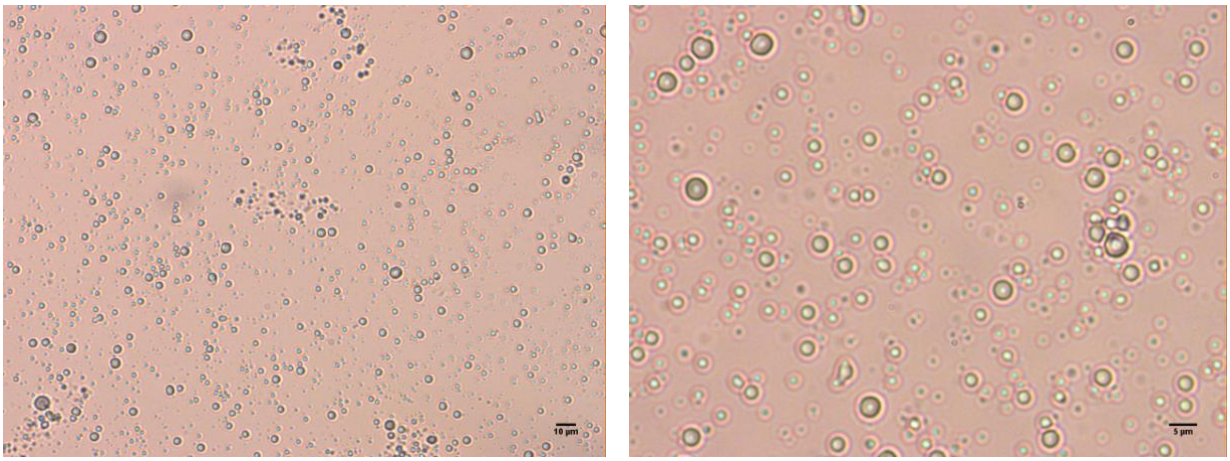

Figure 9: Light microscopy image of spray-dried 10Leu at magnification x20 (left) and x50 (right).

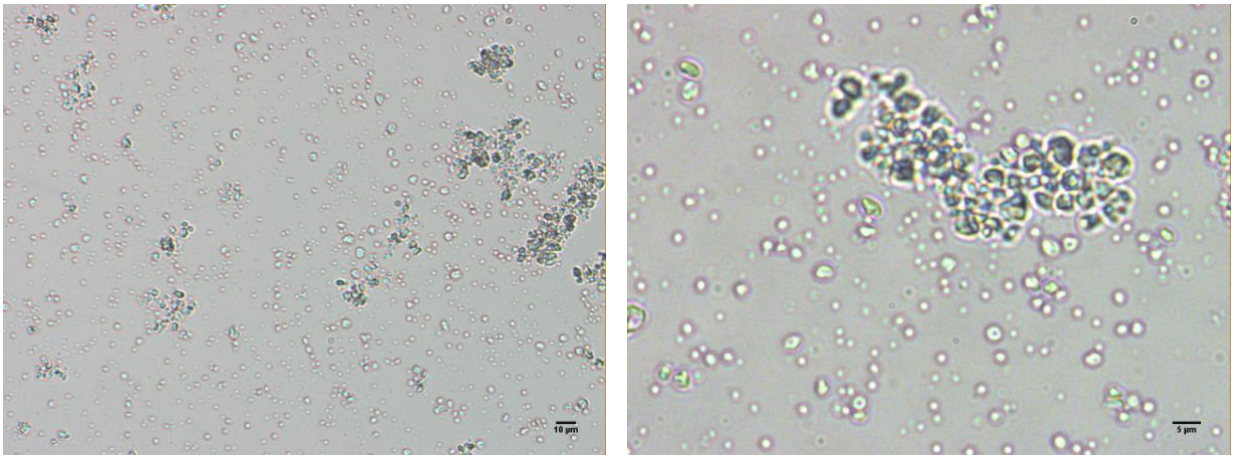

Figure 10: Light microscopy image of spray-dried 10BSA_10Leu at magnification x20 (left) and x50 (right).

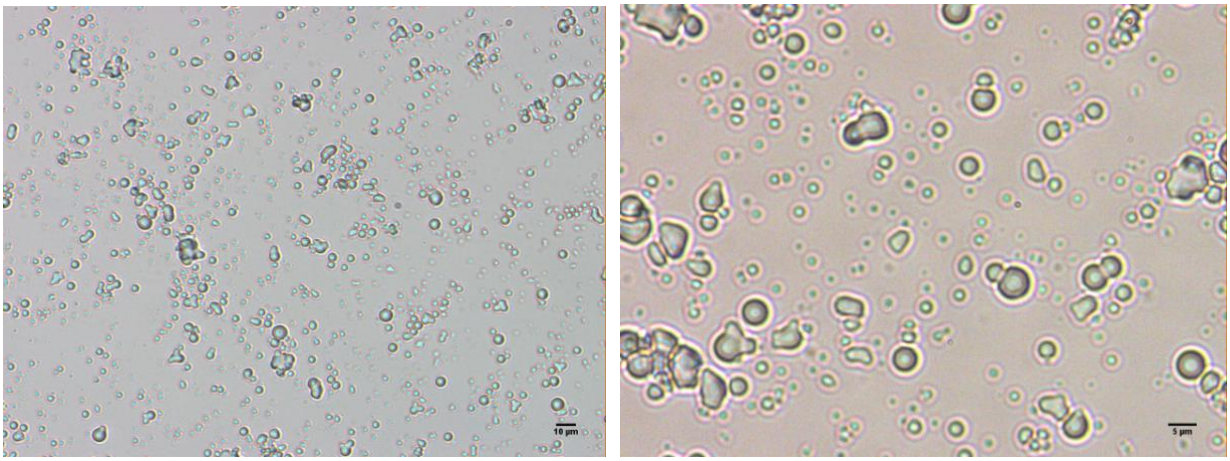

Figure 11: Light microscopy image of spray-dried Tre at magnification x20 (left) and x50 (right).

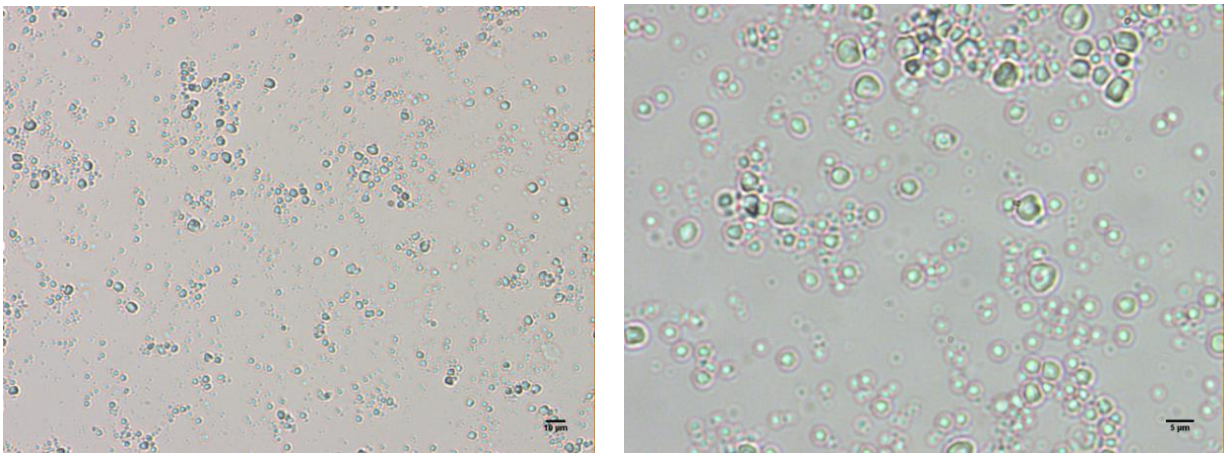

Figure 12: Light microscopy image of spray-dried 10BSA_20Leu at magnification x20 (left) and x50 (right).

SEM images of the samples are provided below (Figure 13-Figure 17). Tre particles appeared spherical with smooth surfaces, whereas 10Leu showed a more corrugated morphology with surface shriveling compared to pure trehalose, likely due to the crystallization behavior of L-leucine during drying. 10BSA particles exhibited raisin-like shapes, where smaller particles appeared heavily wrinkled with shaper ridges. 10BSA_10Leu and 10BSA_20Leu displayed corrugated particles with dents, thick ridges and shrivels on their surface due to a mixed surface of leucine and BSA. 10BSA_10Leu had more wrinkled particles compared with 10BSA_20Leu, despite containing a lower proportion of leucine. 10BSA_20Leu particles presented more distinct flake-like surface features, suggesting that higher leucine content may promote more structured surface morphology and reduce excessive wrinkling. As previously observed in trehalose/leucine systems, the appearance of protrusions or flake-like features on only some particles has been linked to the randomness of the onset of nucleation during particle formation (Wang et al., 2021).

Compared with the SEM images from Kousouli (2024), the ridge and dent morphology were not observed in 10Leu, potentially due to the lower amount of leucine present in the formulation. The morphologies of Tre, 10BSA and 10BSA_10Leu were similar to those reported by Kousouli, whereas 10BSA_20Leu displayed a more flake-like structure. This difference may be due to variations in leucine concentration and spray-drying conditions.

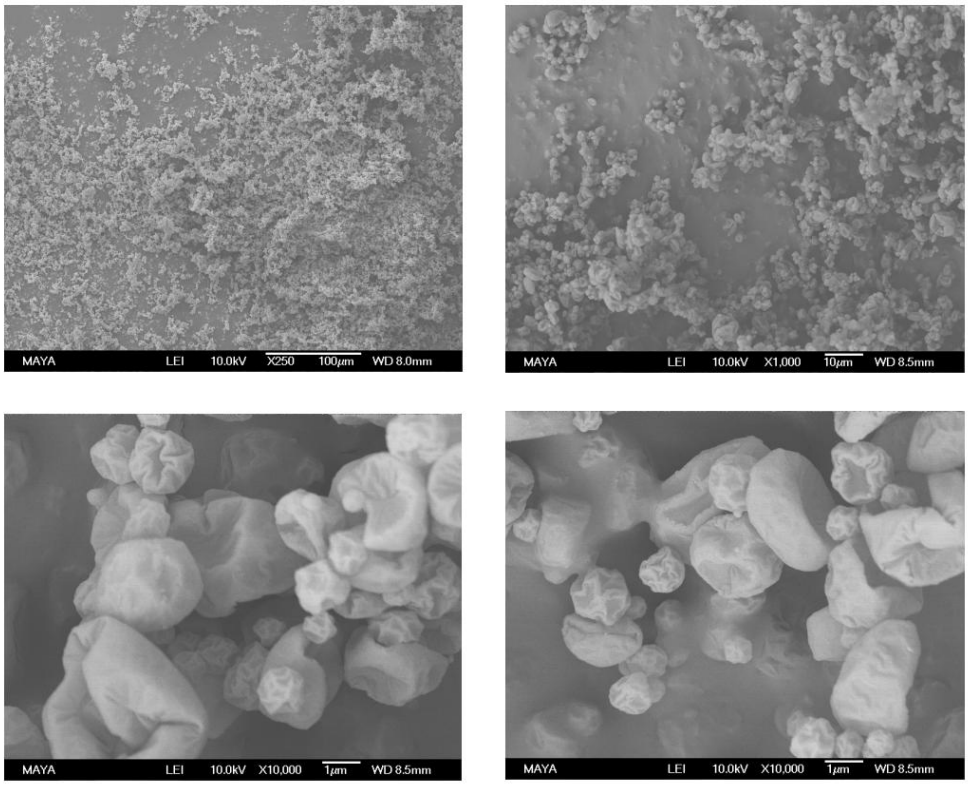

Figure 13: SEM images of spray-dried 10BSA at magnifications x250, x1000, x10000

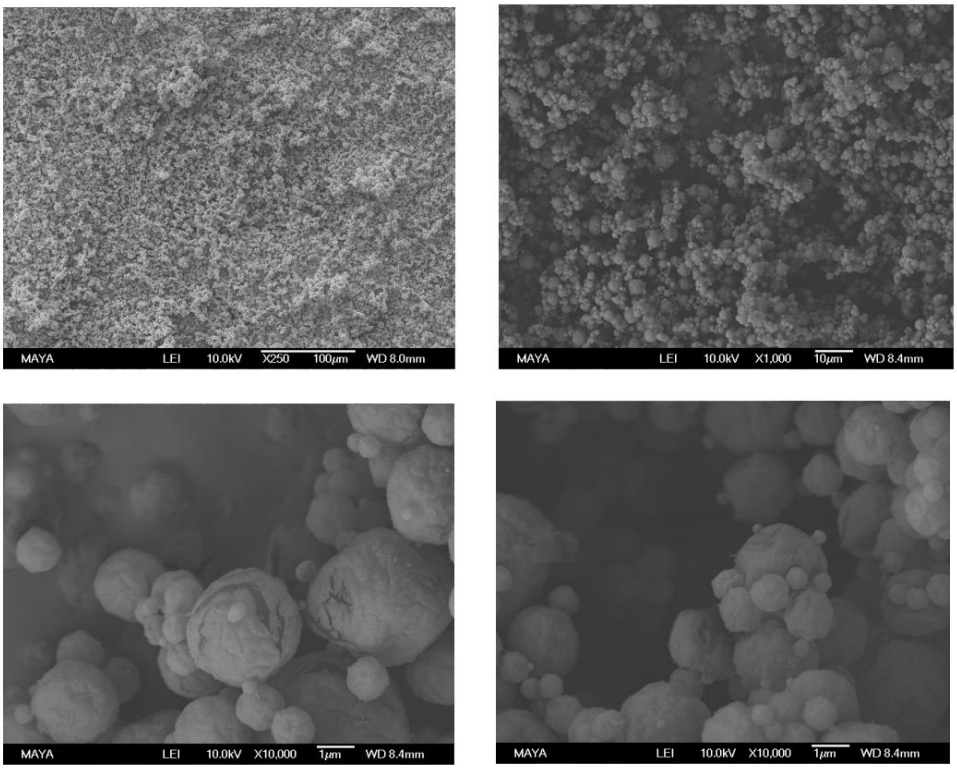

Figure 14: SEM images of spray-dried 10Leu at magnifications x250, x1000, x10000

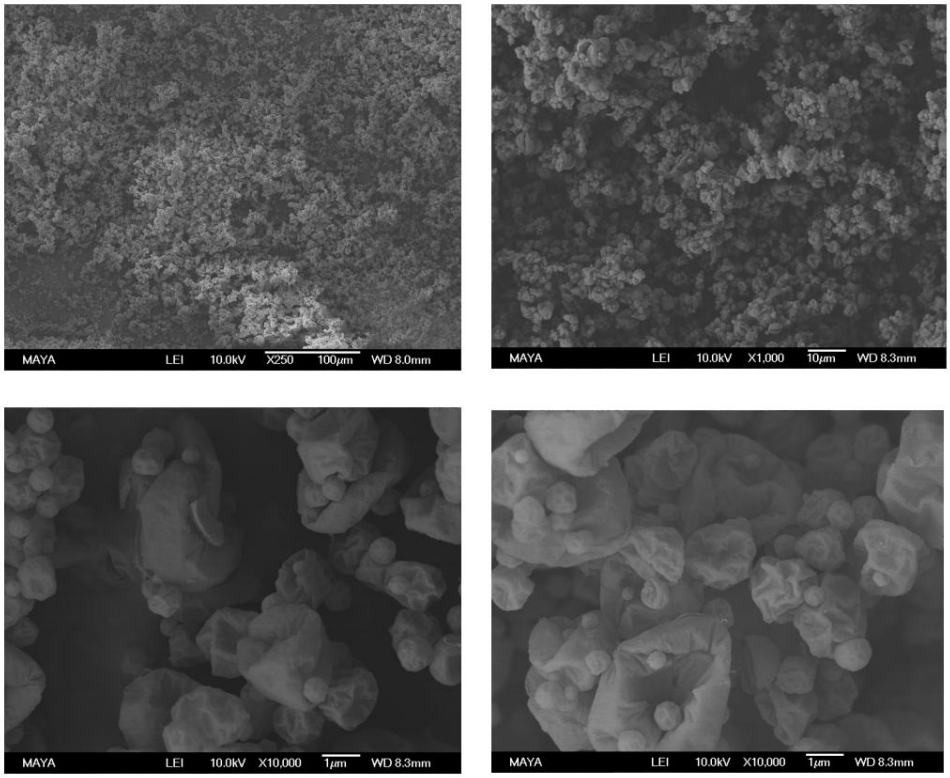

Figure 15: SEM images of spray-dried 10BSA_10Leu at magnifications x250, x1000, x10000

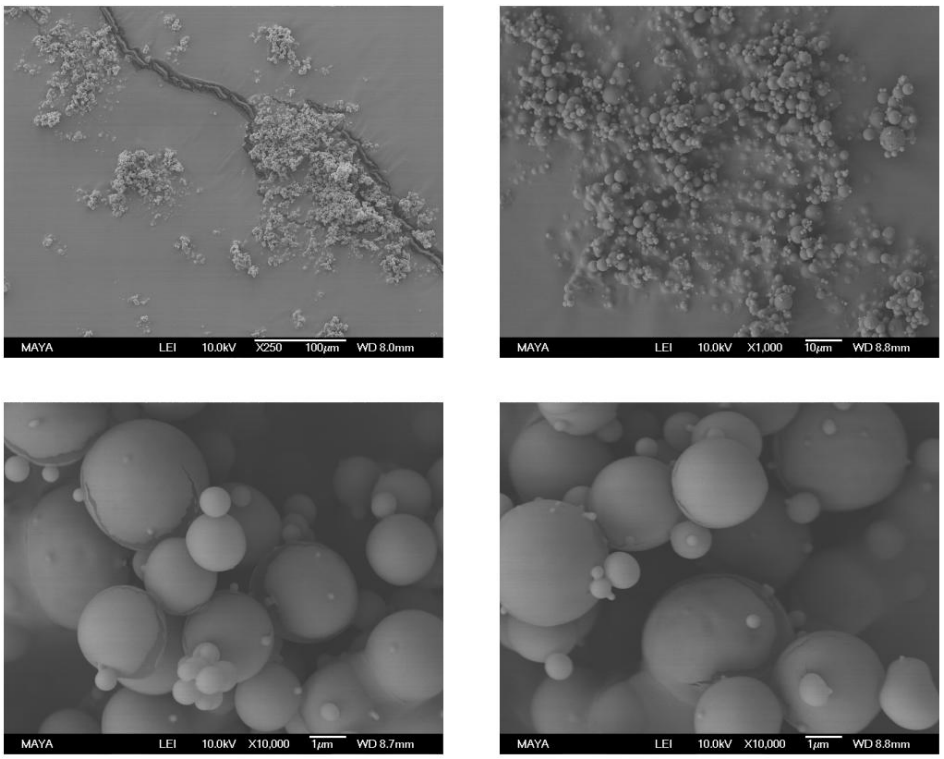

Figure 16: SEM images of spray-dried Tre at magnifications x250, x1000, x10000

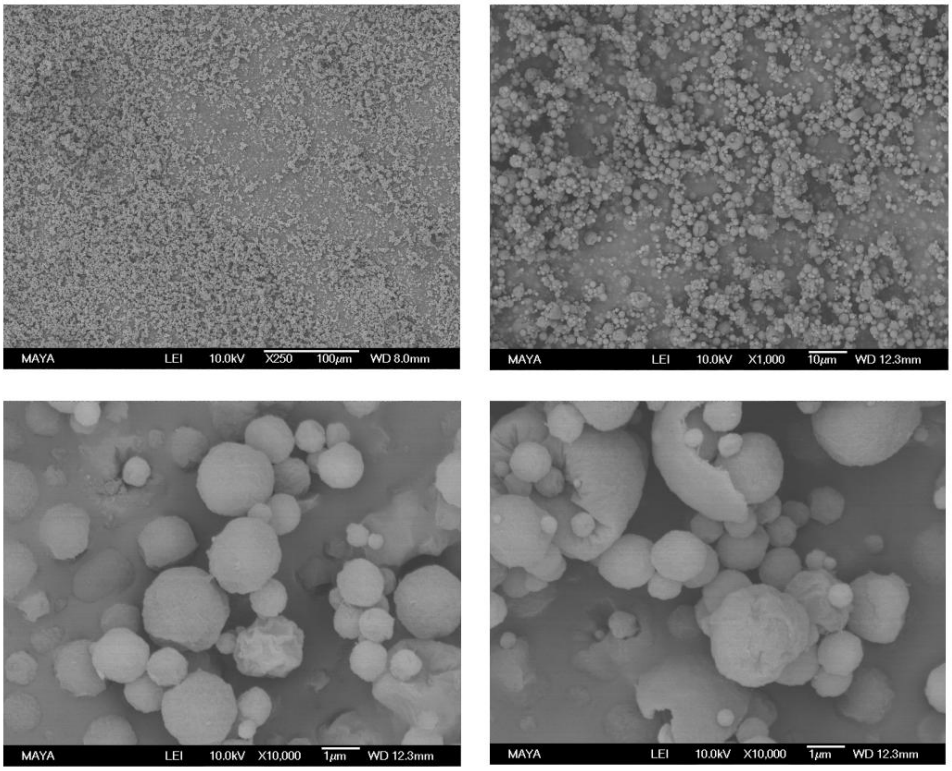

Figure 17: SEM images of spray-dried 10BSA_20Leu at magnifications x250, x1000, x10000

3.2.2 Particle size distribution by Laser diffraction

In line with the findings from the pre-study, the Fraunhofer theory yielded slightly smaller particle sizes and lower weighted residuals compared to the Mie model in the main study; therefore, only results based on the Fraunhofer model are presented here. Comparison of particle size between five formulations (Figure 18) are based on the particle size distribution images shown below (Figure 19-23), 10Leu exhibited the smallest d(0.5) value. Among the formulations containing BSA, the 10BSA sample had the smallest particle size, followed by 10BSA_20Leu and then 10BSA_10Leu. Tre showed a particle size distribution similar to that of 10BSA_20Leu, except that there was a small peak between 10 and 100 µm. A similar peak was also detected in the 10Leu formulation. This additional peak is likely indicative of particle agglomeration, potentially resulting from a suboptimal concentration of Span20 in the lamp oil. Table 10 presents the particle size and the span values of the spray-dried formulations. All samples exhibited a span value below 2, indicating relatively narrow particle size distributions. This suggests a good level of uniformity in particle formation. All of the formulations exhibited particle sizes with d(0.5) values below 3.5 µm. This indicates their potential suitability for deep lung deposition.

Compared with the particle sizes reported by Kousouli (2024), our formulations exhibited smaller particle sizes, likely due to the use of a lower inlet temperature and a higher spray gas flow rate during spray-drying.

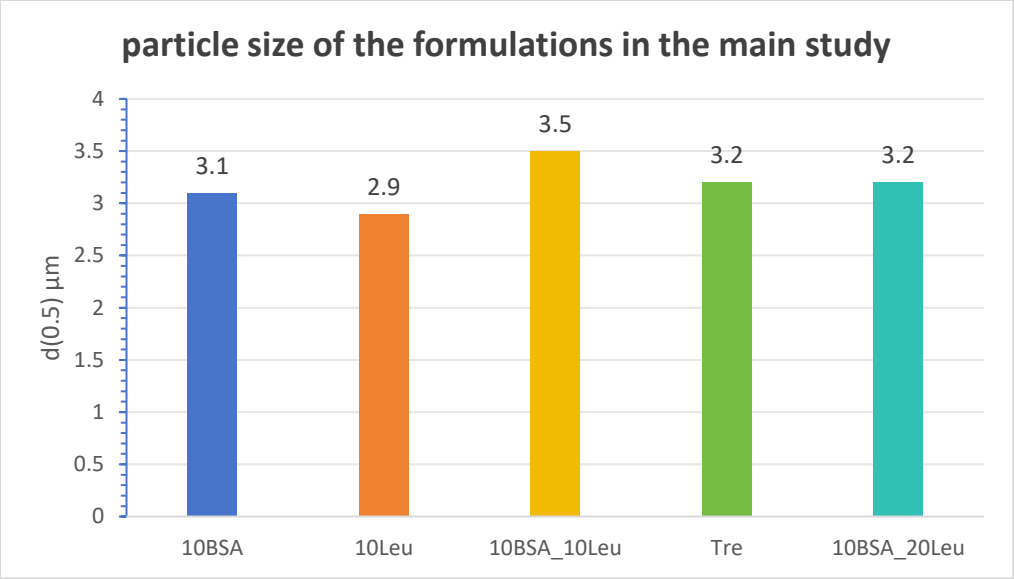

Figure 18: Comparison of particle size of the formulations in the main study.

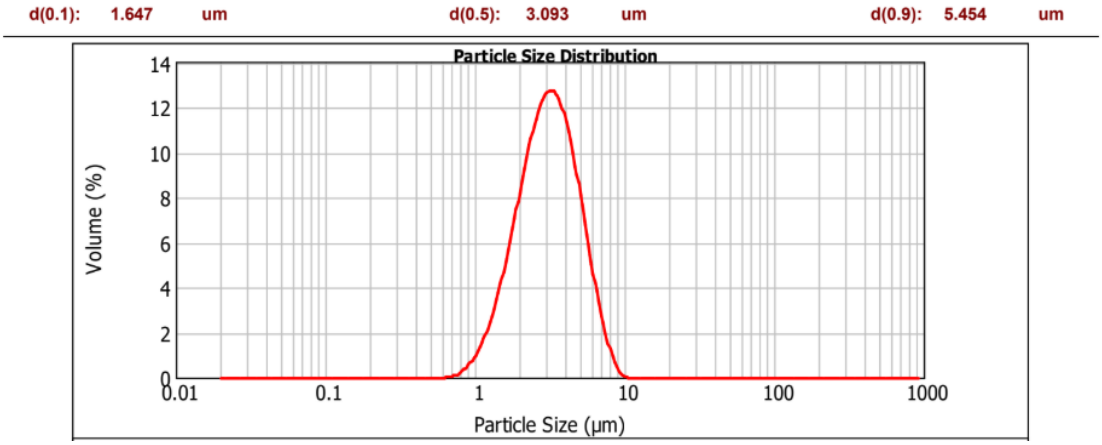

Figure 19: Particle size distribution of sample 10BSA (Fraunhofer theory).

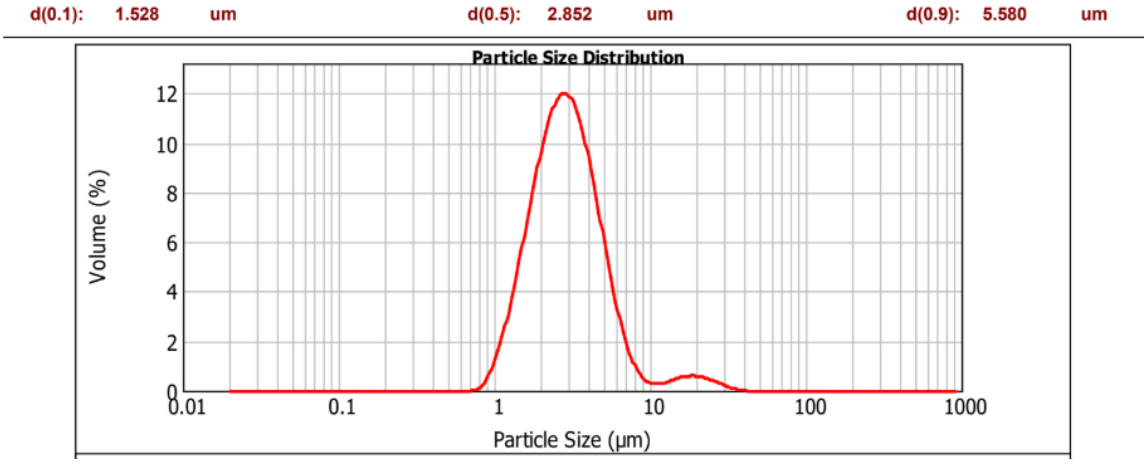

Figure 20: Particle size distribution of sample 10Leu (Fraunhofer theory).

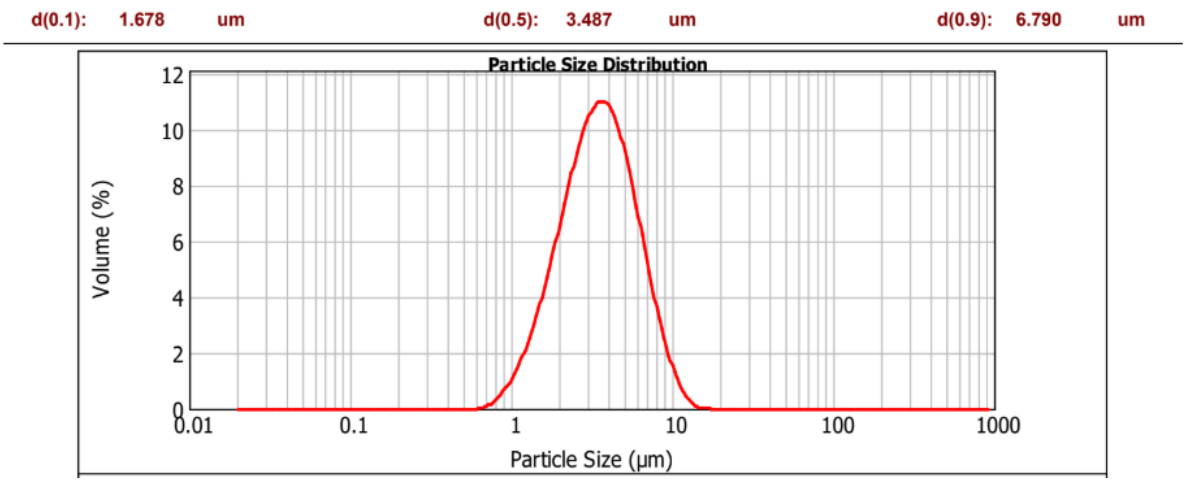

Figure 21: Particle size distribution of sample 10BSA_10Leu (Fraunhofer theory).

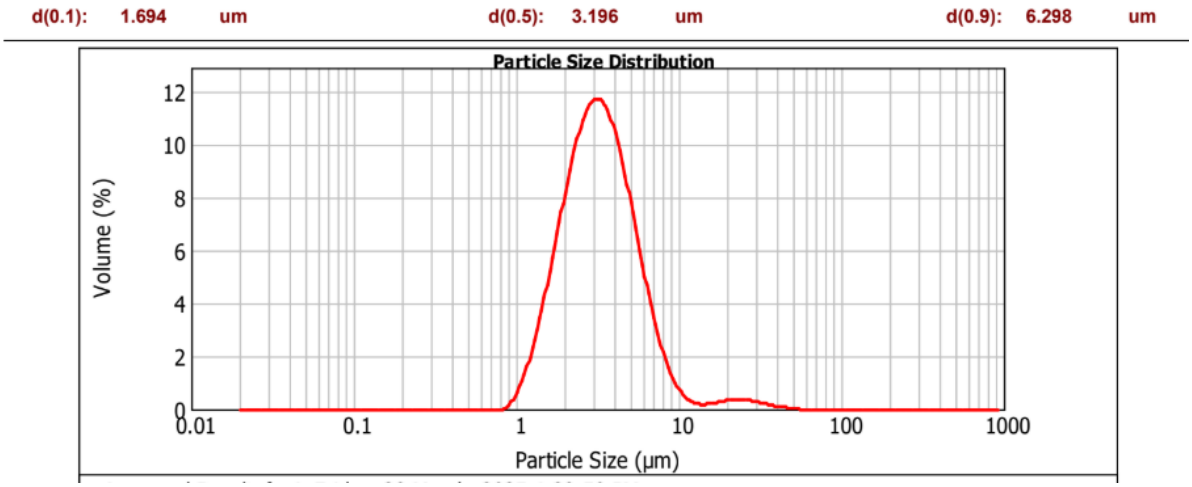

Figure 22: Particle size distribution of sample Tre (Fraunhofer theory).

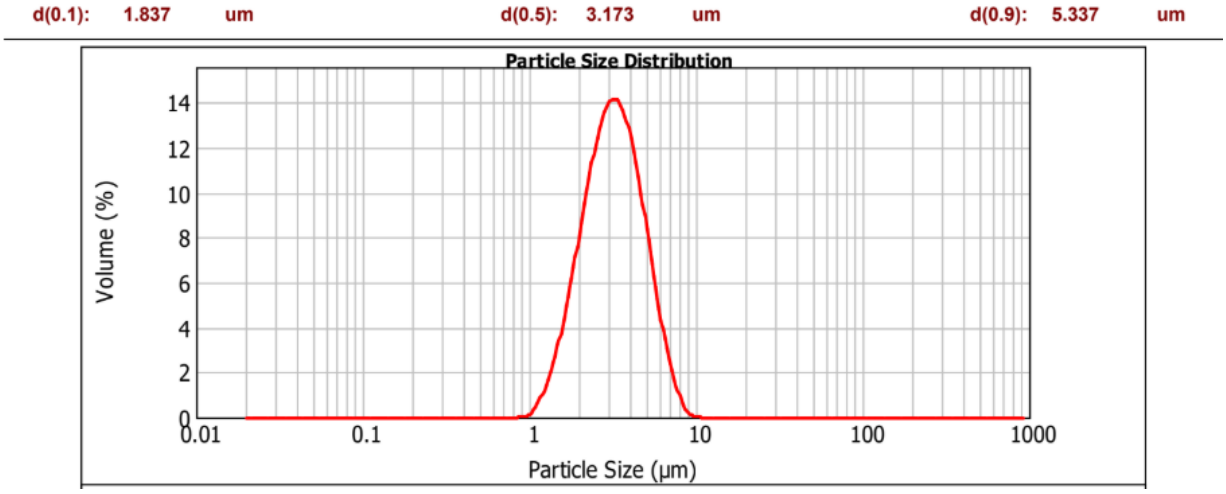

Figure 23: Particle size distribution of sample 10BSA_20Leu (Fraunhofer theory).

Table 10: Laser diffraction results of samples in the main study.

Batch	d(0.1) µm	d(0.5) µm	d(0.9) µm	span
10BSA	1.6	3.1	5.5	1.2
10Leu	1.5	2.9	5.6	1.4
10BSA_10Leu	1.7	3.5	6.8	1.5
Tre	1.7	3.2	6.3	1.4
10BSA_20Leu	1.8	3.2	5.3	1.1

3.2.3 Water content

The water content values in Figure 24 were measured within one week after the spray-drying process; all formulations showed a higher value at 2 hours compared to 1 hour. This may reflect that complete drying was not achieved within 1 hour.

Tre exhibited the lowest water content among the five formulations in both time points, reflecting its good drying characteristics. This implies that the accumulation of components like leucine and BSA at the particle surface reduces drying efficiency. 10BSA consistently maintained the highest amount of moisture while leucine-containing samples generally showed lower water content, suggesting that leucine contributes to better moisture reduction during drying. Among the BSA-containing formulations, 10BSA_20Leu had the lowest water content, suggesting that a higher proportion of leucine improves drying efficiency of BSA-based powders. This effect may be attributed to the tendency of leucine to crystallize during the drying process, forming a water-free crystalline phase that limits moisture retention.

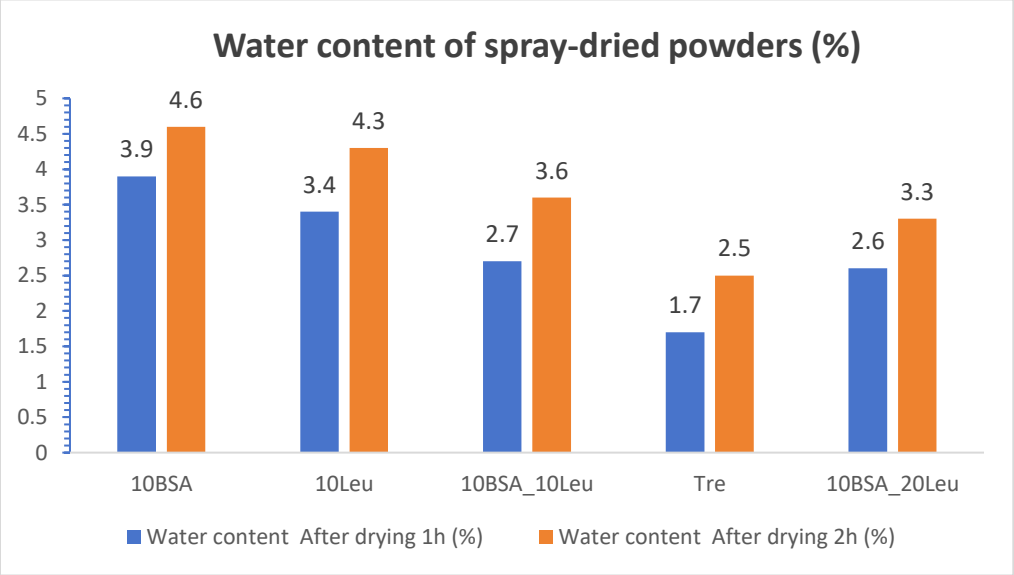

Figure 24: Graph depicting the water content values of the spray-dried powders.

3.2.4 Bulk density

Figure 25 illustrates a comparison of the bulk densities of the various spray-dried powders. The standard deviation for each sample was calculated to assess the variability in the measurements. 10Leu shows the highest bulk density, suggesting that L-Leucine with Trehalose particles is more compact or denser when settled, possibly due to their morphology or particle packing behavior. The relatively smooth and discrete particles observed in 10Leu support this, with no evident signs of agglomeration or electrostatic interactions. The high bulk density also reflects the surface enrichment of leucine, along with its low surface energy and lubricating properties. In contrast, Tre exhibited the lowest bulk density among all formulations. This is likely due to strong electrostatic interactions between particles, which make the powder more cohesive, and it is harder to pack efficiently into a defined volume. The addition of leucine to BSA-based formulations increases bulk density, with a greater effect observed at higher leucine ratios. 10BSA_20Leu exhibits the highest bulk density at 0.35 g/cm³. This trend suggests that leucine enhances particle packing, likely due to its surface-active properties and influences on powder morphology. Such improvements are beneficial for dry powder inhalation, contributing to better flowability and more consistent dosing.

Dry powders with a bulk density below 1 g/cm³ have been suggested suitable for pulmonary delivery, as this promotes effective aerosolization and deep lung deposition (Chaurasiya & Zhao, 2020). Thus, all formulations meet this bulk density requirement for deep lung deposition.

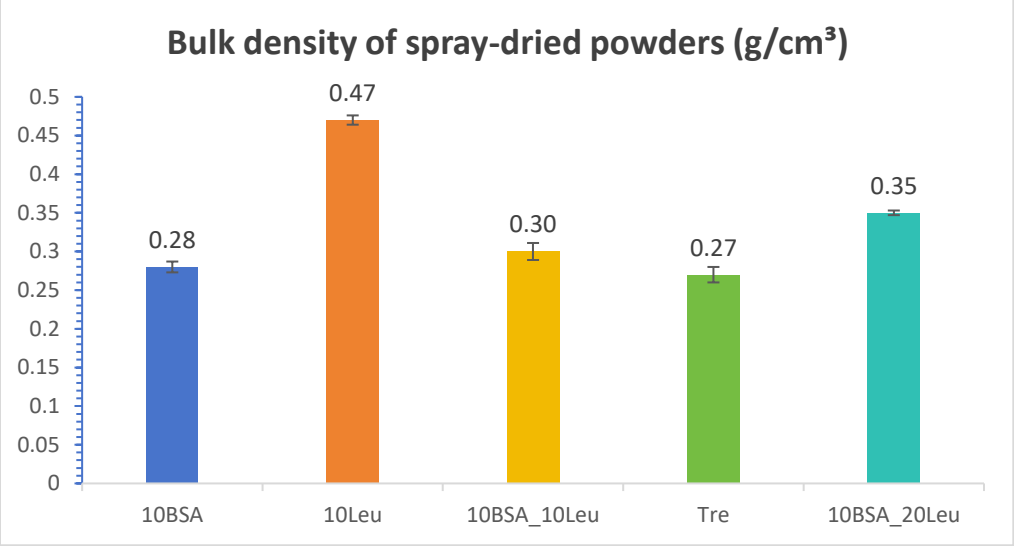

Figure 25: Graph depicting the bulk density values with the standard deviation of the spray-dried powders.

3.2.5 Humidity study

In this experiment, the five formulations and their duplicates were named 10BSA (1a and 1b), 10Leu (2a, 2b), 10BSA_10Leu (3a, 3b), Tre (4a, 4b), and 10BSA_20Leu (5a, 5b) were kept in a desiccator which maintained an environment with 21.5℃ and 72% RH. After overnight storage, the capsules were opened, and the powder was poured out for observation, as shown in Figure 26.

Table 11: Observation results at three time points: 1 hour, 3 hours, and overnight.

Time	Results
1 hour	Only No. 4 (Tre) had a little clogging. The other formulations were normal.
3 hours	No. 2 (10Leu) still had no clogging. No. 1 (10BSA), 3 (10BSA_10Leu), and 5 (10BSA_20Leu) showed slight clogging. No. 4 (Tre) showed more obvious clogging.
Overnight	All formulations were clogged.

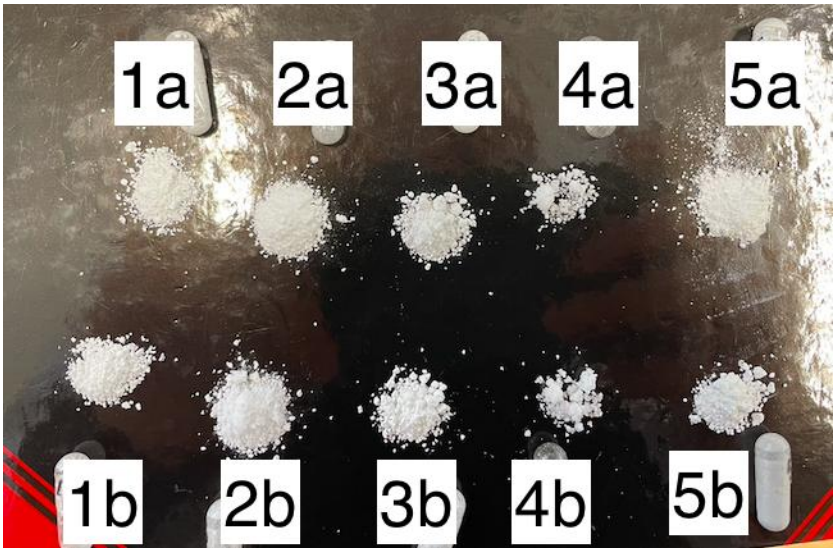

Figure 26: Results of overnight observation: 1a, 1b (10BSA): Slight aggregation, the powder is still relatively loose. 2a, 2b (10Leu): The morphology is the loosest and most uniform, the powder is fluffy and dispersed, and there are no obvious lumps. 3a, 3b (10BSA_10Leu): Slight lumps appear, but the overall dispersion is good. 4a, 4b (Tre): The lumps are the most obvious, the particles are coarse, and the agglomeration is serious. 5a, 5b (10BSA_20Leu): Between 1 and 3, there are some slight lumps, but still dispersed.

The 10Leu (No. 2) was in the best condition, and there was no *aggregation* even after 3 hours of exposure. The combination of 10BSA_10Leu (No. 3) was also good, with slight aggregation but better than the 10BSA. The combination of 10BSA_20Leu (No. 5) also had slight agglomeration after 3 hours, and the effect was not as good as the 10% Leucine alone formula (No. 2). Leucine can significantly improve moisture resistance and dispersibility.

The Tre (No. 4) began to agglomerate in 1 hour, was obviously blocked in 3 hours, and completely lost its powder properties overnight. This is consistent with the physical property of Trehalose's high hygroscopicity.

The 10BSA (No. 1) was slightly better than pure Trehalose, but it still began to aggregate after 3 hours. This suggests that 10BSA itself helps slightly alleviate hygroscopicity but is not enough to resist high humidity.

3.2.6 Aerodynamic particle sizing by Next Generation Impactor (NGI)

Due to the limitation of our HPLC quantitative detection method, only three BSA containing formulations were tested for NGI at 30% RH and 50% RH. Three replicates were tested for each formulation, and the average was calculated to minimize the errors. In order to avoid the impact of the weight difference of each dose, we focus on comparing the FPF diagrams. FPD data are shown in Appendix 6.4.2. In the Deposition profile, we compare the proportion of each part to the total.

3.2.6.1 FPF, MMAD, and capsule retention comparison

First, in terms of FPF (Figure 27), the FPF of the three formulations all have a very high FPF at 30% RH and 50% RH, with minimal variation between humidity conditions. In comparison, the BSA-containing formulation reported by Kousouli (2024) achieved FPF values ranging from 29.6% to 49.3%. The three BSA-based formulations developed in this study showed significantly higher FPFs, indicating superior aerosolization performance and strong potential for efficient pulmonary drug delivery.

In terms of MMAD (Figure 28), the particle size of all formulations increased with increasing humidity, indicating that high humidity may cause particle agglomeration or hygroscopic expansion. The particle size of 10BSA_20Leu was always the smallest (2.69-2.88 μm) under 30% and 50% RH conditions, indicating that it has good lung deposition potential under different humidity conditions, which is related to better dispersibility when the leucine content level is higher. There is no significant difference in the change of particle size with increasing humidity.

In terms of capsule retention rate (Figure 29), the capsule retention values obtained for the three formulations at 30% RH and 50% RH were all below very low values (5%), which means that the capsule emptying effects of the three formulations were very good. However, the 10BSA increased significantly under high humidity conditions (from 1.6% to 3.7%), which may be due to its enhanced adhesion in the device due to hygroscopicity. 10BSA_10Leu and 10BSA_20Leu showed lower and more stable retention rates, especially 10BSA_20Leu, which showed almost no change (1.8% vs. 1.7%), showing good humidity protection.

Finally, in terms of GSD (Figure 30), Obviously, the GSD value of 10BSA is always the lowest under both 30% RH and 50% RH conditions, indicating that its size distribution is the narrowest. And the 10BSA slightly widened the distribution when the humidity increased (from 2.26 to 2.48), while the Leu-added formulations maintained their distribution ranges, especially 10BSA_20Leu, which showed almost no change at two humidity levels (2.93 vs. 2.95), showing excellent uniformity.

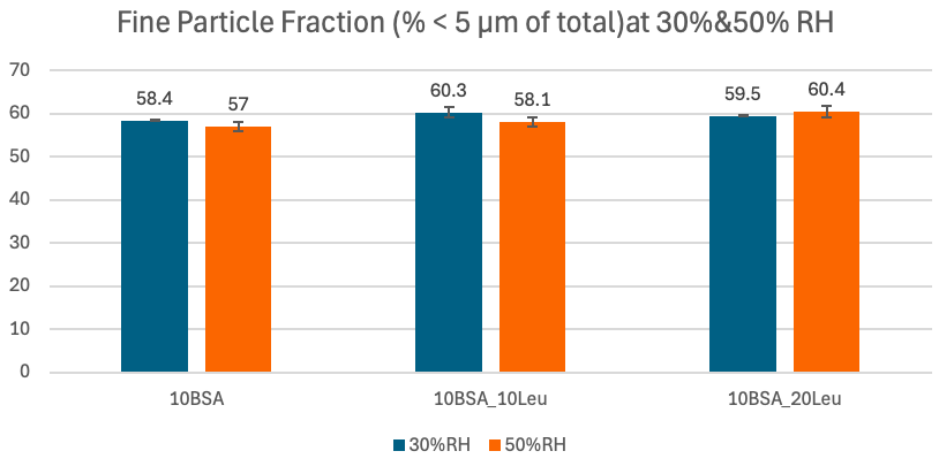

Figure 27: Fine particle fraction (% of particles < 5 µm) of three formulations (10BSA, 10BSA_10Leu, and 10BSA_20Leu) measured under 30% and 50% relative humidity (RH) using NGI analysis. The Error bars in the graph shows SEM (Standard Error of the Mean).

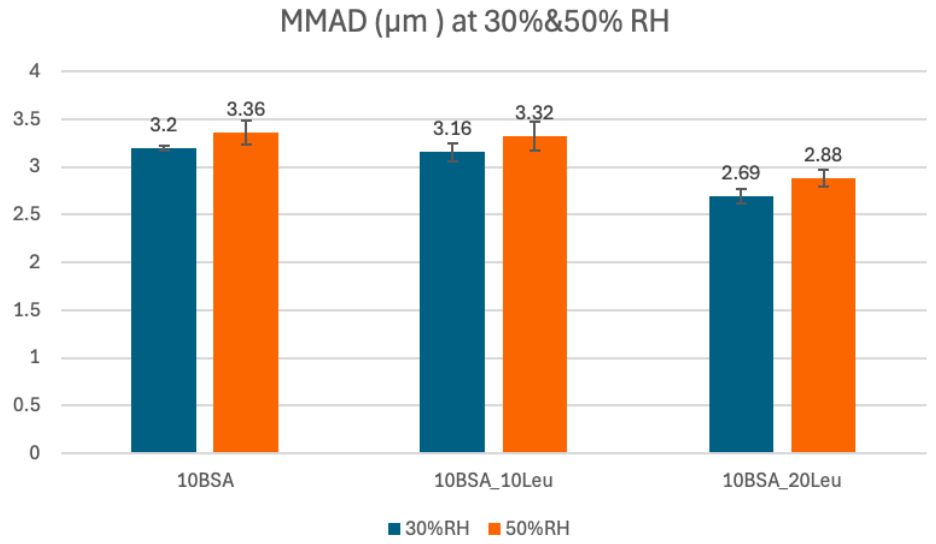

Figure 28: Mass median aerodynamic diameter (MMAD, µm) of three formulations (10BSA, 10BSA_10Leu, and 10BSA_20Leu) measured under 30% and 50% relative humidity (RH) using NGI analysis. The Error bars in the graph shows SEM (Standard Error of the Mean).

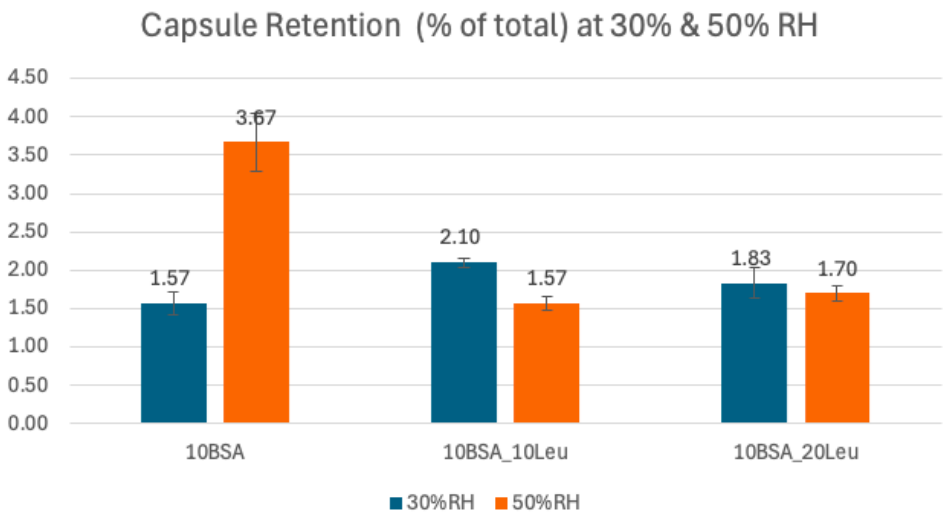

Figure 29. Caplule retention (% of total emitted dose) of 10BSA, 10BSA_10Leu, and 10BSA_20Leu formulations measured under 30% and 50% relative humidity (RH). The Error bars in the graph shows SEM (Standard Error of the Mean).

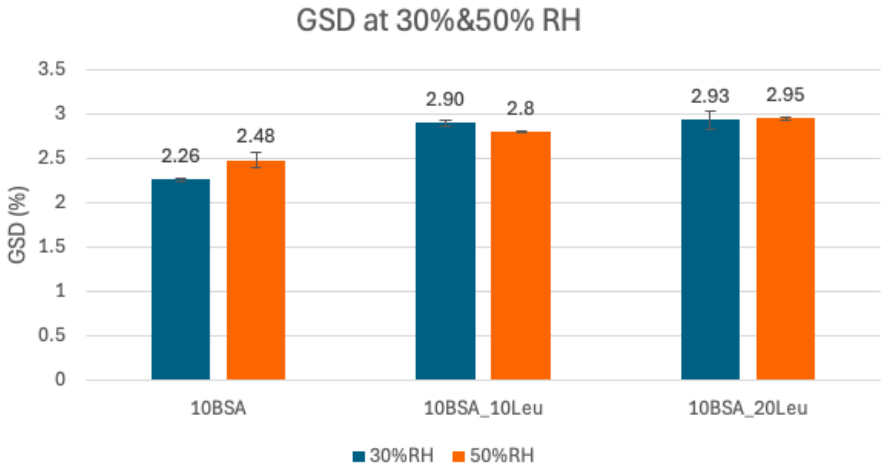

Figure 30: GSD of three formulations (10BSA, 10BSA_10Leu, and 10BSA_20Leu) measured under 30% and 50% relative humidity (RH) using NGI analysis. The Error bars in the graph shows SEM (Standard Error of the Mean).

The MMAD values of all three formulations were within the optimal range for inhalation (<5 μm), and both FPF and capsule retention were satisfactory. Among them, 10BSA_20Leu showed slightly better aerodynamic performance and moisture resistance, suggesting that higher leucine content may improve formulation stability under humid conditions. This aligns with findings by Wang et al. (2021), who reported that a crystalline leucine shell helps maintain dispersibility even in moisture-rich particles.

On the other hand, the GSD values of the three BSA containing formulations are all higher than 2, with 10BSA having the lowest GSD, and 10BSA_20Leu being higher than 10BSA_10Leu, which may be caused by the rebound effect during the NGI experiment. The rebound effect

refers to the fact that when particles hit the surface of the impact stage plates, some particles are not firmly captured but bounce back into the airflow and deposit at a later stage. According to Mitchell and Nagel (2003) and Khalili et al. (2018), this effect is common in NGI measurements and can result in underestimation of deposition in the early stages and overestimation in the later stages, thereby distorting the actual particle size distribution.

3.2.6.2 Deposition Pattern Comparison of three formulations

By observing the deposition profile (Figure 31), we can see that the amount of residue in the capsule position of the three formulations was very low. A graph of the actual deposition mass in each size bin is also plotted, as shown in appendix 6.4.3. The cumulative NGI relative particle size distributions at two relative humidity conditions for the three formulations (10BSA, 10BSA_10Leu, and 10BSA_20Leu) are plotted in Appendix 6.4.4. The data were plotted as cumulative mass fraction versus aerodynamic diameter to assess particle deposition behavior in relation to inhalation performance.

In terms of throat deposition, the 10BSA_10Leucine formula showed the lowest deposition at 30% RH and 50% RH conditions, which were 267 μg/dose and 335 μg/dose, respectively, which were significantly lower than the Leucine-free formula (492 μg/dose and 381 μg/dose). In contrast, the throat deposition of the 10BSA_20Leucine at 30% RH increased to 412 μg/dose, suggesting that too high a Leucine ratio may have an adverse effect on particle flight and impact behavior.

The distribution of PS and stage 1 in each formulation was not significantly different. At 30% RH and 50% RH humidity, the 10BSA_10Leu had the highest deposition peak at Stage 2. The 10BSA is slightly lower than the 10BSA_10Leu, and 10BSA_10Leu is significantly lower than the first two formulations. The 10BSA with different humidity levels has the highest distribution in Stage 3, followed by 10BSA_10Leu, and the 10BSA_10Leu is the lowest. However, the distribution in the later sections is significantly reduced, while 10BSA_20Leu gradually increases, and the data is almost the same as that of the 10BSA10Leu in stage 4 and then surpasses from stage 5.

After adding Leucine (especially 20%), the powder deposition distribution migrates to the small particle area, and the fine particle output ratio increases significantly, while maintaining good dispersion and deposition uniformity under high humidity conditions; however, when there is too much Leucine (20%), it may also lead to enhanced aggregation of large particles in the PS segment. The particle size distribution profiles (Figure 31) show that all BSA formulations, regardless of relative humidity (RH) and leucine (Leu) content, exhibit a unimodal distribution centered around 7.9 μm. With the addition of leucine, especially at higher concentrations (20%), the distribution shifts slightly toward smaller particle sizes and reduces the fraction of larger particles.

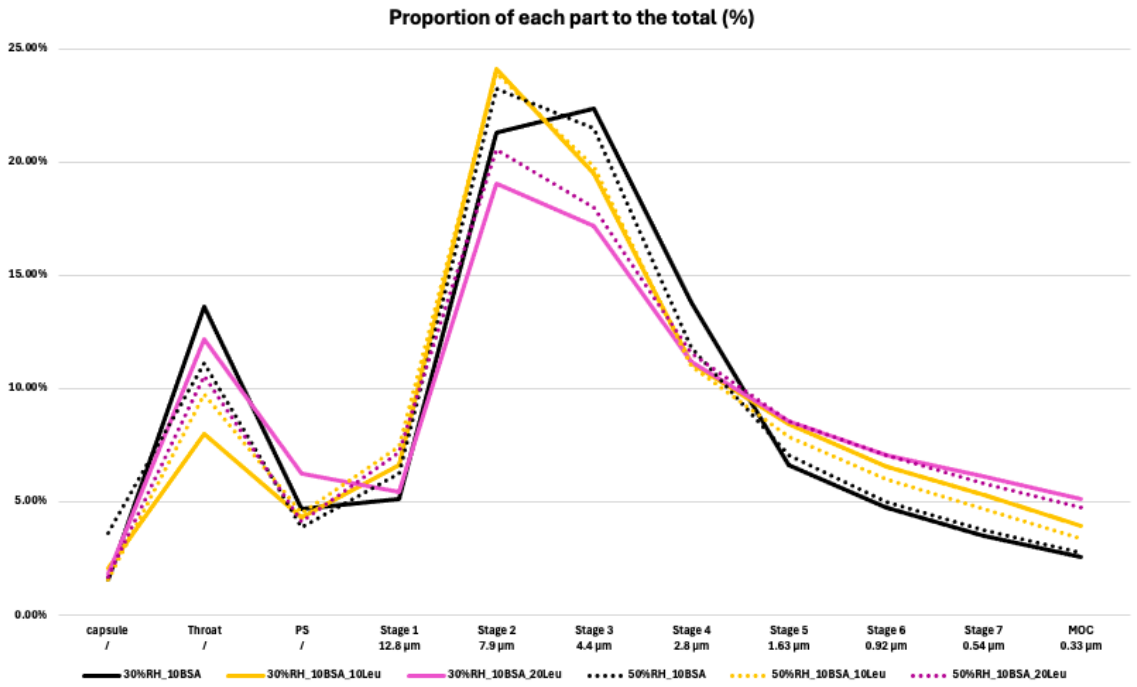

Figure 31. Deposition profile of three BSA containing formulations across impactor stages under different relative humidity (RH) conditions and leucine contents. The y-axis shows the proportion of each particle size fraction relative to the total, while the x-axis represents the stage particle deposited and particle size (µm). Formulations include BSA with 0%, 10%, and 20% leucine at 30% and 50% RH.

Formulations without leucine show higher deposition in capsule and throat regions, while leucine-containing formulations—especially those with 20% Leu—exhibit increased deposition in peripheral regions such as Stage 5 to Stage 7. This suggests that the addition of leucine helps improve the aerodynamic properties of the powder, forming smaller, more inhalable particles after spraying, thereby promoting deeper lung penetration.

As shown in the deposition curves, the formulations at 30% RH exhibited a more pronounced tailing from stage 5 to MOC, especially in the 10BSA formulation without leucine. This suggests enhanced particle bounce, likely due to increased particle rigidity and reduced surface adhesion under low humidity conditions—an effect consistent with the findings of Yu et al. (2017) and Young et al. (2007), who reported that low RH increases electrostatic charge and decreases adhesion. At 50% RH, deposition was more uniform with reduced tailing, indicating improved particle retention. The inclusion of leucine mitigated bounce across both humidity levels, with 20% leucine yielding the most consistent aerodynamic performance.

3.2.6.3 Particle Size Distribution from NGI: Comparison of three formulations

As shown in Figure 32A, the 10BSA formulation without leucine showed significant differences under different humidity conditions. The distribution under 50% RH conditions shifted slightly toward larger particle sizes, indicating that higher humidity may lead to particle agglomeration or reduced dispersibility. However, there is a possibility of the bounce effect.

When 10% leucine was added (Figure 32B), the particle size distribution curves under the two humidity conditions almost completely overlapped, indicating that leucine significantly weakened the effect of RH on aerodynamic performance. This may be attributed to the surface activity and anti-hygroscopic properties of leucine, which improved the dispersibility of the powder. In contrast, when the leucine addition was increased to 20% (Figure 32C), the distribution difference between 30% and 50% RH conditions became obvious again. Although the distribution of particles larger than 4.4 μm under 50% RH was slightly higher than that of the 30% RH sample. This may be because the large-sized particles under 30% RH conditions escaped to the position of small-sized particles due to not being captured. We will make a more in-depth comparison in the data comparison between APS and NGI.

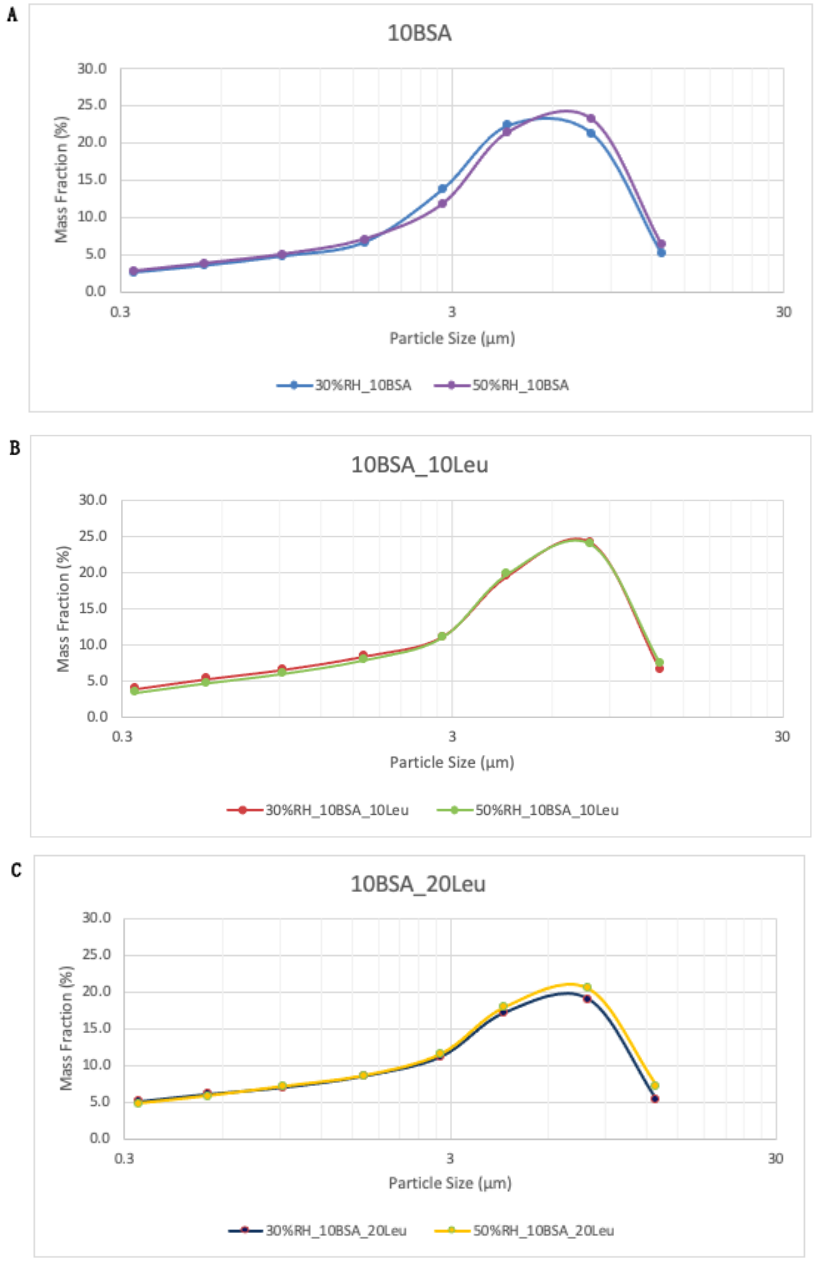

Figure 32: Particle size distributions of 10BSA-based formulations under 30% and 50% relative humidity. (A) 10BSA; (B) 10BSA_10Leu; (C) 10BSA_20Leu. All distributions were obtained using NGI , with particle size (X-axis) displayed on a base-10 logarithmic scale and mass fraction (Y-axis) expressed as a percentage of total collected dose.

3.2.7 Aerodynamic Particle Sizing by APS instrument (APS)

The five formulations were tested for APS operation at 30% RH and 50% RH, and the 30% RH humidity condition was tested at 4kPa and 2kPa inside the device. Three replicates were tested for each sample, and the average was calculated to reduce the error. Although each sample was run 10 times for APS measurement, considering that the concentration data after three minutes are too low and may not have statistical value, only the first three minutes (the first six measurements) will be included in the calculations (as shown in Appendix 6.5.2).

3.2.7.1 MMAD, GSD, and Total concentration comparison

Under 30% relative humidity (RH) (Figure 33), the MMAD of the 10BSA, 10Leu, 10BSA_10Leu, and the Tre did not change much, ranging from 2.4 to 2.6 μm, regardless of whether it was at 2kPa or 4kPa pressure. However, at 50% RH_4kPa conditions, the particle size of the formulation containing a high proportion of leucine (Leu) tended to increase, with the MMAD of the 10Leu and the 10BSA_20Leu reaching 2.68 μm and 2.71 μm, respectively, which were 0.2–0.3 μm higher than the other conditions. Overall, an increase in humidity (to 50% RH) tended to increase the particle size of the Leu-rich formulation, while a decrease in pressure from 4 kPa to 2 kPa had little effect on the particle size, with no significant changes.

Under most conditions (Figure 34), the GSD value at 30% RH was relatively high, close to 1.9–2.0, indicating a wide particle size distribution. However, under 50% RH conditions, GSD decreased significantly, which indicates that the particle distribution was more concentrated and uniform. In general, increasing humidity helps to improve the concentration of particle size distribution, especially in the Leu-containing formulation. Furthermore, the higher the Leu content, the smaller the GSD after the humidity rises, indicating that the particles are more concentrated. The effect of pressure changes (2 kPa and 4 kPa) on GSD was not significant besides Tre and 10BSA_20Leu.

The concentration under 30% RH conditions (Figure 35) is generally low, especially at 2 kPa. It can be seen that increasing the suction pressure helps to increase the mass concentration of particles in the Leu-containing formulation. Regardless of the RH and air pressure conditions, the particle concentration of the Tre formula is lower than that of other formulas, indicating that the aerosol generation efficiency after spray drying is poor. At 50% RH_4kPa conditions, the total particle concentration generally reaches the highest value, especially 10Leu, which is the most significant, reaching 3.23 mg/m³, and 10BSA_20Leu also increases significantly to 2.85 mg/m³. It was noted that during the experiment, due to the high humidity of 50% RH, the diluter was easily blocked by particles larger than 20 μm, which affected the measurement of the total concentration and caused the total concentration given by the APS to be not a very good metric We believe this may be an experimental challenge and subsequent optimization of the experimental method may be necessary.

In general, at high humidity (50% RH) and high pressure (4 kPa), formulations containing a higher proportion of leucine showed larger particle size (MMAD) and higher particle concentration. This may be related to the migration of leucine to the particle surface during spray drying to form a hydrophobic protective layer.

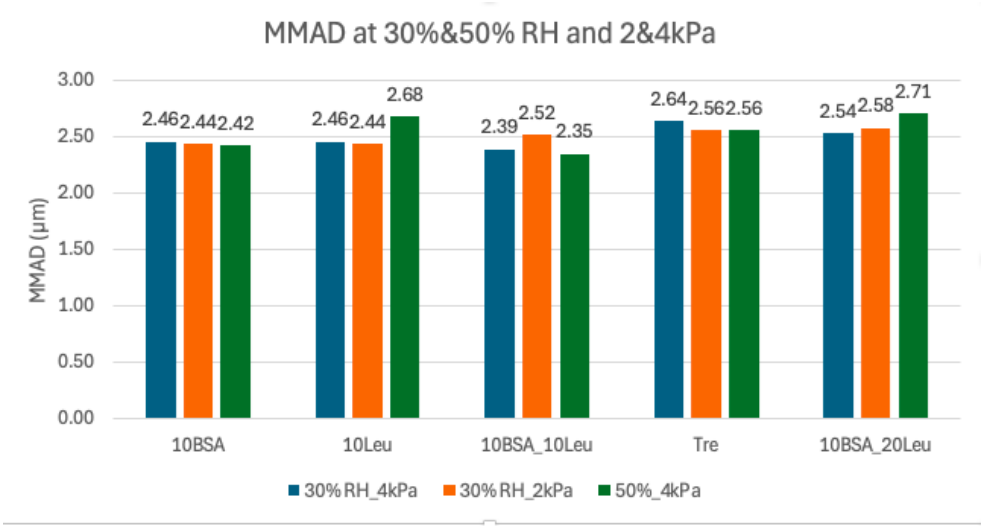

Figure 33: Mass median aerodynamic diameter (MMAD, μm) of five spray-dried formulations (10BSA, 10Leu, 10BSA_10Leu, Tre, 10BSA_20Leu) measured by APS under 2 kPa and 4 kPa at 30% relative humidity (RH), and under 4 kPa at 50% RH.

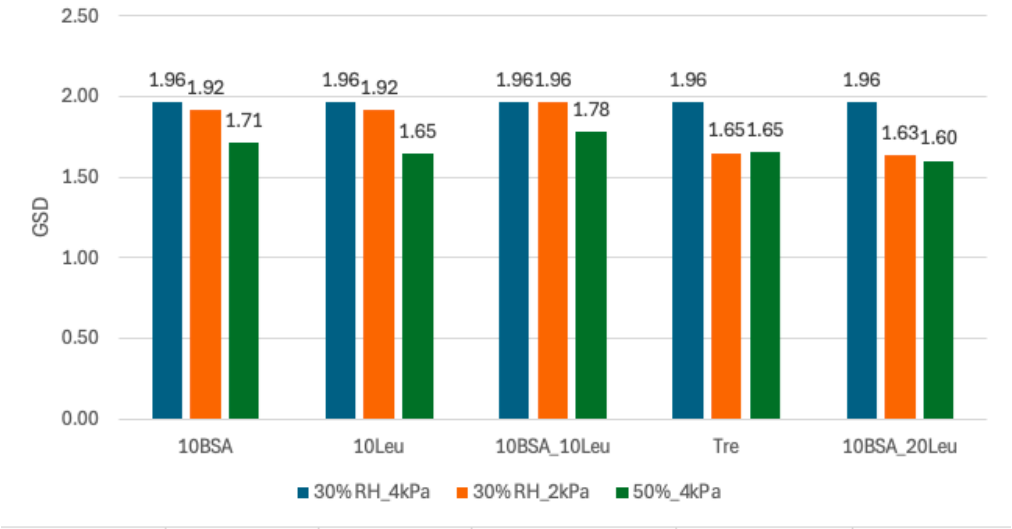

Figure 34: GSD of five spray-dried formulations (10BSA, 10Leu, 10BSA_10Leu, Tre, 10BSA_20Leu) measured by APS under 2 kPa and 4 kPa at 30% relative humidity (RH), and under 4 kPa at 50% RH.

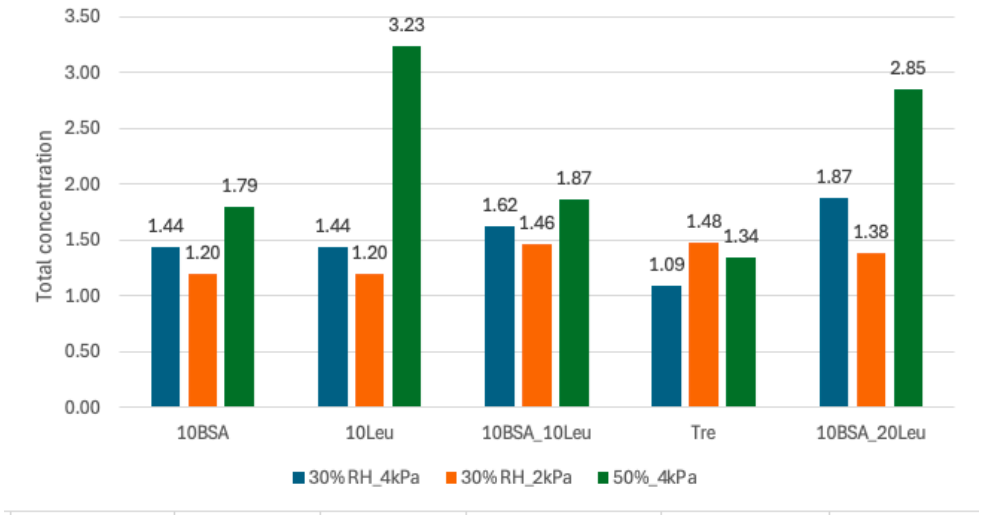

Figure 35: Total concentration (mg/m³) of five spray-dried formulations (10BSA, 10Leu, 10BSA_10Leu, Tre, 10BSA_20Leu) measured by APS under 2 kPa and 4 kPa at 30% relative humidity (RH), and under 4 kPa at 50% RH.

3.2.7.2 Aerodynamic Particle Size Distribution in APS

Figure 36 shows the normalized APS aerodynamic particle size distribution of the five spray-dried powders (10BSA, 10Leu, 10BSA_10Leu, Tre, 10BSA_20Leu) under different relative humidity (30% and 50% RH) and suction pressure (2 kPa and 4 kPa). The unnormalized original distribution is shown in Appendix 6.5.3.

In Figure 36A, 10BSA samples generally show bimodal distribution characteristics, with the main peak at 2–4 μm and the shoulder peak at 10-15 μm, indicating that the aerosol contains a certain proportion of large particles. The distribution profile under different suction conditions changes little, but the main peak is slightly more prominent at 50% RH, suggesting that higher humidity may promote the formation of smaller particles.

The 10Leu sample in Figure 36B shows a more concentrated single-peak distribution, with the main peak at 2–3 μm, a sharper overall distribution, and a shoulder peak at 10-15μm. Under 50% RH conditions, its main peak height is the largest and the shoulder peak is reduced. Compared with the 10BSA, the 10Leu samples are more concentrated under high humidity conditions and have a lower proportion of large particles.

In Figure 36C, the distribution morphology of 10BSA_10Leu samples under various conditions is highly consistent, and the main peak is stable at 2–4 μm, indicating that the addition of leucine may effectively inhibit the large particle aggregation phenomenon generated when BSA is sprayed alone, thereby improving the controllability of particle distribution. Compared with 10BSA or 10Leu alone, 10BSA_10Leu showed better particle size stability and stronger adaptability.

The particle size distribution of the Tre formulation is shown in Figure 36D. The main peak was centered around 2-3 μm under all conditions tested. Although the overall distribution pattern remained consistent across conditions, the Tre formulation had a wider peak and a flatter curve

compared to 10Leu and 10BSA_20Leu, indicating greater particle size heterogeneity and slightly less uniform distribution. In addition, although trehalose tends to agglomerate, no shoulder peak was observed, possibly because high humidity hindered the detection of aggregates, leading to inaccurate measurements.

In Figure 36E, the 10BSA_20Leu formula shows the most concentrated distribution curve, with the main peaks all focused on 2–3 μm, almost no obvious drift with changes in humidity or pressure, and a good shoulder peak suppression effect. Compared with the other four formulas, 10BSA_20Leu has the sharpest and most stable distribution, showing excellent humidity resistance and potential lung deposition efficiency.

From a horizontal comparison, the addition of leucine has a positive regulatory effect on distribution: the distribution of 10BSA_10Leu is more concentrated than that of BSA; and 10BSA_20Leu is superior to Tre and 10Leu alone in terms of distribution concentration and humidity resistance environmental. Previous studies have shown that pure trehalose tends to aggregate under high humidity conditions, so it is suspected that potential limitations of the analytical method may result in aggregates larger than 20 μm not being captured within the measurement range. Therefore, further optimization of the analytical method may be required to fully characterize the formulation under such conditions.

In summary, the higher the leucine content in the formula, the more the particles generated tend to be concentrated in the particle size range that can be deposited in the lungs, and the sensitivity to the operating environment is lower. The 10BSA_20Leu formulation shows the best performance. The results also showed that humidity was the main factor affecting particle size distribution, while the effect of pressure was generally small, but there were noteworthy exceptions in some formulations.

The 10Leu shows a more concentrated and sharp particle size distribution, which is more prominent under 50% RH conditions, showing its good powder consistency and structural stability. 10BSA_20Leu shows a more significant synergistic optimization effect compared to 10BSA_10Leu. And the 10BSA_20Leu not only significantly suppresses the large particle size shoulder peak generated when BSA is used alone but also improves the consistency of the overall particle size distribution and the stability of the main peak.

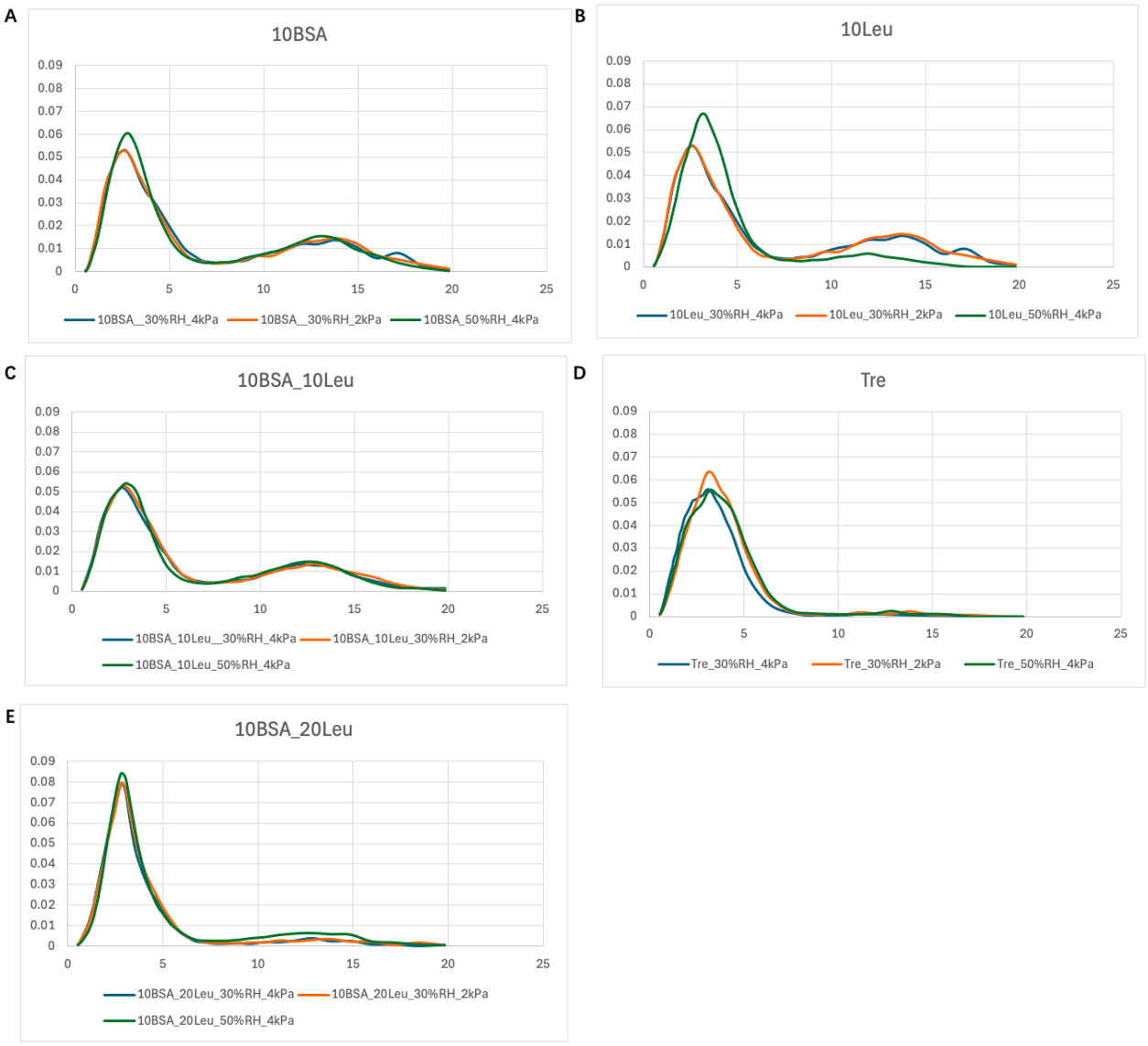

Figure 36: Normalized APS Particle Size Distribution (by Total Concentration) of aerodynamic diameters for different spray-dried powder formulations under varying relative humidity (RH) and drying pressure conditions. (A) 10BSA; (B) 10Leu; (C) 10BSA_10Leu; (D) Tre; (E) 10BSA_20Leu. The x-axis indicates aerodynamic diameter (μm), and the y-axis represents the relative proportion of particles in each size bin normalized to the total aerosol concentration measured by APS. Each subplot compares formulations processed at 30% or 50% RH under either 2 kPa or 4 kPa pressure. The differences in peak positions and distribution profiles reflect the impact of excipient composition and drying conditions on particle aerodynamic behavior and potential lung deposition performance.

3.2.7.3 Cumulative Particle Size Distribution: Performance of Different Formulations

The cumulative relative particle size distribution obtained from the APS measurements was analyzed and plotted. A comprehensive comparison was made for different formulations, suction pressure and relative humidity. Detailed distribution diagrams are given in Appendix 6.5.4.

Under 30% RH conditions (shown in Appendix 6.5.4.1), different pressures (2 kPa and 4 kPa) have different effects on the particle size distribution of each formula. In the 10Leu and Tre, the cumulative distribution curve under 4 kPa conditions is more to the left than that under 2 kPa, indicating that the particle size is relatively small, which may be related to the stronger a dispersion effect under higher pressure. For 10BSA, 10BSA_10Leu, and 10BSA_20Leu, the distribution curves under 2 kPa and 4 kPa conditions are almost the same, indicating that in these systems, pressure changes have little effect on particle formation and the particle size distribution is stable.

As shown in Appendix 6.5.4.2, a horizontal comparison between formulas under three typical conditions (30% RH_2kPa, 30% RH_4kPa, 50% RH_4kPa) found that the slope of the cumulative distribution curves of the 10BSA and 10BSA_10Leu formulations under all conditions was significantly slower, indicating that their particle size distribution is wider and may contain more large particles.

Under 4 kPa conditions (shown in Appendix 6.5.4.3), the effects of different relative humidity (30% RH and 50% RH) on the particle size distribution of each formula showed a differentiated trend. The cumulative distribution curves of 10Leu and 10BSA_20Leu at 30% RH shifted slightly to the left than 50% RH, indicating that the particle size was small, and the increase in humidity may cause the particles to aggregate, resulting in a larger particle size. The distribution curves of 10BSA, 10BSA_10Leu and Tre under different humidity conditions were highly overlapped, with only a slight shift in the local domain, indicating that humidity had little effect on these formulas and the system was less responsive to changes in external humidity.

3.2.8 Comparison Between Aerodynamic and Laser Diffraction Particle Sizing

The cumulative distributions of aerodynamic particle size (APS) of five different formulations at 30% RH and 4 kPa were compared with the laser diffraction particle size (Laser) measured in a liquid medium (lamp oil). This provided a further understanding of the differences in particle behavior in gas and liquid environments, as well as the effects of excipients on particle structure and dispersibility.

The particle size range obtained by laser diffraction is between 0-100 μm, while that of APS is 0-20 μm. Comparative data shows that except for the 10Leu and the Tre in APS, which have very few particles larger than 20 μm, all other particles are within this range. Therefore, the particle cumulative relative size distribution of APS and laser diffraction is only performed in the range of 0-20 μm. Detailed distribution diagrams are given in Figure 37.

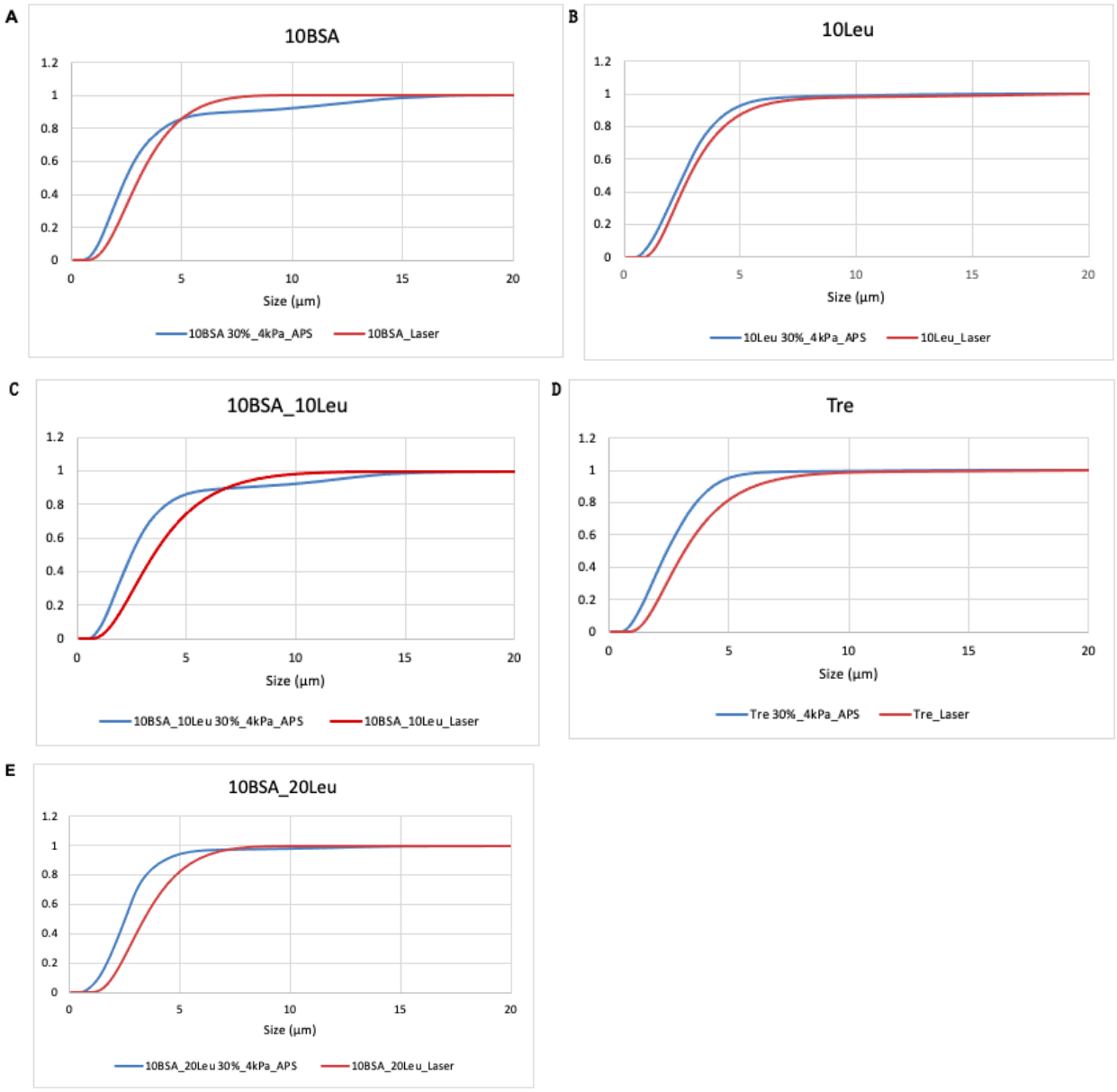

Figure 37: Normalized cumulative particle size distributions of five formulations between APS (blue) and laser diffraction in lamp oil (red). (A) 10BSA; (B) 10Leu; (C) 10BSA_10Leu; (D) Tre; (E) 10BSA_20Leu. The x-axis in the figure is the particle diameter (µm), and the y-axis is the normalized cumulative volume fraction (0–1), which indicates the proportion of particles below each particle size in the total particle volume.

Compared with Figure 37, the APS-measured particle size distribution curves (blue lines) of all formulations rise faster in the small particle size section, and the overall curve is biased to the left compared to the laser diffraction result, indicating that the particle size measured in the gas phase is smaller and the particle distribution is more concentrated; while the particle size measured by the laser diffraction method is generally larger, and the cumulative rise rate is slower. This phenomenon is consistent with the comparison results of the MMAD measured by APS and the d(0.5) value measured by laser diffraction.

APS directly reflects the particle size characteristics of the powder in the gas phase by analyzing the particles in the aerosol state; while the laser diffraction method evaluates the particle size distribution in the liquid phase (kerosene in this study). In order to achieve uniform dispersion of the powder in the liquid phase, this experiment used 20% w/w Span as a dispersant. However, during the data analysis process, it is speculated that the concentration of Span may be too high, causing the powder particles to absorb water and swell during the suspension process, thereby making the measured particle size larger.

Therefore, it is necessary to optimize the liquid phase dispersion method in future studies, especially the screening of dispersant types and dosages, to improve the accuracy and representativeness of laser diffraction measurements.

3.2.9 Comparison of APS and NGI Measurements

Looking back at the data in APS and NGI, it is found that the particle size parameters (such as MMAD, GSD, span) obtained by different analytical methods may be significantly different. This is due to the significant differences in the measurement principles and operation methods of the two methods. APS measures the response of a single particle to the time of passing through the laser beam, while NGI calculates the particle size based on the accumulation of mass, and the operating parameters of the two methods are different, such as sampling time, airflow rate, and pressure. This may cause differences in particle size parameters.

The maximum size range measured by APS is 19.81 μm, while the maximum size measured by NGI is 12.8 μm. In order to highlight the difference between the two measurement results, only particles with a size of 12.86 μm and below are included in the statistics in APS.

As shown in Figure 38, in the smaller particle size range, the cumulative mass fraction measured by NGI is generally higher than that of APS, suggesting that there may be a particle bounce effect. Specifically, the difference mainly appears in the particle size range of about 0–1.7 μm in the 10BSA formulation (Figure 38A); in the formulation with 10Leu, the range extends to 0–2.0 μm (Figure 38B); and in 10BSA_20Leu, it further expands to 0–2.4 μm (Figure 38C). This trend may indicate that as the amount of leucine added increases, the particles are more likely to bounce on the NGI impact plate.

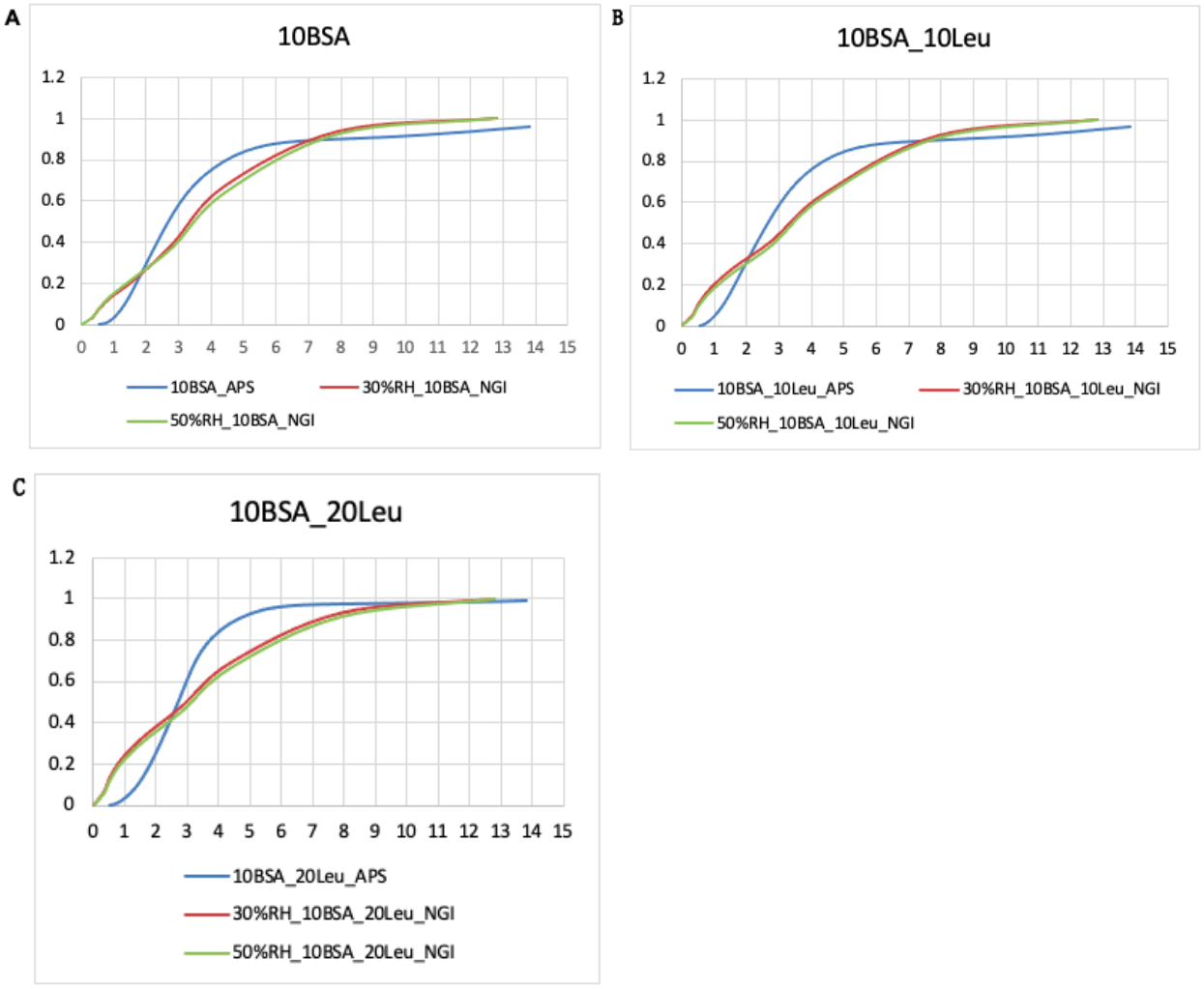

Figure 38: Comparison of the cumulative distribution of particle sizes of APS and NGI samples containing BSA under different humidity conditions. (A) 10BSA; (B) 10BSA_10Leu; (C) 10BSA_20Leu. The figures show the normalized cumulative distribution curves obtained by the aerodynamic particle spectrometer (APS) and the next generation impactor (NGI). The horizontal axis is the particle size (μm) and the vertical axis is the normalized cumulative mass fraction.

4 CONCLUSIONS

This study systematically investigated spray-dried powder formulation composed of bovine serum albumin (BSA), L-leucine (Leu) and trehalose dihydrate, aiming to develop a dry powder formulation for pulmonary inhalation with good aerodynamic properties and humidity resistance. Through preliminary formulation screening and process parameter optimization, the optimal spray conditions (inlet air temperature 120 °C, feed rate 1.7 mL/min, spray gas flow rate 2.3 m^3/h) were determined. Under these conditions, the remaining formulations were successfully produced with a median volume distribution particle size (d(0.5)) less than 3.5 μm and a yield higher than 75% (except for the pure trehalose), meeting basic spray drying particle size requirements for pulmonary delivery.

The experimental results showed that the aerodynamic particle size (MMAD) of all composite formulations was in the range of 2.3–3.4 μm, with a narrow particle size distribution and good deep lung deposition potential. The formulations containing only BSA tends to form wrinkled particle morphology, while the formulation with leucine added forms a characteristic "wrinkled shell" structure, indicating that leucine migrates to the surface of the droplets during the drying process and constructs a hydrophobic protective layer, thereby significantly improving the dispersibility and structural stability of the powder.

In terms of humidity resistance, the formulation with a high leucine content (especially 20%) shows the best anti-caking ability, and its effect is also significantly leucine content dependent. At 72% relative humidity, the pure trehalose group agglomerated significantly within 1 hour, while the 10Leu formulation still maintained a good powder state, indicating that leucine plays a key role in inhibiting hygroscopic agglomeration, which not only improves the dispersion performance, but also enhances the humidity resistance of the dry powder inhalation system.

A strong bounce-back phenomenon was also observed in the NGI experiment, suggesting that it may interfere with the particle deposition trajectory in the impactor. It should be pointed out that this phenomenon only occurs in experimental equipment and does not occur in the actual human respiratory tract. Therefore, this observation suggests that we need to further optimize the experimental design and measurement methods in subsequent studies to improve the representativeness and accuracy of the data. Comprehensively considering various performance indicators, the 10BSA_20Leu formulation performed the best in BSA-containing formulations and had an optimal size for inhalation. Under high humidity conditions, the formulation can still maintain excellent aerodynamic behavior, making it an ideal candidate for pulmonary delivery.

In summary, this study shows that leucine has multiple functions in the design of protein inhalation formulations: it can improve particle size control, enhance anti-hygroscopicity, and lead to optimized aerodynamic performance. However, its dosage needs to be reasonably regulated. Future studies can further explore the synergistic mechanism between leucine and other biomacromolecules or excipients and evaluate their actual impact on in vivo delivery efficiency and therapeutic efficacy.

5 REFERENCES

Alhajj, N., O'Reilly, N. J., & Cathcart, H. (2021). Designing enhanced spray dried particles for inhalation: A review of the impact of excipients and processing parameters on particle properties. Powder Technology, 384, 313–331. https://doi.org/10.1016/j.powtec.2021.02.03

Andrade, J.D., Flady, V., Wei, A-P. and Gölander, C-G. (1990) Croatica Chemica Acta, 63, 527-538.

B-290 Mini Spray Dryer Operation Manual. (2018). BÜCHI Labortechnik AG.

Chang, Y.-X., Yang, J.-J., Pan, R.-L., Chang, Q., & Liao, Y.-H. (2014). Anti-hygroscopic effect of leucine on spray-dried herbal extract powders. Powder Technology, 266, 388–395. https://doi.org/10.1016/j.powtec.2014.06.058

Chaurasiya, B., & Zhao, Y. Y. (2020). Dry Powder for Pulmonary Delivery: A Comprehensive Review. Pharmaceutics, 13(1), 31. https://doi.org/10.3390/pharmaceutics13010031

Crowder, T. M., Rosati, J. A., Schroeter, J. D., Hickey, A. J., & Martonen, T. B. (2002). Fundamentals of particle formulation for pulmonary delivery. Pharmaceutical Science & Technology Today, 5(7), 288–296. Pharmaceutical Research, 19(3), 239–245. https://doi.org/10.1023/A:1014426530935

Darder, M. L., Paz-González, A., García-Tomillo, A., Lado, M., & Wilson, M. G. (2021). Comparing multifractal characteristics of soil particle size distributions calculated by Mie and Fraunhofer models from laser diffraction measurements. Applied Mathematical Modelling, 94, 36–48. https://doi.org/10.1016/j.apm.2020.12.044

Douafer, H., Andrieu, V., & Brunel, J. M. (2020). Scope and limitations on aerosol drug delivery for the treatment of infectious respiratory diseases. Journal of Controlled Release, 325, 276–292. https://doi.org/10.1016/j.jconrel.2020.07.002

Garcia-Contreras, L., Ibrahim, M., & Verma, R. (2015). Inhalation drug delivery devices: Technology update. Medical Devices: Evidence and Research, 131. https://doi.org/10.2147/MDER.S48888

Gréhan, G., Gouesbet, G., Guilloteau, F., & Chevaillier, J. P. (1992). Comparison of the diffraction theory and the generalized Lorenz-Mie theory for a sphere arbitrarily located into a laser beam. Optics Communications, 90(1–3), 1–6. https://doi.org/10.1016/0030-4018(92)90315-I

Healy, A. M., McDonald, B. F., Tajber, L., & Corrigan, O. I. (2008). Characterisation of excipient-free nanoporous microparticles (NPMPs) of bendroflumethiazide. European Journal of Pharmaceutics and Biopharmaceutics, 69(3), 1182–1186. https://doi.org/10.1016/j.ejpb.2008.04.020

Khalili, N., Young, P. M., Traini, D., & Scalia, S. (2018). The effect of different coating materials on the prevention of powder bounce in the Next Generation Impactor. *International Journal of Pharmaceutics*, 548(1), 92–100. https://doi.org/10.1016/j.ijpharm.2018.06.008

Kousouli, E. M. (2024). Spray-dried powders for inhalation (Master's thesis). Faculty of Engineering, Department of Process and Life Science Engineering, Lund University.

Landström, K. (2000). Competitive protein adsorption during spray-drying [Doctoral dissertation, Lund University]. Lund University Publications. https://lup.lub.lu.se/search/publication/40637

Lechanteur, A., & Evrard, B. (2020). Influence of Composition and Spray-Drying Process Parameters on Carrier-Free DPI Properties and Behaviors in the Lung: A review. Pharmaceutics, 12(1). https://doi.org/10.3390/pharmaceutics12010055

Mensink, M. A., Frijlink, H. W., Van Der Voort Maarschalk, K., & Hinrichs, W. L. J. (2017). How sugars protect proteins in the solid state and during drying (review): Mechanisms of stabilization in relation to stress conditions. European Journal of Pharmaceutics and Biopharmaceutics, 114, 288–295. https://doi.org/10.1016/j.ejpb.2017.01.024

Mitchell, J. P., & Nagel, M. W. (2003). Cascade impactors for the size characterization of aerosols from medical inhalers: Their uses and limitations. Journal of Aerosol Medicine, 16(4), 341–377. https://doi.org/10.1089/089426803771771269

Moon, R., Johnston, L., Land-Hensdal, C. et al. Perspectives on cellulose nanofibril size measurement using scanning electron microscopy. Cellulose 32, 2793–2810 (2025). https://doi.org/10.1007/s10570-025-06458-2

Ordoubadi, M., Shepard, K. B., Wang, H., Wang, Z., Pluntze, A. M., Churchman, J. P., & Vehring, R. (2023). On the Physical Stability of Leucine-Containing Spray-Dried Powders for Respiratory Drug Delivery. Pharmaceutics, 15(2), 435. https://doi.org/10.3390/pharmaceutics15020435

Osman, A., Goehring, L., Patti, A., Stitt, H., & Shokri, N. (2017). Fundamental Investigation of the Drying of Solid Suspensions. Industrial & Engineering Chemistry Research, 56(37), 10506–10513. https://doi.org/10.1021/acs.iecr.7b02334

Patton, J. S., & Byron, P. R. (2007). Inhaling medicines: Delivering drugs to the body through the lungs. Nature Reviews Drug Discovery, 6(1), 67–74. https://doi.org/10.1038/nrd2153

Pilcer, G., & Amighi, K. (2010). Formulation strategy and use of excipients in pulmonary drug delivery. International Journal of Pharmaceutics, 392(1–2), 1–19. https://doi.org/10.1016/j.ijpharm.2010.03.017

Price, D. N., Kunda, N. K., & Muttil, P. (2019). Challenges Associated with the Pulmonary Delivery of Therapeutic Dry Powders for Preclinical Testing. KONA Powder and Particle Journal, 36(0), 129–144. https://doi.org/10.14356/kona.2019008

Shoyele, S. A., & Slowey, A. (2006). Prospects of formulating proteins/peptides as aerosols for pulmonary drug delivery. International Journal of Pharmaceutics, 314(1), 1–8. https://doi.org/10.1016/j.ijpharm.2006.02.014

Sosnik, A., & Seremeta, K. P. (2015). Advantages and challenges of the spray-drying technology for the production of pure drug particles and drug-loaded polymeric carriers. Advances in Colloid and Interface Science, 223, 40–54. https://doi.org/10.1016/j.cis.2015.05.003

Sou, T., Meeusen, E. N., De Veer, M., Morton, D. A. V., Kaminskas, L. M., & McIntosh, M. P. (2011). New developments in dry powder pulmonary vaccine delivery. Trends in Biotechnology, 29(4), 191–198. https://doi.org/10.1016/j.tibtech.2010.12.009

Stranzinger, S., Faulhammer, E., Li, J., Dong, R., Zeitler, J. A., Biserni, S., Calzolari, V., Khinast, J. G., & Markl, D. (2019). Predicting capsule fill weight from in-situ powder density measurements using terahertz reflection technology. International journal of pharmaceutics: X, 1, 100004. https://doi.org/10.1016/j.ijpx.2018.100004

Tan, C. P., & Nakajima, M. (2005). β-Carotene nanodispersions: Preparation, characterization and stability evaluation. Food Chemistry, 92(4), 661–671. https://doi.org/10.1016/j.foodchem.2004.08.044

Tsapis, N.; Bennett, D.; Jackson, B.; Weitz, D. A.; Edwards, D. A. Trojan particles: Large porous carries of nanoparticles for drug delivery Proc. Natl. Acad. Sci. U. S. A. 2002, 99, 12001– 12005 DOI: 10.1073/pnas.182233999

Wang, Z., Wang, H., & Vehring, R. (2021). Leucine enhances the dispersibility of trehalose-containing spray-dried powders on exposure to a high-humidity environment. *International journal of pharmaceutics*, *601*, 120561. https://doi.org/10.1016/j.ijpharm.2021.120561

Young, P. M., Sung, A., Traini, D., Kwok, P. C. L., & Chan, H.-K. (2007). Influence of humidity on the electrostatic charge and aerosol performance of dry powder inhaler carrier based systems. *Pharmaceutical Research*, 24(5), 963–970. https://doi.org/10.1007/s11095-006-9218-8

Yu, J., Wong, J., Ukkonen, A., & Chan, H.-K. (2017). Effect of relative humidity on bipolar electrostatic charge profiles of dry powder aerosols. *Pharmaceutical Research*, 34(8), 1646–1654. https://doi.org/10.1007/s11095-017-2160-5

Vehring, R. (2008). Pharmaceutical Particle Engineering via Spray Drying. Pharmaceutical Research, 25(5), 999–1022. https://doi.org/10.1007/s11095-007-9475-1

6 APPENDIX

6.1 Conversion tables for spray drying parameters

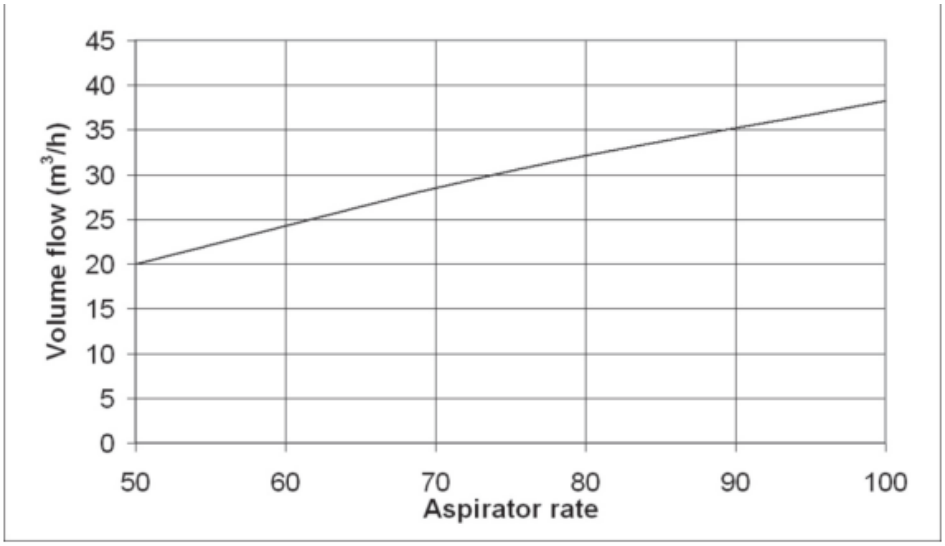

Figure 6.1: Aspirator settings (%) vs actual volumetric flow (m³/h) (B-290 Mini Spray Dryer Operation Manual, 2018).

6.2 Light Microscopy images in the pre-study

6.2.1 Spray-dried Trehalose dihydrate

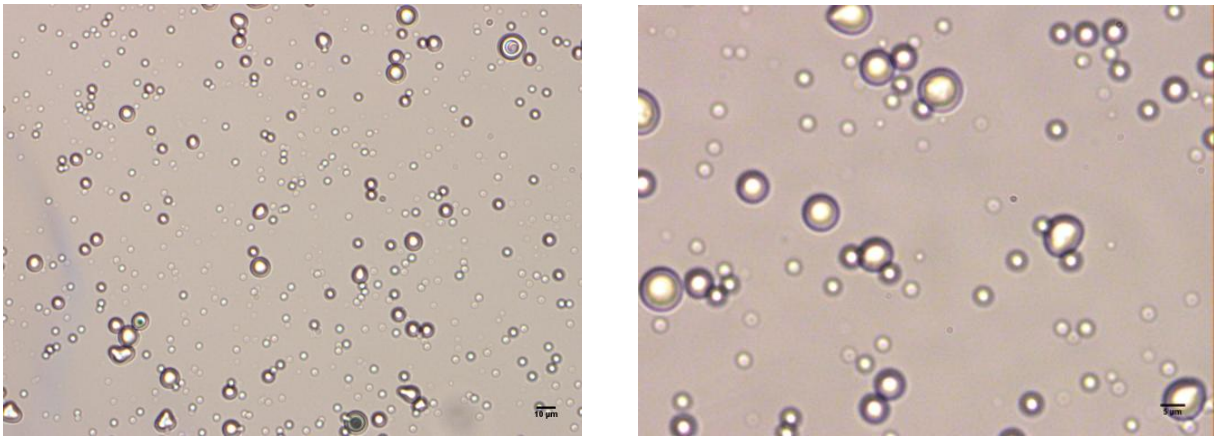

Figure 6.2.1.1: Light microscopy image of spray-dried Tre_01 at magnification x20 (left) and x50 (right).

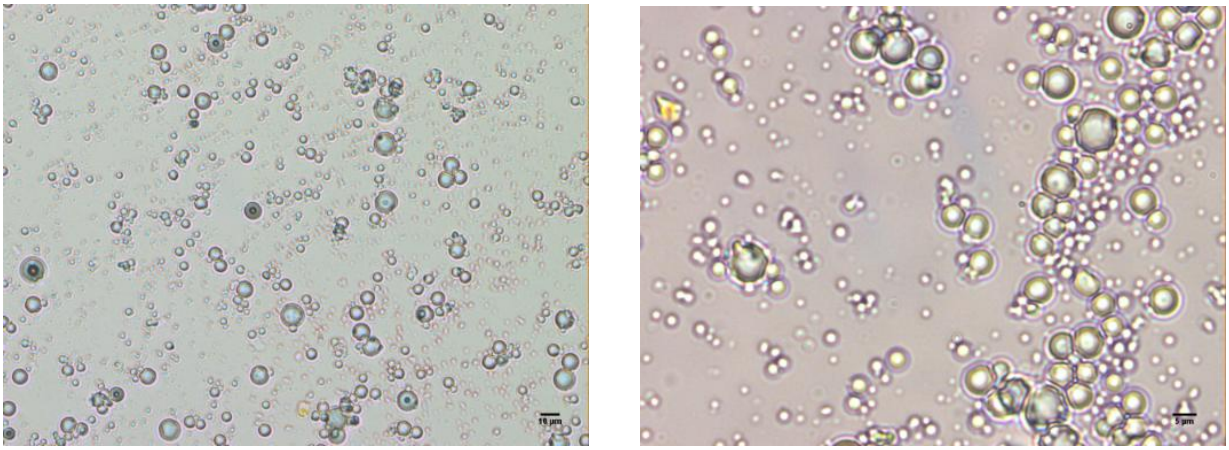

Figure 6.2.1.2: Light microscopy image of spray-dried Tre_02 at magnification x20 (left) and x50 (right).

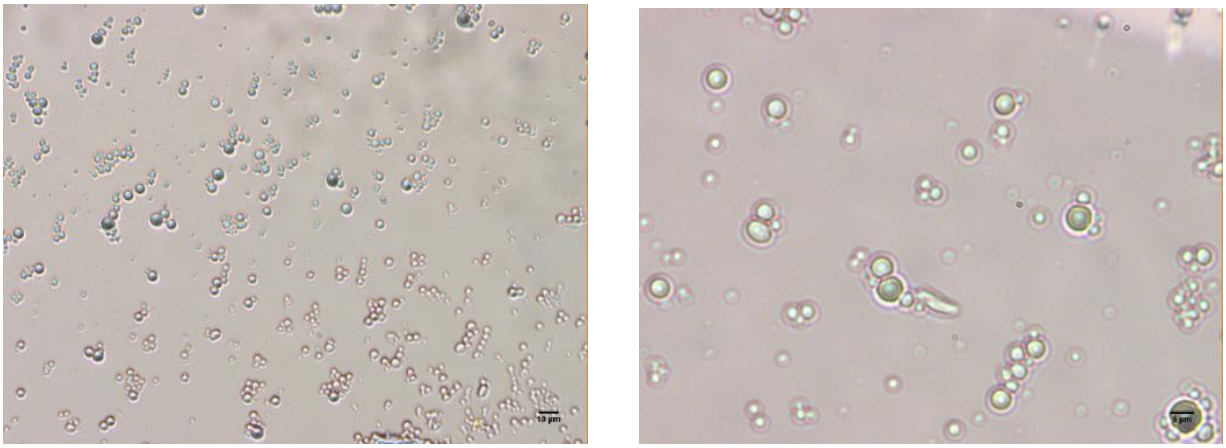

Figure 6.2.1.3: Light microscopy image of spray-dried Tre_03 at magnification x20 (left) and x50 (right).

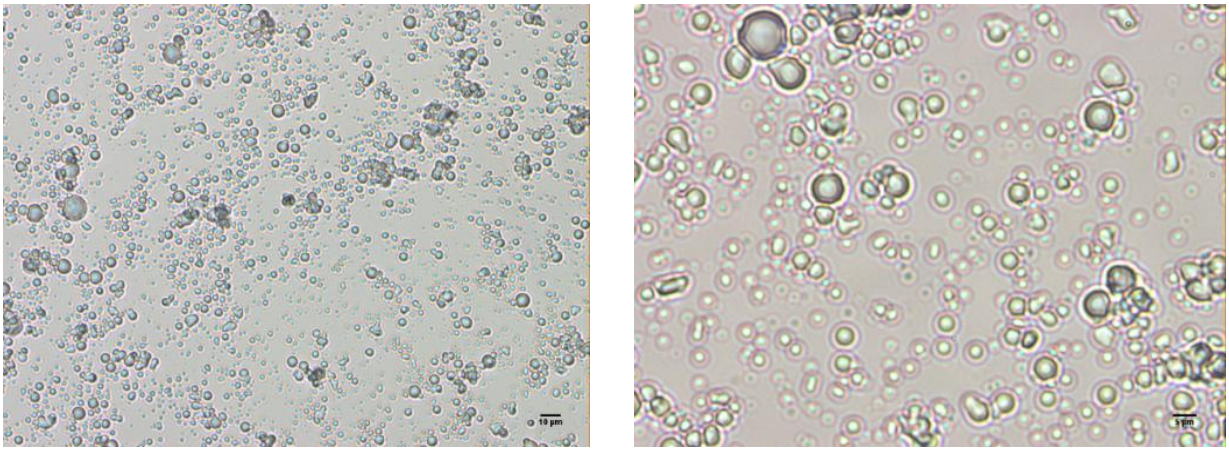

Figure 6.2.1.4: Light microscopy image of spray-dried Tre_04 at magnification x20 (left) and x50 (right).

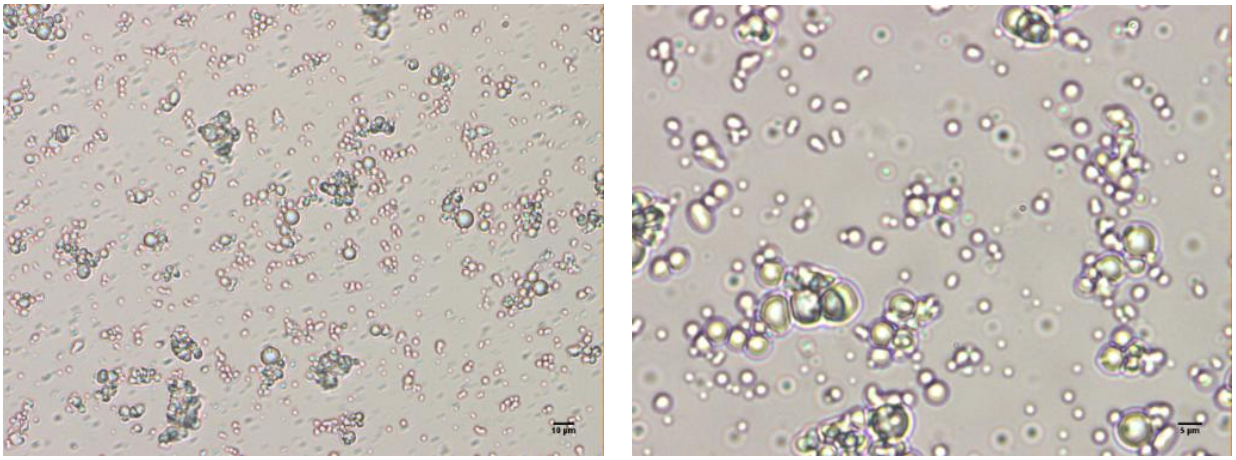

Figure 6.2.1.5: Light microscopy image of spray-dried Tre_05 at magnification x20 (left) and x50 (right).

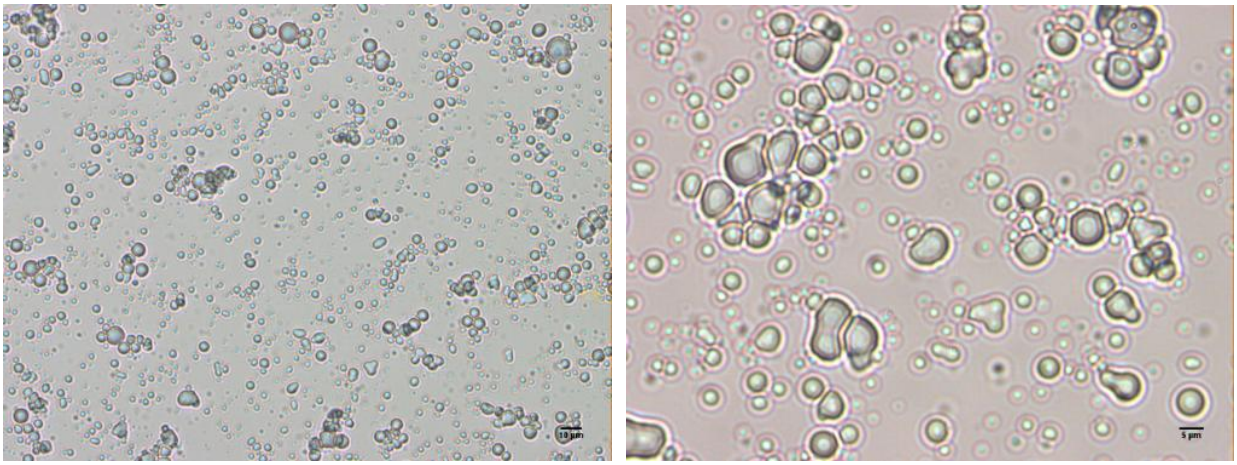

Figure 6.2.1.6: Light microscopy image of spray-dried Tre_06 at magnification x20 (left) and x50 (right).

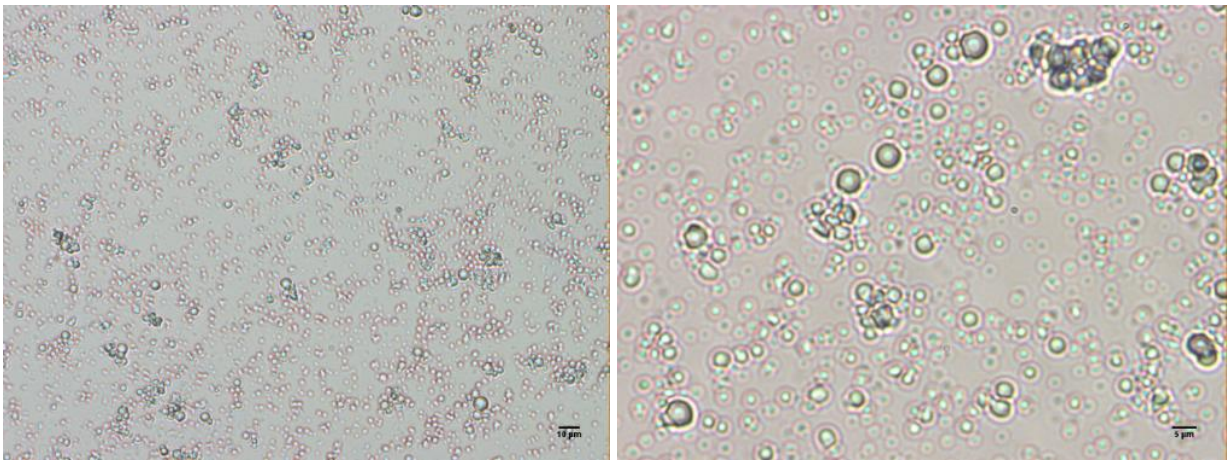

Figure 6.2.1.7: Light microscopy image of spray-dried Tre_07 at magnification x20 (left) and x50 (right).

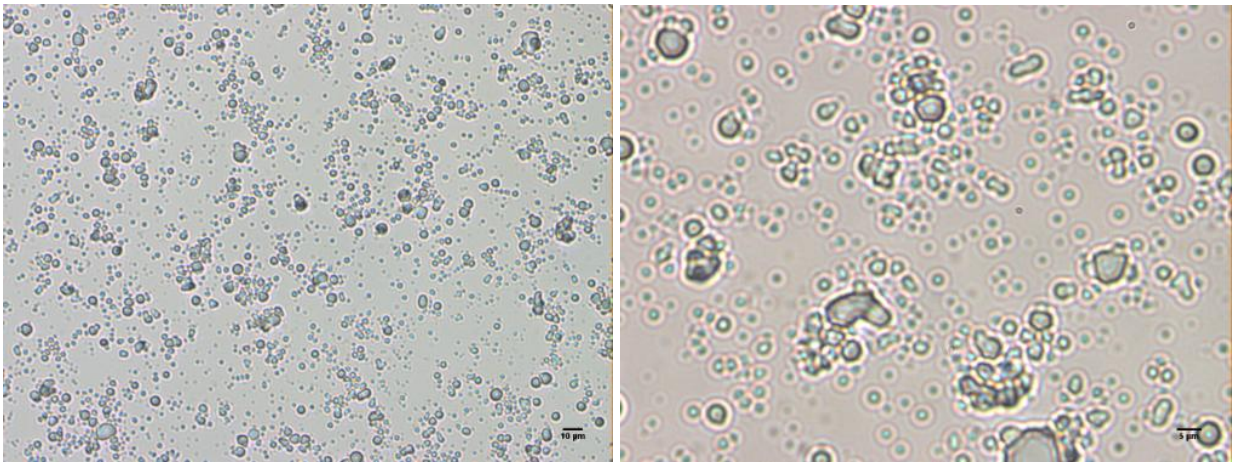

Figure 6.2.1.8 Light microscopy image of spray-dried Tre_08 at magnification x20 (left) and x50 (right).

6.2.2 Spray-dried L-leucine with Trehalose Dihydrate

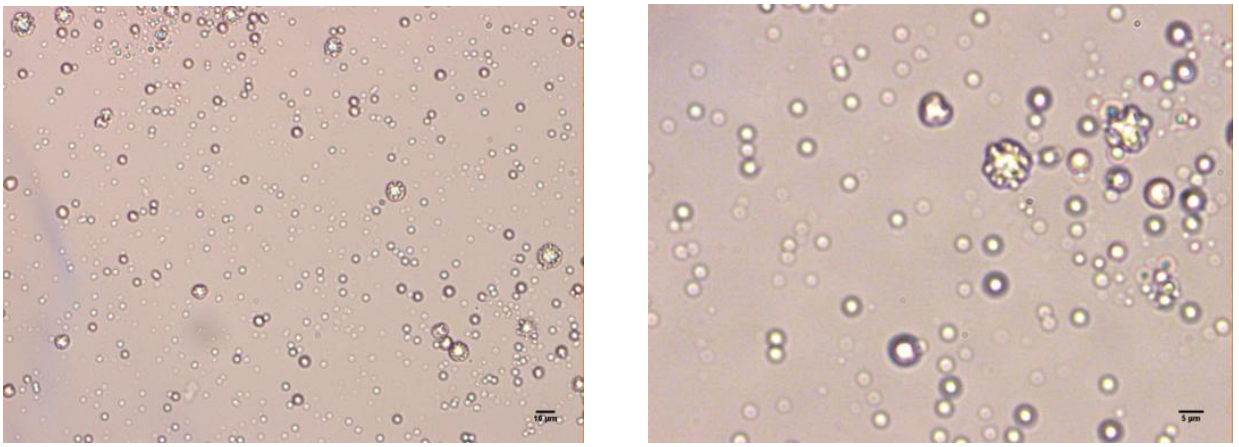

Figure 6.2.2.1: Light microscopy image of spray-dried 10Leu_01 at magnification x20 (left) and x50 (right).

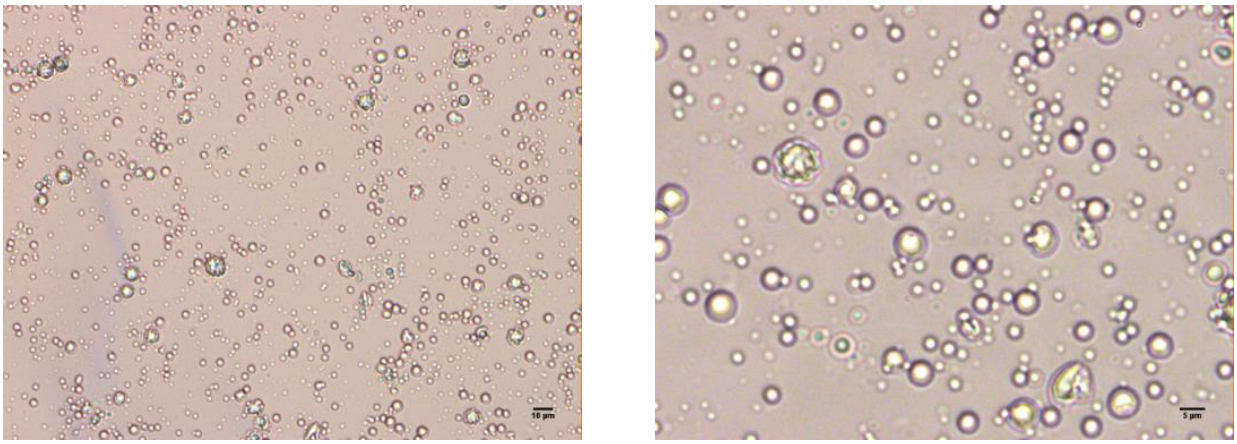

Figure 6.2.2.2: Light microscopy image of spray-dried 10Leu_02 at magnification x20 (left) and x50 (right).

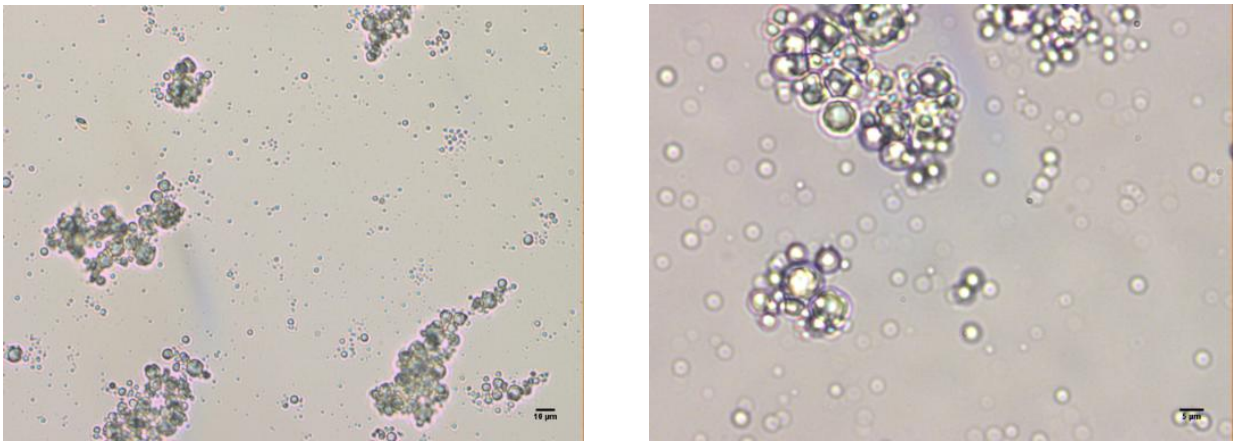

Figure 6.2.2.3: Light microscopy image of spray-dried 10Leu_03 at magnification x20 (left) and x50 (right).

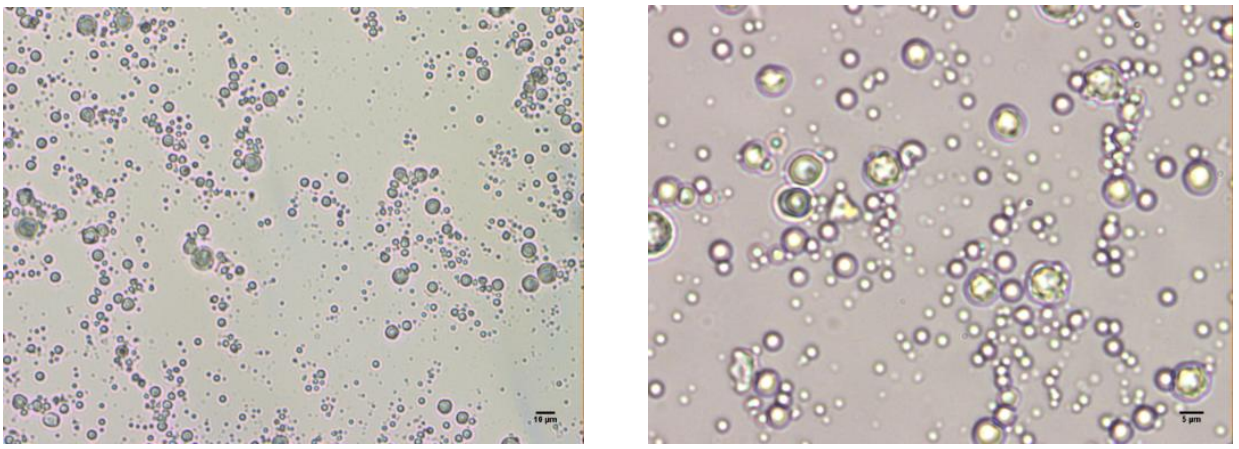

Figure 6.2.2.4: Light microscopy image of spray-dried 10Leu_04 at magnification x20 (left) and x50 (right).

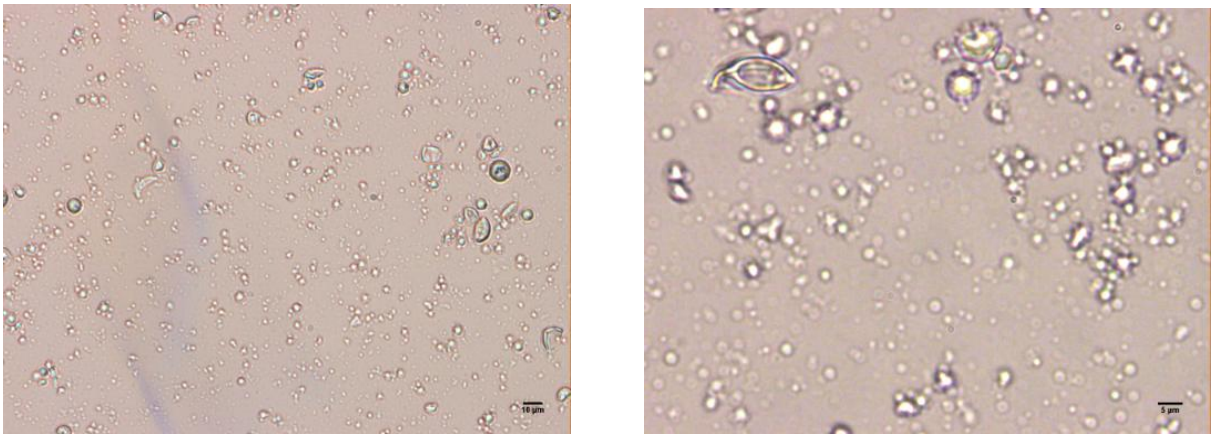

Figure 6.2.2.5: Light microscopy image of spray-dried 20Leu_01 at magnification x20 (left) and x50 (right).

6.2.3 Spray-dried BSA with Trehalose Dihydrate

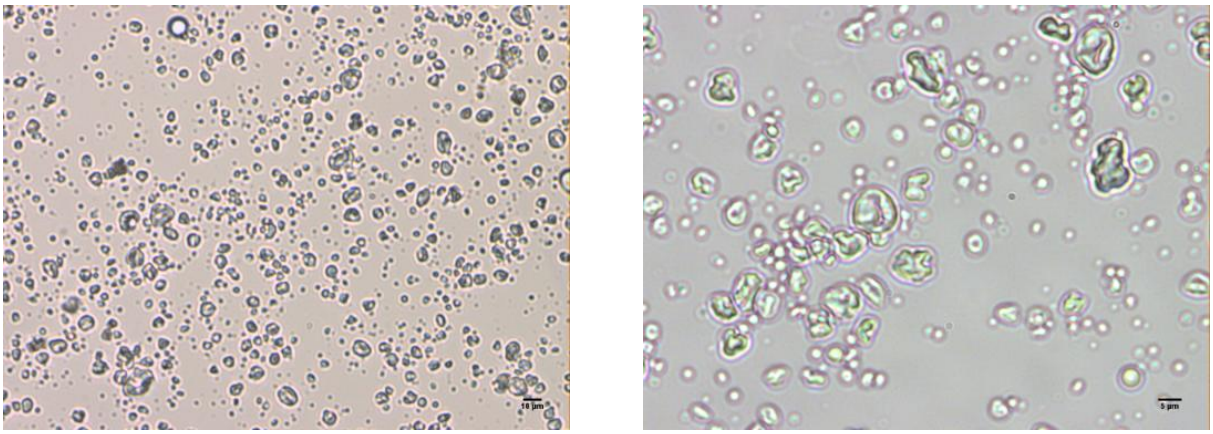

Figure 6.2.3.1: Light microscopy image of spray-dried 10BSA_01 at magnification x20 (left) and x50 (right).

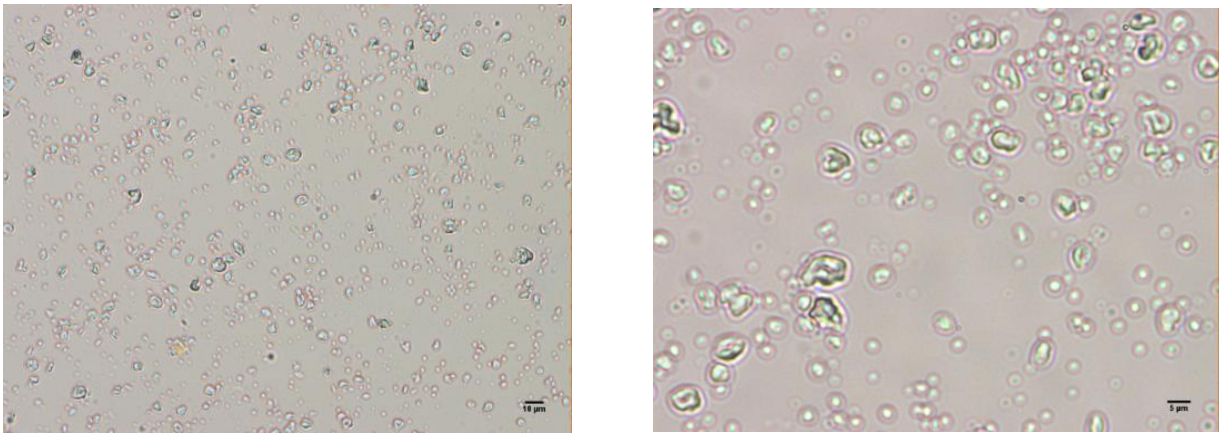

Figure 6.2.3.2: Light microscopy image of spray-dried 10BSA_02 at magnification x20 (left) and x50 (right).

6.2.4 Spray-dried BSA, L-leucine with Trehalose Dihydrate

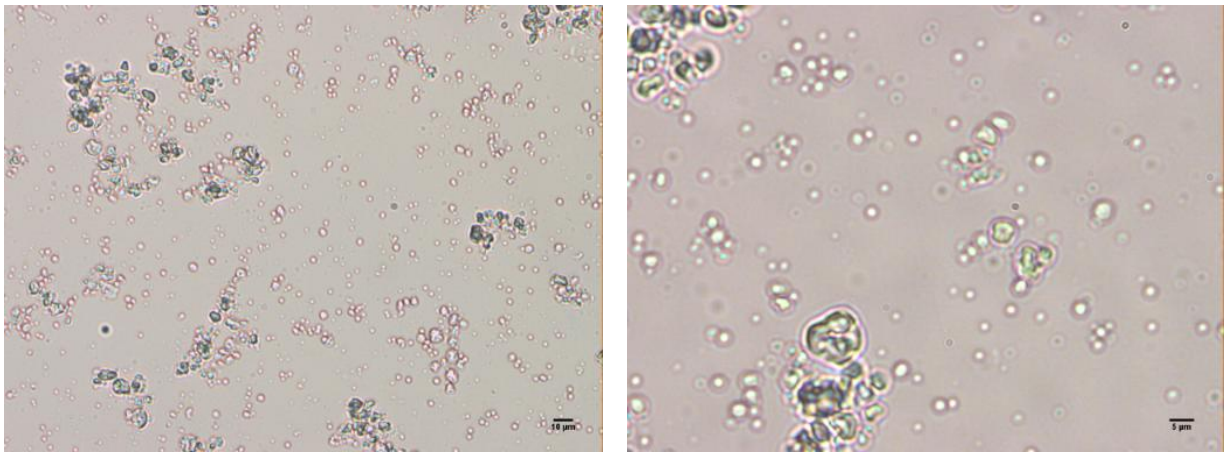

Figure 6.2.4.1: Light microscopy image of spray-dried 10BSA_10Leu_01 at magnification x20 (left) and x50 (right).

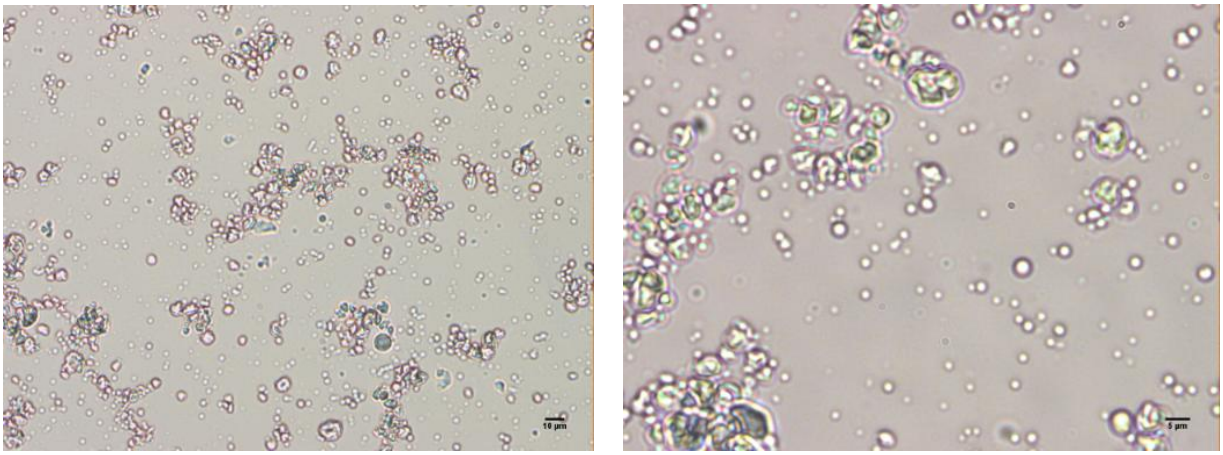

Figure 6.2.4.2: Light microscopy image of spray-dried 10BSA_10Leu_02 at magnification x20 (left) and x50 (right).

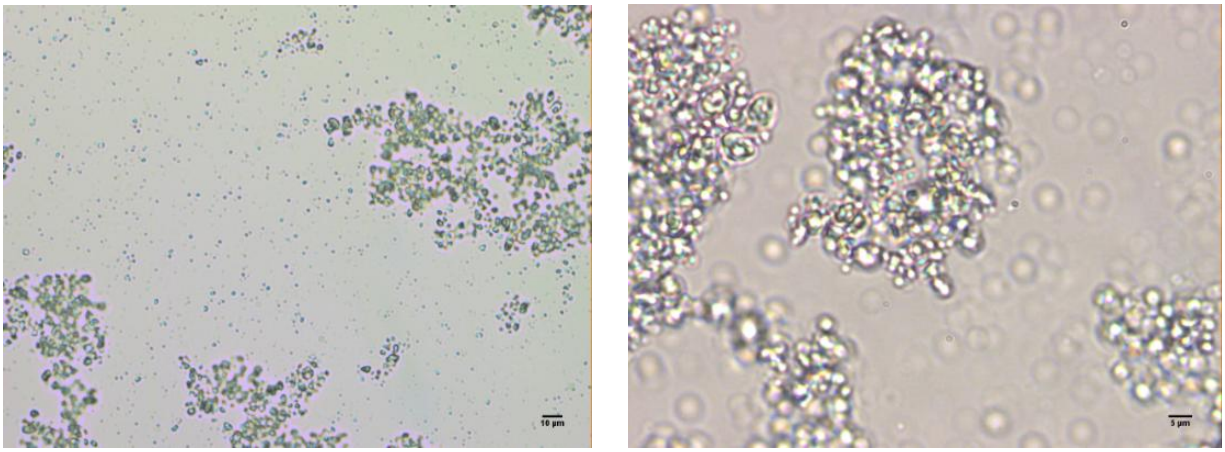

Figure 6.2.4.3: Light microscopy image of spray-dried 10BSA_10Leu_03 at magnification x20 (left) and x50 (right).

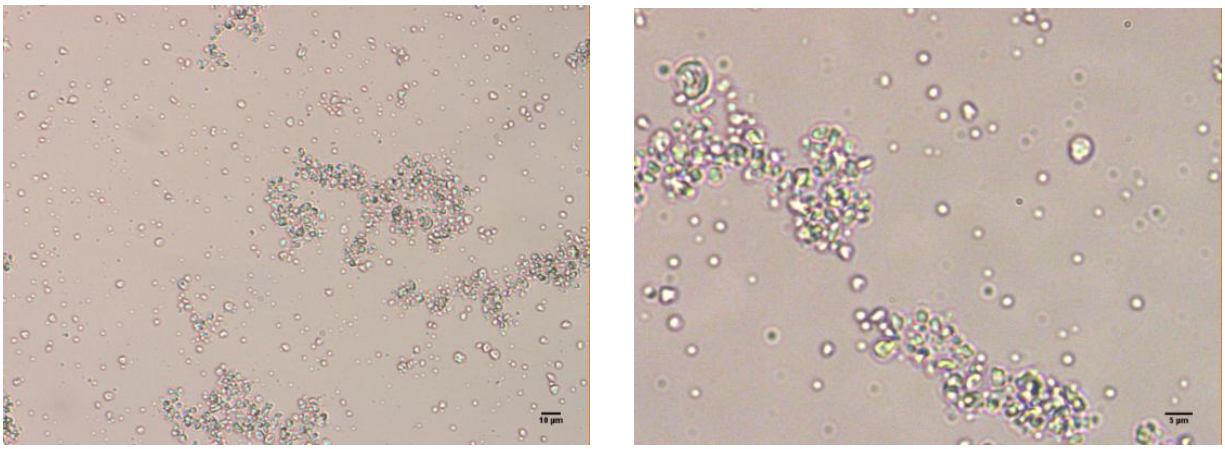

Figure 6.2.4.4: Light microscopy image of spray-dried 10BSA_10Leu_04 at magnification x20 (left) and x50 (right).

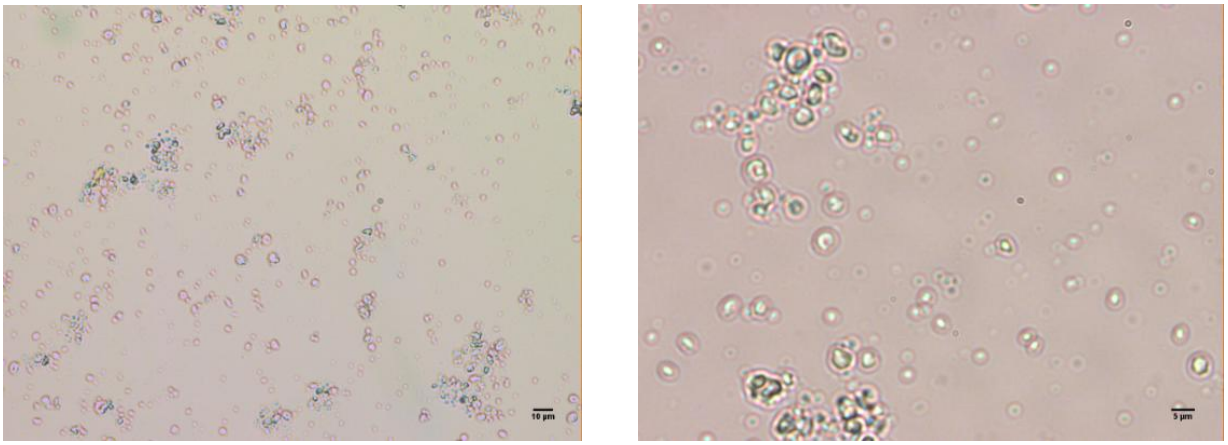

Figure 6.2.4.5: Light microscopy image of spray-dried 10BSA_10Leu_05 at magnification x20 (left) and x50 (right).

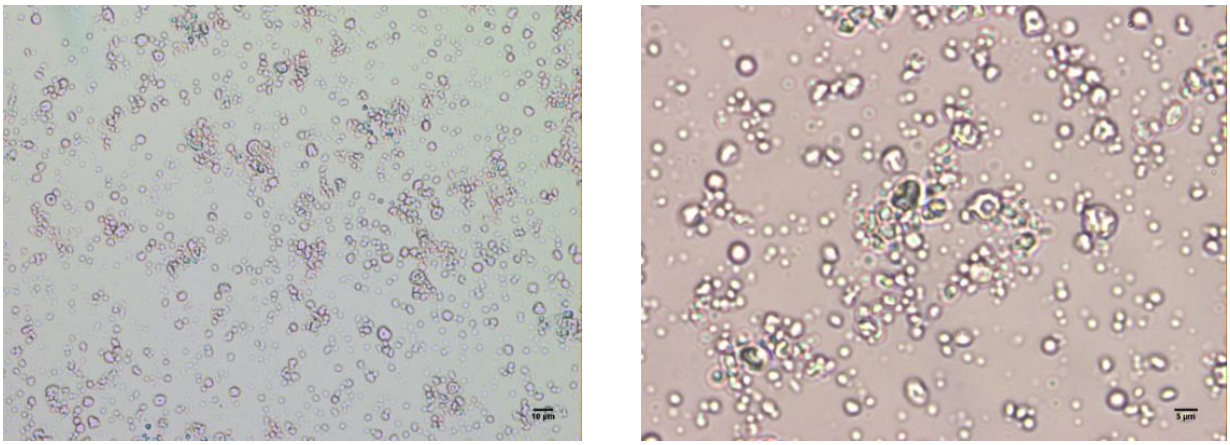

Figure 6.2.4.6: Light microscopy image of spray-dried 10BSA_10Leu_06 at magnification x20 (left) and x50 (right).

6.3 Laser diffraction results in the pre-study

6.3.1 Spray-dried Trehalose dihydrate

Table 6.3.1 Laser diffraction results of Spray-dried Trehalose dihydrate in the pre-study.

Batch	d(0.1) µm	d(0.5) µm	d(0.9) µm	span
Tre_01	1.8	4.8	11.8	2.1
Tre_02	1.7	3.8	8.9	1.9
Tre_03	1.7	3.2	6.3	1.4
Tre_04	1.9	3.5	6.6	1.3
Tre_05	1.9	3.7	7.5	1.5
Tre_06	2.0	3.8	7.1	1.4
Tre_07	1.7	2.9	4.7	1.0
Tre_08	1.8	3.2	5.5	1.2

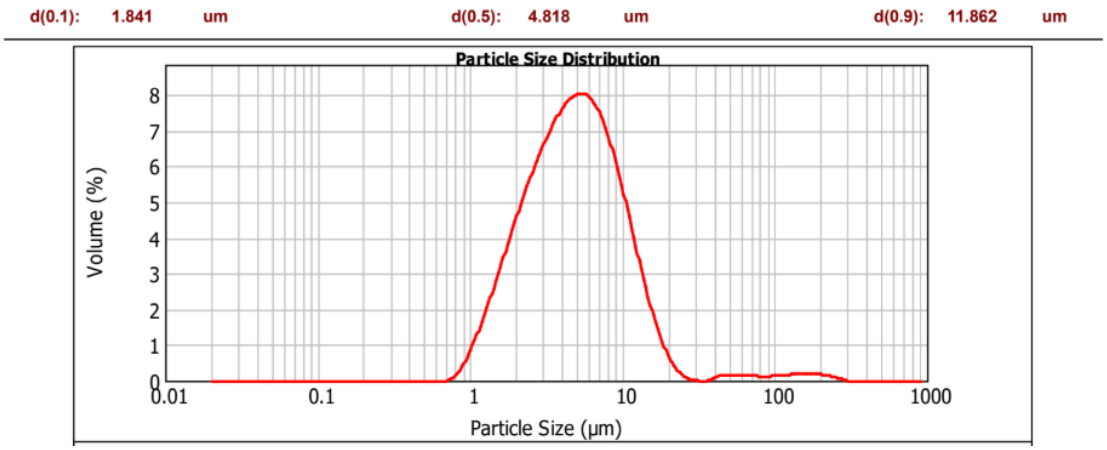

Figure 6.3.1.1: Particle size distribution of sample Tre_01 (Fraunhofer theory).

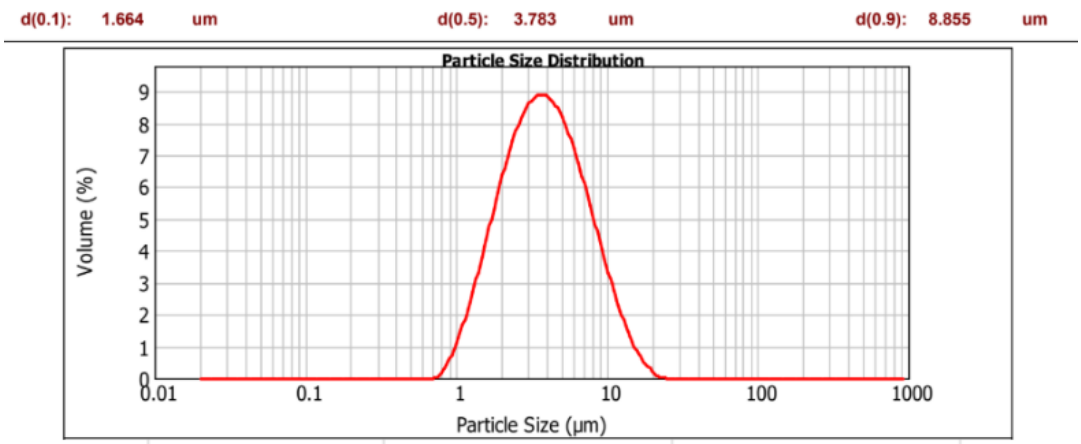

Figure 6.3.1.2: Particle size distribution of sample Tre_02 (Fraunhofer theory).

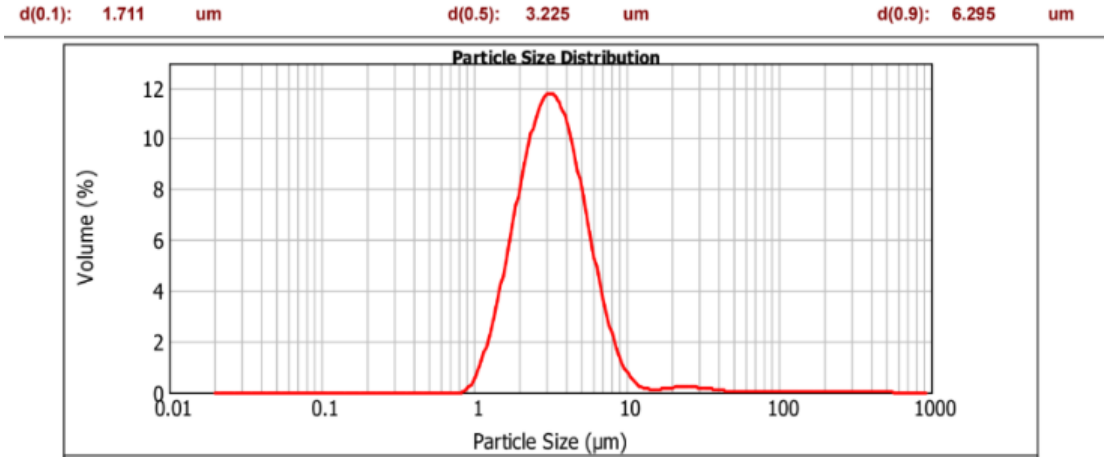

Figure 6.3.1.3: Particle size distribution of sample Tre_03 (Fraunhofer theory).

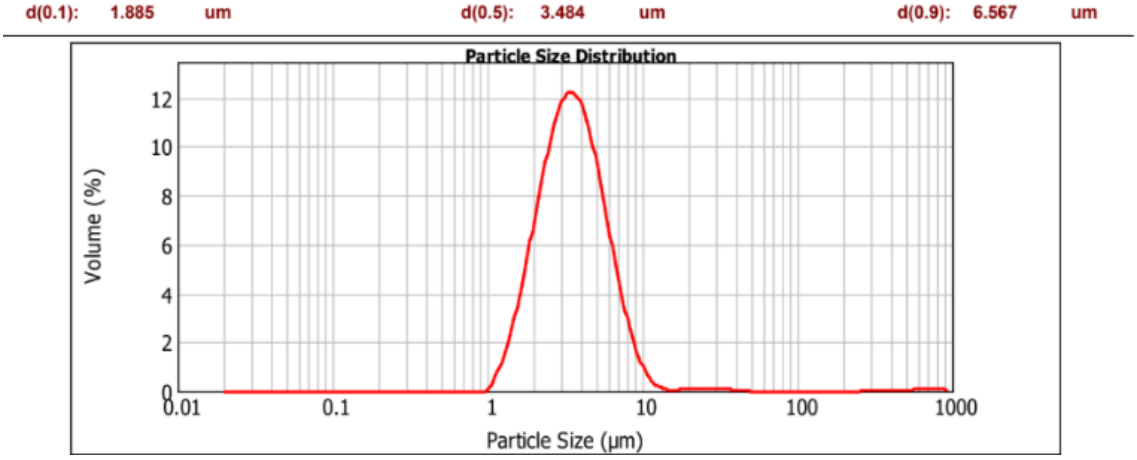

Figure 6.3.1.4: Particle size distribution of sample Tre_04 (Fraunhofer theory).

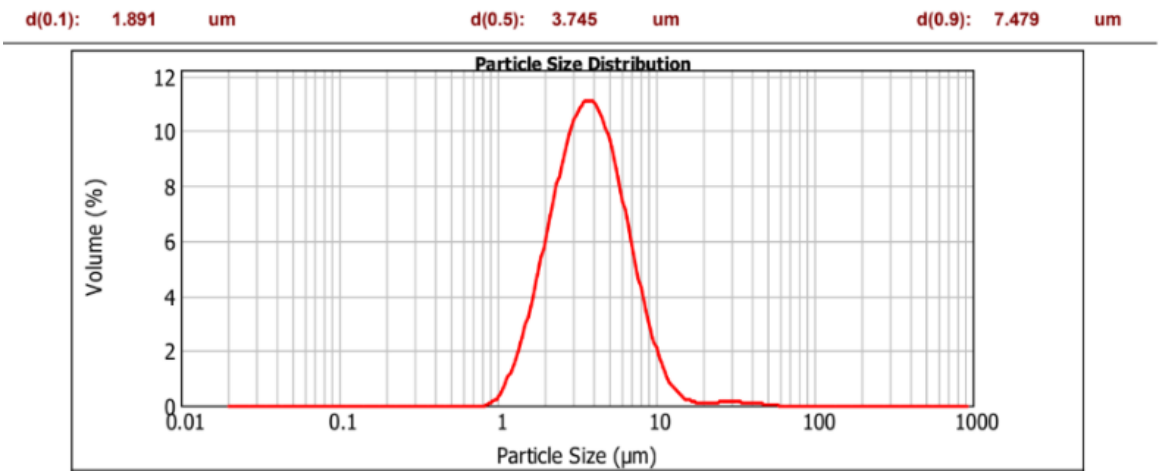

Figure 6.3.1.5: Particle size distribution of sample Tre_05 (Fraunhofer theory).

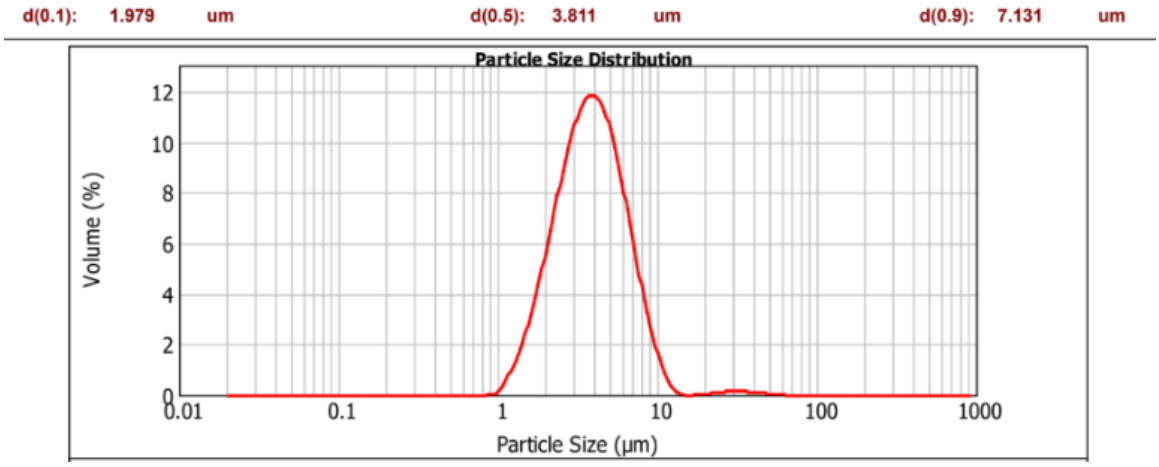

Figure 6.3.1.6: Particle size distribution of sample Tre_06 (Fraunhofer theory).

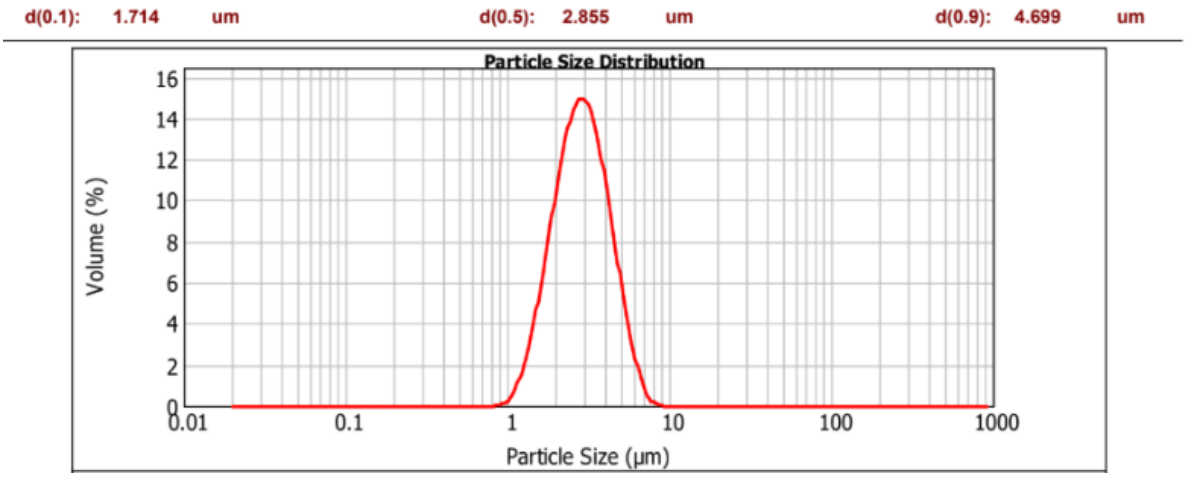

Figure 6.3.1.7: Particle size distribution of sample Tre_07 (Fraunhofer theory).

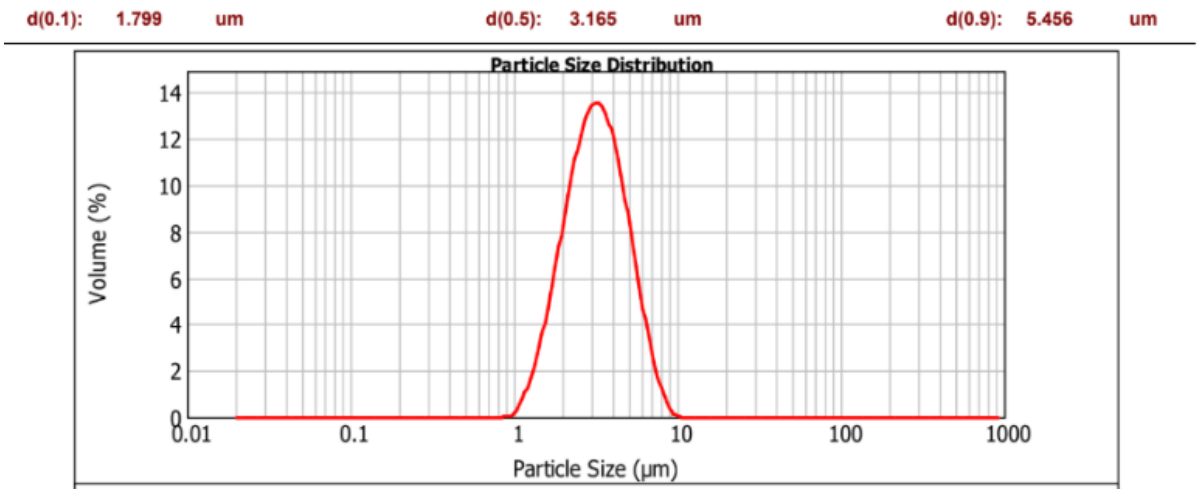

Figure 6.3.1.8: Particle size distribution of sample Tre_08 (Fraunhofer theory).

6.3.2 Spray-dried L-leucine with Trehalose Dihydrate

Table 6.3.2 Laser diffraction results of Spray-dried L-leucine with Trehalose Dihydrate in the pre-study.

Batch	d(0.1) µm	d(0.5) µm	d(0.9) µm	span
10Leu_01	1.9	4.8	11.9	2.1
10Leu_02	1.9	4.3	10.1	1.9
10Leu_03	1.8	4.3	11.4	2.2
10Leu_04	1.7	3.5	8.1	1.8
20Leu_01	2.2	4.9	10.7	1.7

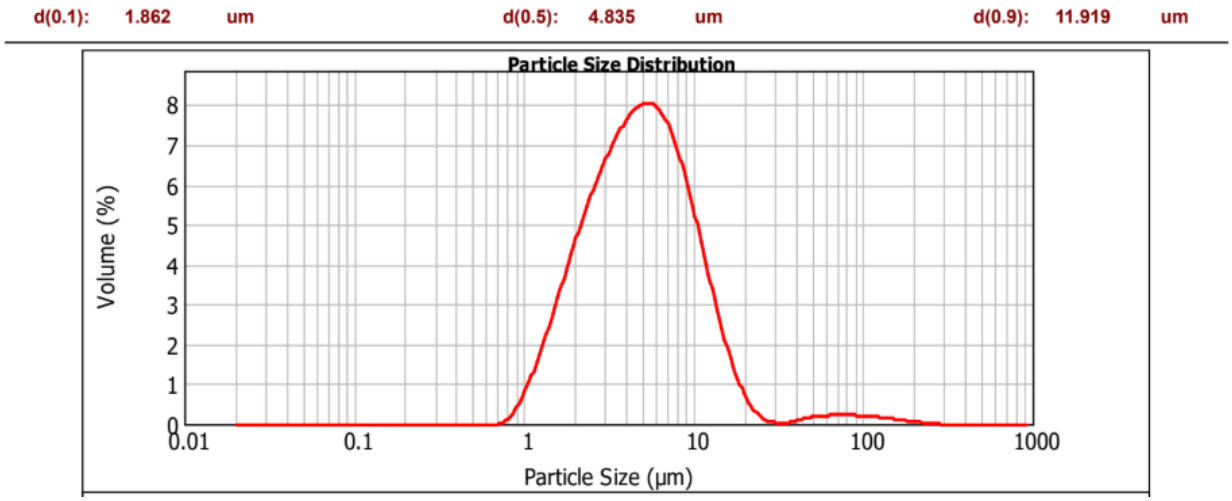

Figure 6.3.2.1: Particle size distribution of sample 10Leu_01 (Fraunhofer theory).

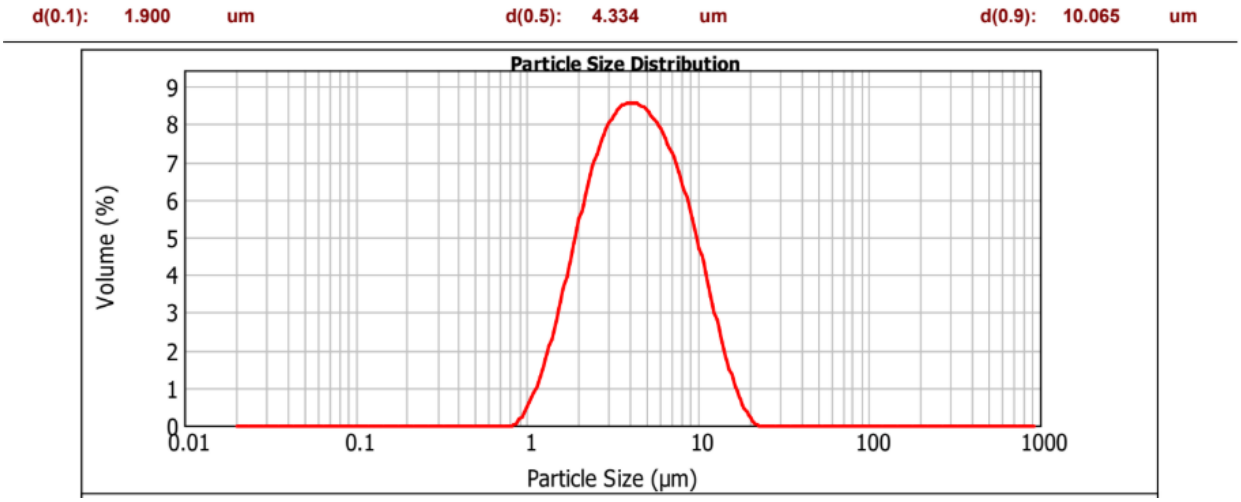

Figure 6.3.2.2: Particle size distribution of sample 10Leu_02 (Fraunhofer theory).

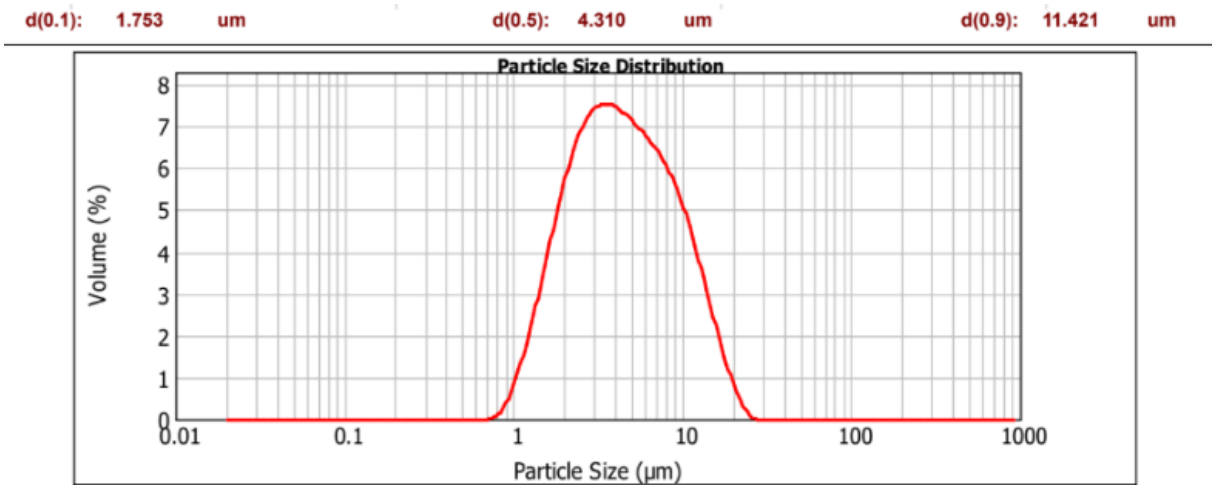

Figure 6.3.2.3: Particle size distribution of sample 10Leu_03 (Fraunhofer theory).

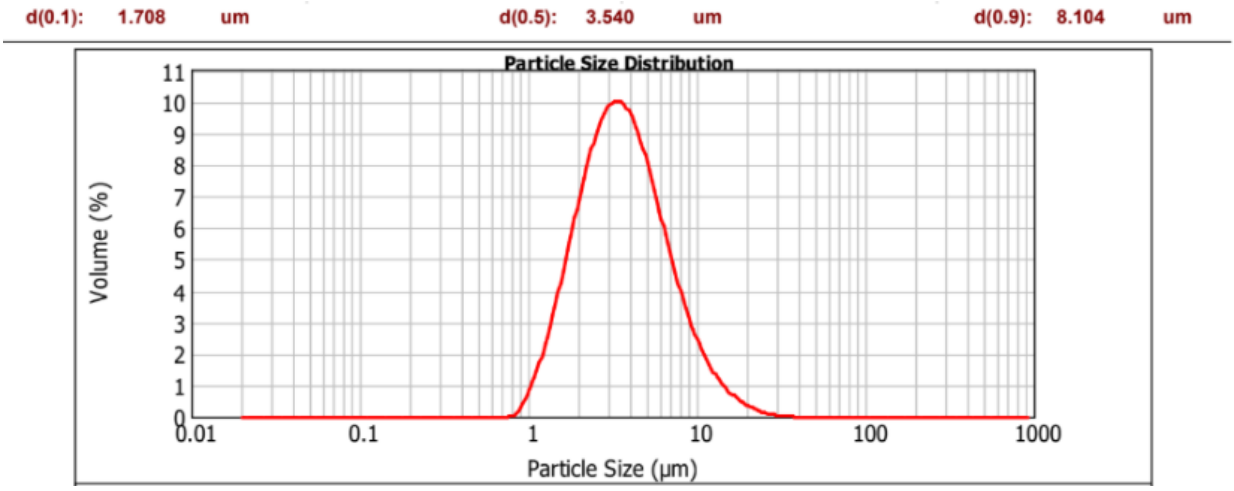

Figure 6.3.2.4: Particle size distribution of sample 10Leu_04 (Fraunhofer theory).

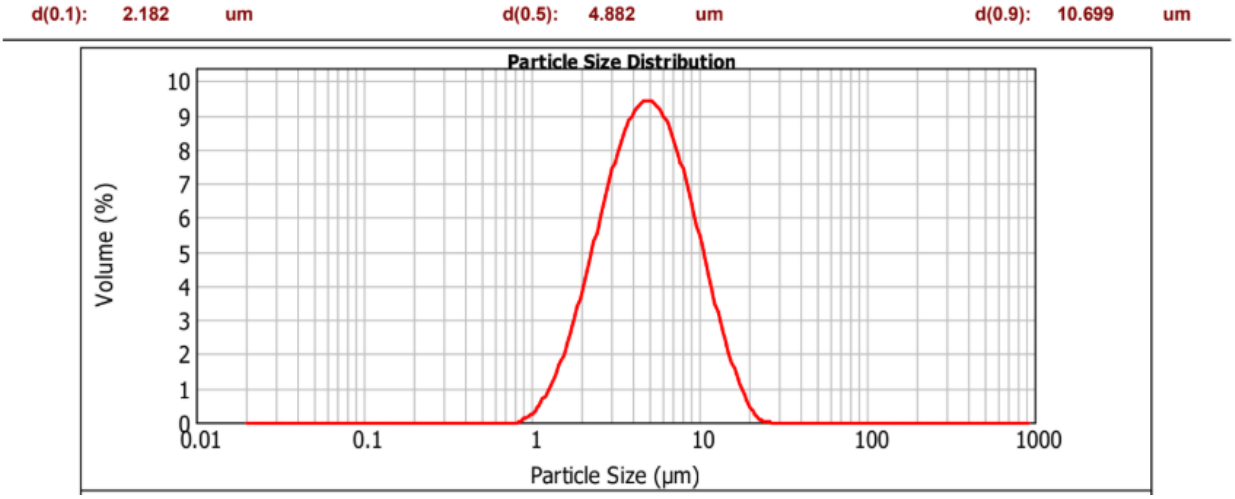

Figure 6.3.2.5: Particle size distribution of sample 20Leu_01 (Fraunhofer theory).

6.3.3 Spray-dried BSA with Trehalose Dihydrate

Table 6.3.3 Laser diffraction results of Spray-dried BSA with Trehalose Dihydrate in the pre-study.

Batch	d(0.1) µm	d(0.5) µm	d(0.9) µm	span
10BSA_01	2.0	4.6	9.4	1.6
10BSA_02	2.0	4.6	9.3	1.6

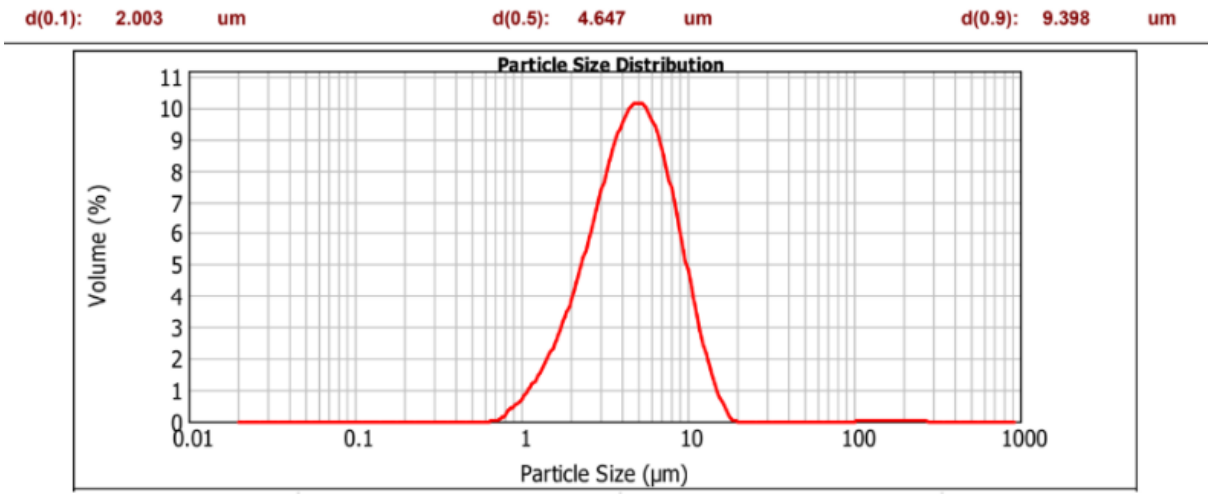

Figure 6.3.3.1: Particle size distribution of sample 10BSA_01 (Fraunhofer theory).

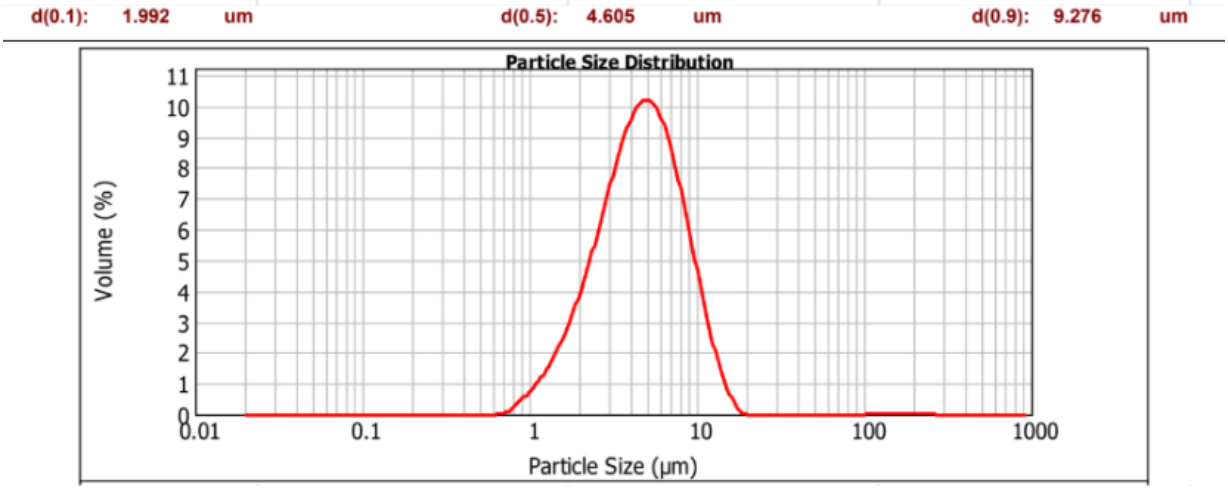

Figure 6.3.3.2: Particle size distribution of sample 10BSA_02 (Fraunhofer theory).

6.3.4 Spray-dried BSA, L-leucine with Trehalose Dihydrate

Table 6.3.4 Laser diffraction results of Spray-dried BSA, L-leucine with Trehalose Dihydrate in the pre-study.

Batch	d(0.1) µm	d(0.5) µm	d(0.9) µm	span
10BSA_10Leu_01	2.1	4.8	9.7	1.6
10BSA_10Leu_02	2.0	4.8	9.7	1.6
10BSA_10Leu_03	1.7	3.9	7.7	1.5
10BSA_10Leu_04	1.6	3.5	7.1	1.6
10BSA_10Leu_05	1.8	3.5	6.3	1.3
10BSA_10Leu_06	1.7	3.5	6.7	1.4

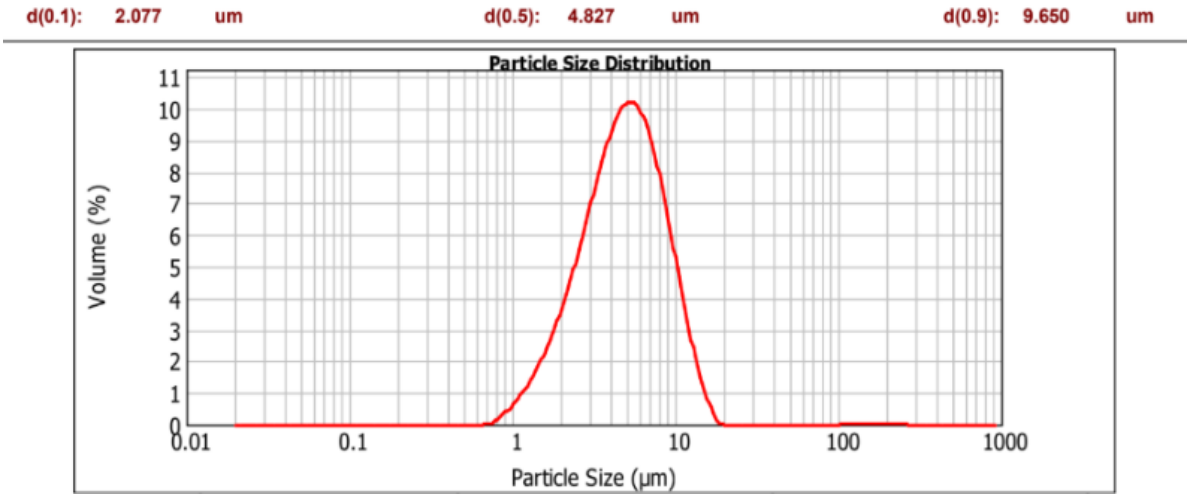

Figure 6.3.4.1: Particle size distribution of sample 10BSA_10Leu_01 (Fraunhofer theory).

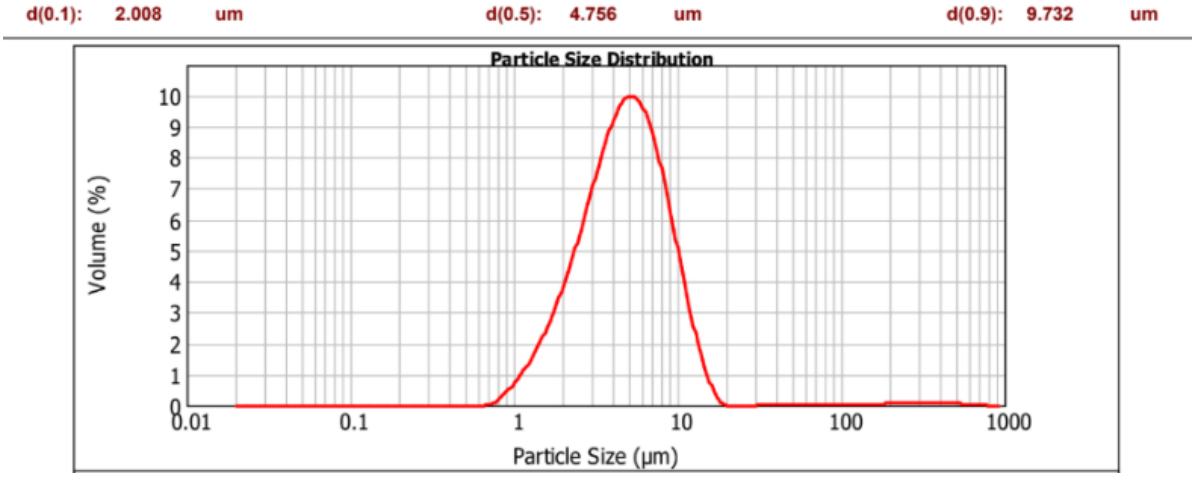

Figure 6.3.4.2: Particle size distribution of sample 10BSA_10Leu_02 (Fraunhofer theory).

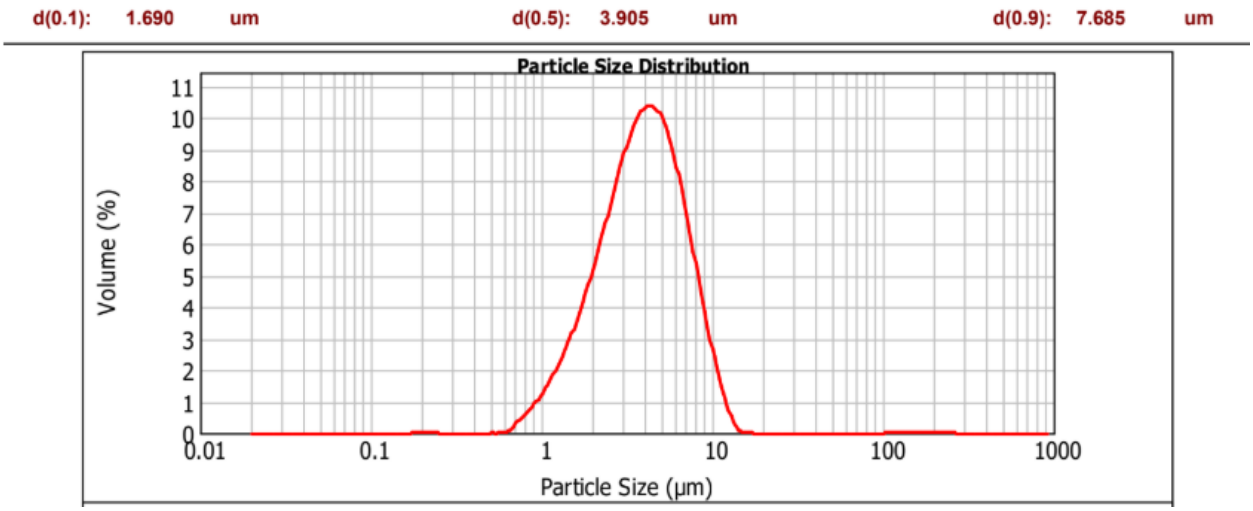

Figure 6.3.4.3: Particle size distribution of sample 10BSA_10Leu_03 (Fraunhofer theory).

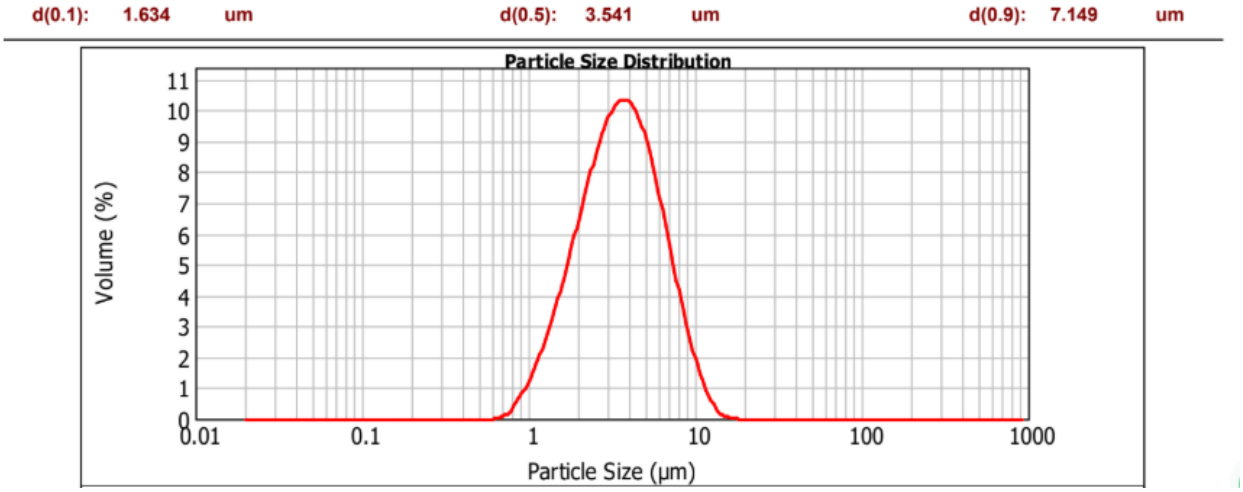

Figure 6.3.4.4: Particle size distribution of sample 10BSA_10Leu_04 (Fraunhofer theory).

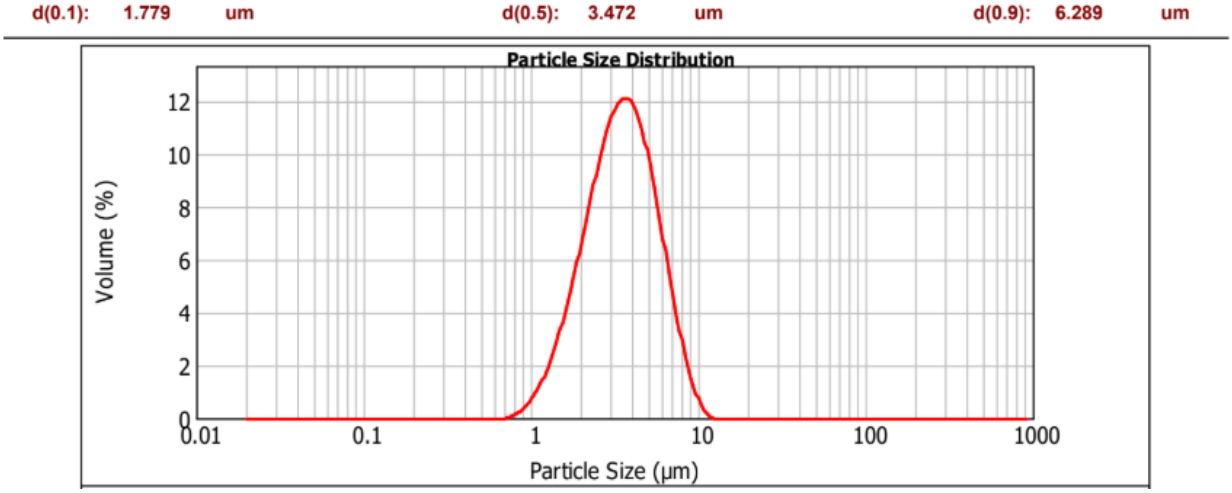

Figure 6.3.4.5: Particle size distribution of sample 10BSA_10Leu_05 (Fraunhofer theory).

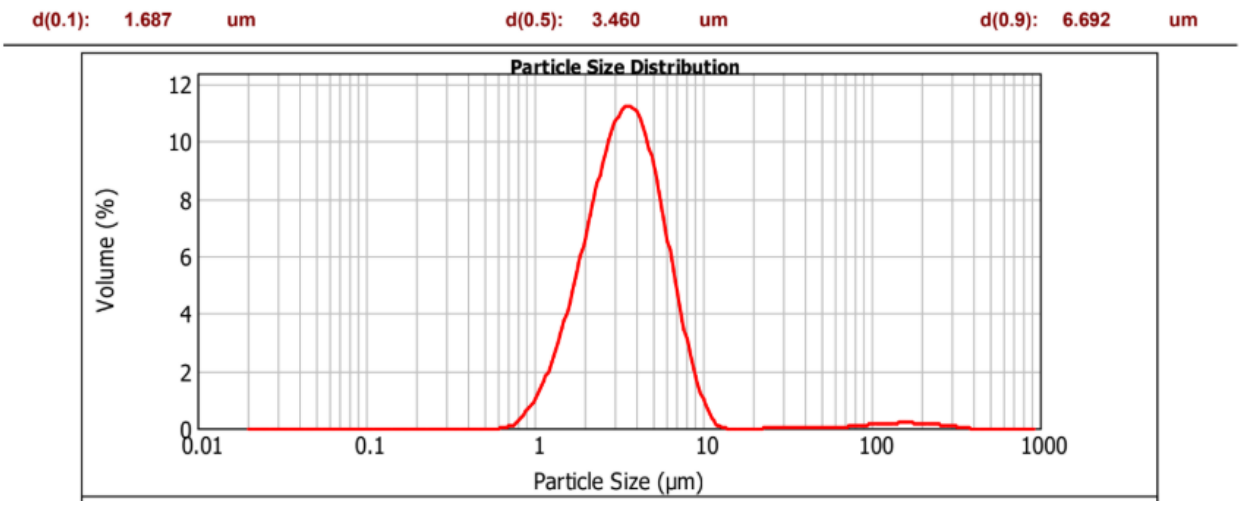

Figure 6.3.4.6: Particle size distribution of sample 10BSA_10Leu_06 (Fraunhofer theory).

6.4 NGI Graphs

6.4.1 Weight of Powder Loaded into Capsules for NGI Measurements

Formulation	2 capsules	Group 1(mg)	Group 2(mg)	Group 3(mg)	Averageg (mg)
10BSA_30%RH	Capsule 1	23.2	22.3	23.9	23.2
	Capsule 2	23.8	23.3	22.7	
10BSA_10Leu_30%RH	Capsule 1	19.2	23.3	22.2	22.2
	Capsule 2	22.8	21.2	24.5	
10BSA_20Leu_30%RH	Capsule 1	23	23.2	24.9	23.35
	Capsule 2	23.9	20.8	24.3	
10BSA_50%RH	Capsule 1	22.7	22.7	21	21.85
	Capsule 2	21	21.4	22.3	
10BSA_10Leu_50%RH	Capsule 1	20.2	21.9	23.7	22.85
	Capsule 2	23.8	23.5	24	
10BSA_20Leu_50%RH	Capsule 1	24.7	23.9	23.5	23.45
	Capsule 2	22.5	24.6	21.5	

Figure 6.4.1: Powder weight (mg) filled into two HPMC capsules for each NGI measurement for three replicates. The table shows data for six different formulations at 30% and 50% relative humidity (RH), with average fill ranging from 21.85 mg to 23.45 mg.

6.4.2 Summary of NGI results

Summary of Results	unit	Triplicates	Triplicates	Triplicates	Triplicates	Triplicates	Triplicates
comment		30%RH	30%RH	30%RH	50%RH	50%RH	50%RH
formulation		10BSA	10BSA_10Leu	10BSA_20Leu	10BSA	10BSA_10Leu	10BSA_20Leu
Flow rate in impactor	L/min	62	62	62	62	62	62
		Mean	Mean	Mean	Mean	Mean	Mean
Total dose	µg/dose	3608.9	3341.1	3385	3430.6	3439.3	3226.5
Delivered dose	µg/dose	3550.9	3271.1	3322.7	3305.7	3385.4	3171.6
Delivered fraction		0.983928621	0.979048816	0.981595273	0.963592375	0.984328206	0.982984658
Throat	% of DD	13.8	8.1	12.4	11.6	9.9	10.7
MP	% of total	1.6	2.1	1.8	3.7	1.6	1.7
Capsue Retention	µg/dose	57.9	70	62.3	124.9	54	55
Capsule Retention	% of total	1.6	2.1	1.8	3.7	1.6	1.7
Fine particle dose	µg/dose <5µm	2108.1	2012.3	2014.3	1957	1998.7	1948.4
Fine particle fraction	%<5µm of total	58.4	60.3	59.5	57	58.1	60.4
Fine particle fraction	%<5µm of DD	59.4	61.6	60.6	59.2	59.1	61.5
Fine particle fraction	%<3µm of DD	35.7	39.6	41.8	35.4	37	41.7
Fine particle fraction	%<1µm of DD	12	17.4	19.8	13	15.4	19.2
MMAD	µm	3.2	3.16	2.69	3.36	3.32	2.88
GSD		2.26	2.9	2.93	2.48	2.8	2.95
R-value		0.9895	0.9837	0.9865	0.9848	0.9838	0.9873

Figure 6.4.2: Summary of NGI test results for each spray-dried powder formulation under different humidity conditions. The table shows the triplicate averages of key aerodynamic parameters such as total dose, delivered dose, lung deposition fraction (FPF), MMAD, GSD, etc. for three formulations of 10BSA, 10BSA_10Leu and 10BSA_20Leu at 30% and 50% relative humidity (RH) to evaluate their inhalation performance and distribution characteristics.

6.4.3 Actual deposition mass in each size bin

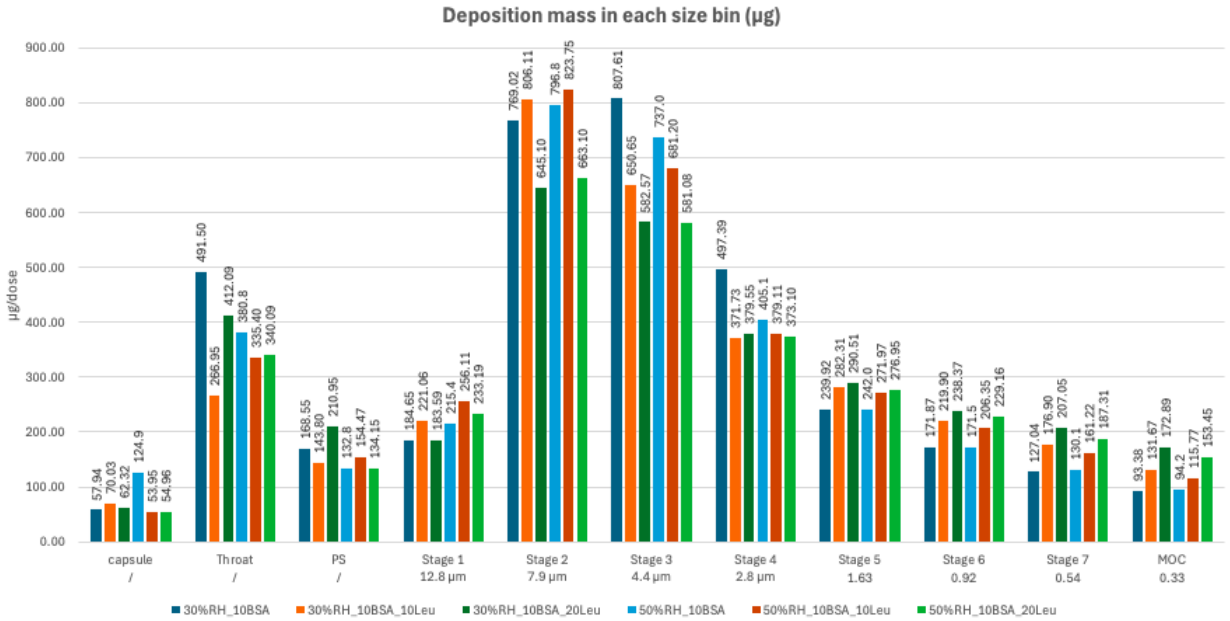

Figure 6.4.3: Deposition profile of three BSA containing formulations across impactor stages under different relative humidity (RH) conditions and leucine contents. The y-axis shows the mass of each particle size fraction relative to the total, while the x-axis represents the stage particle deposited and particle size (μm). Formulations include BSA with 0%, 10%, and 20% leucine at 30% and 50% RH.

6.4.4. Comparison of NGI cumulative size distribution

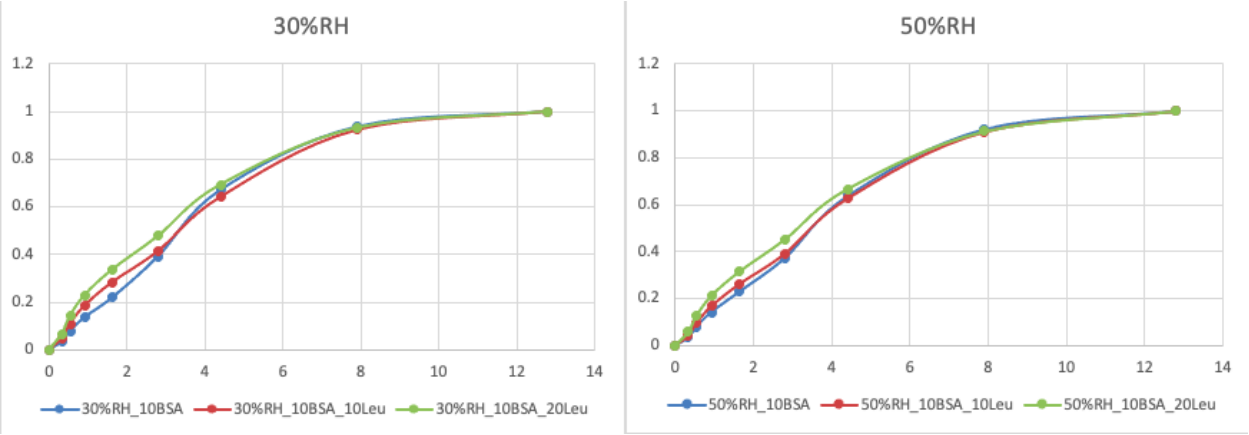

Figure 6.4.4.1: Cumulative NGI particle size distributions of 10BSA, 10BSA10Leu, and 10BSA_20Leu formulations at 30% RH (left) and 50% RH (right). The x-axis in the figure is the particle diameter (μm), and the y-axis is the normalized cumulative volume fraction (0–1), which indicates the proportion of particles below each particle size in the total particle volume. The shape of the curve reflects the characteristics of the sample particle size distribution, where a steeper rise indicates a concentrated particle size distribution, and a gentler rise indicates a wider distribution.

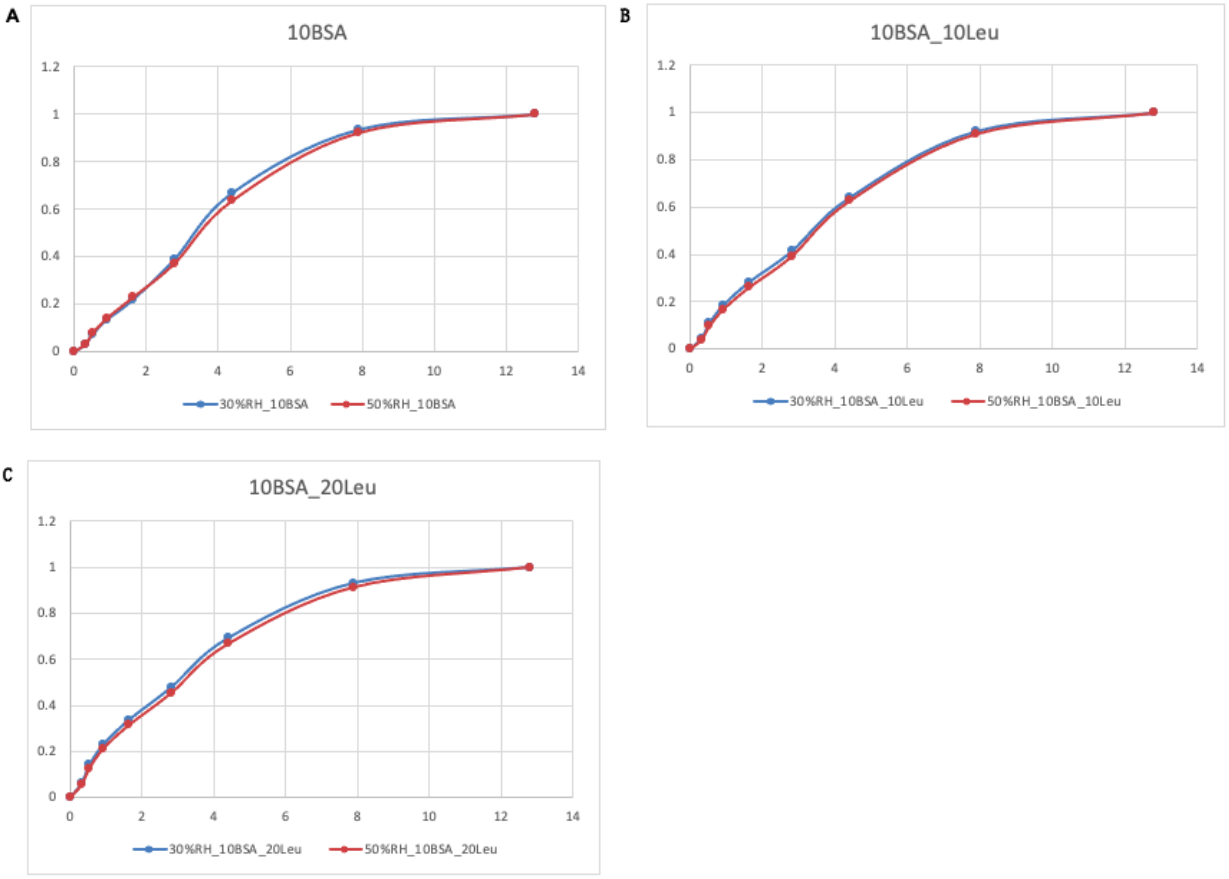

Figure 6.4.4.2: Cumulative size distribution of NGI under different humidity conditions for three formulations. (A) 10BSA; (B) 10BSA_10Leu; (C) 10BSA_20Leu. The blue color is the distribution under 30% RH, and the red color is the distribution under 50% RH.

6.5 APS Graphs

6.5.1 Weight of Powder Loaded into Capsules for APS Measurement

Condition	Group 1(mg)	Group 2(mg)	Group 3(mg)	Averaged (mg)
10BSA__30%RH_4kPa	21.9	21.4	23.3	22.2
10BSA__30%RH_2kPa	21.7	24.8	24	23.5
10BSA_50%RH_4kPa	23.5	20.9	23.2	22.5
10Leu_30%RH_4kPa	21.5	24.2	22.1	22.6
10Leu_30%RH_2kPa	21.4	23.2	23.2	22.6
10Leu_50%RH_4kPa	24.6	20.2	24.4	23.1
10BSA_10Leu__30%RH_4kPa	24.2	21.1	22.7	22.7
10BSA_10Leu_30%RH_2kPa	23.8	23.8	24.1	23.9
10BSA_10Leu_50%RH_4kPa	22.9	20.4	20.6	21.3
Tre_30%RH_4kPa	21.8	19.6	22.8	21.4
Tre_30%RH_2kPa	22.6	23.8	24.2	23.5
Tre_50%RH_4kPa	20.1	21.4	20.1	20.5
10BSA_20Leu_30%RH_4kPa	23.6	24	23.5	23.7
10BSA_20Leu_30%RH_2kPa	22.5	23.7	23.7	23.3
10BSA_20Leu_50%RH_4kPa	20.3	22.3	21.5	21.4

Figure 6.5.1: Powder weight (mg) filled into two HPMC capsules per APS measurement within three replicates. The table shows data for five formulations at 30% and 50% relative humidity (RH) and 2kPa or 4kPa pressure for three experimental parameter combinations, with average fill ranging from 21.4mg to 23.9mg.

6.5.2 Total Concentration of 10BSA at 4 kPa: Measurements at 50% RH and 30% RH

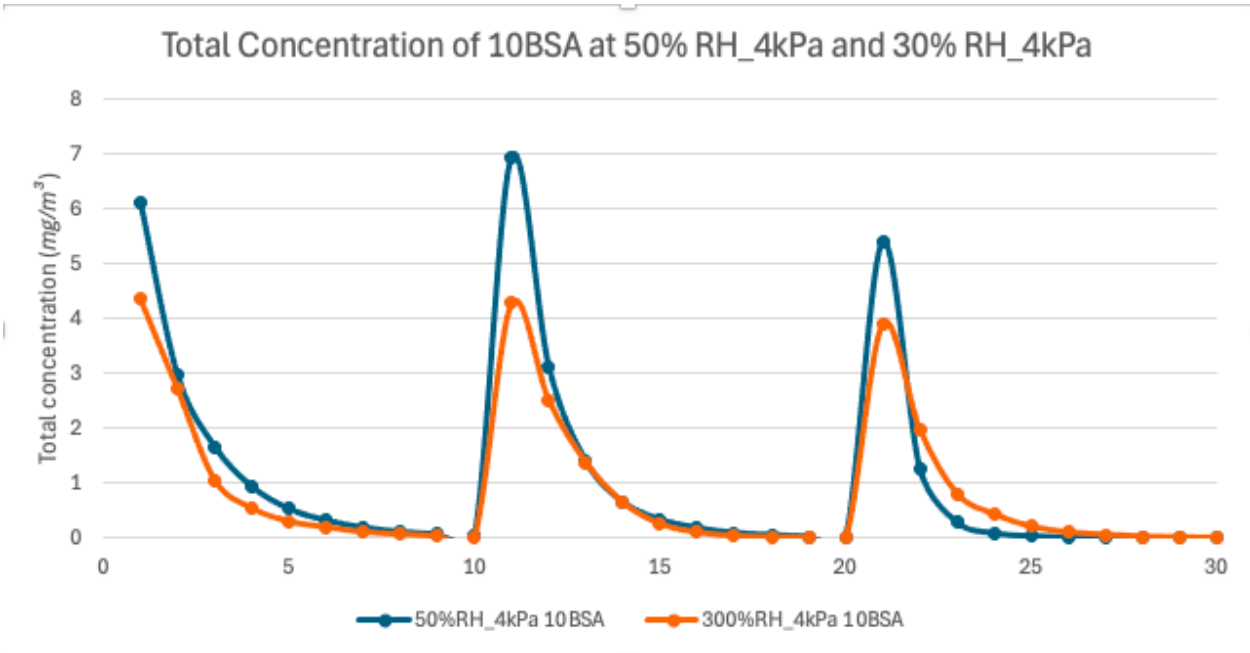

Figure 6.5.2: Total concentration curves of 10BSA formulations measured at 30% and 50% relative humidity (RH) at 4 kPa pressure. The blue curve represents the data at 50% RH, and the orange curve represents the data at 30% RH. The x-axis is the number of tests, with each ten measurements as a group of samples, and all three replicates are from the same formulation. It can be seen in the figure that each sample showed a very low concentration at the seventh measurement, so in this study, only the first six measurements were included in the statistics.

6.5.3 *Unnormalized APS Particle Size Distribution*

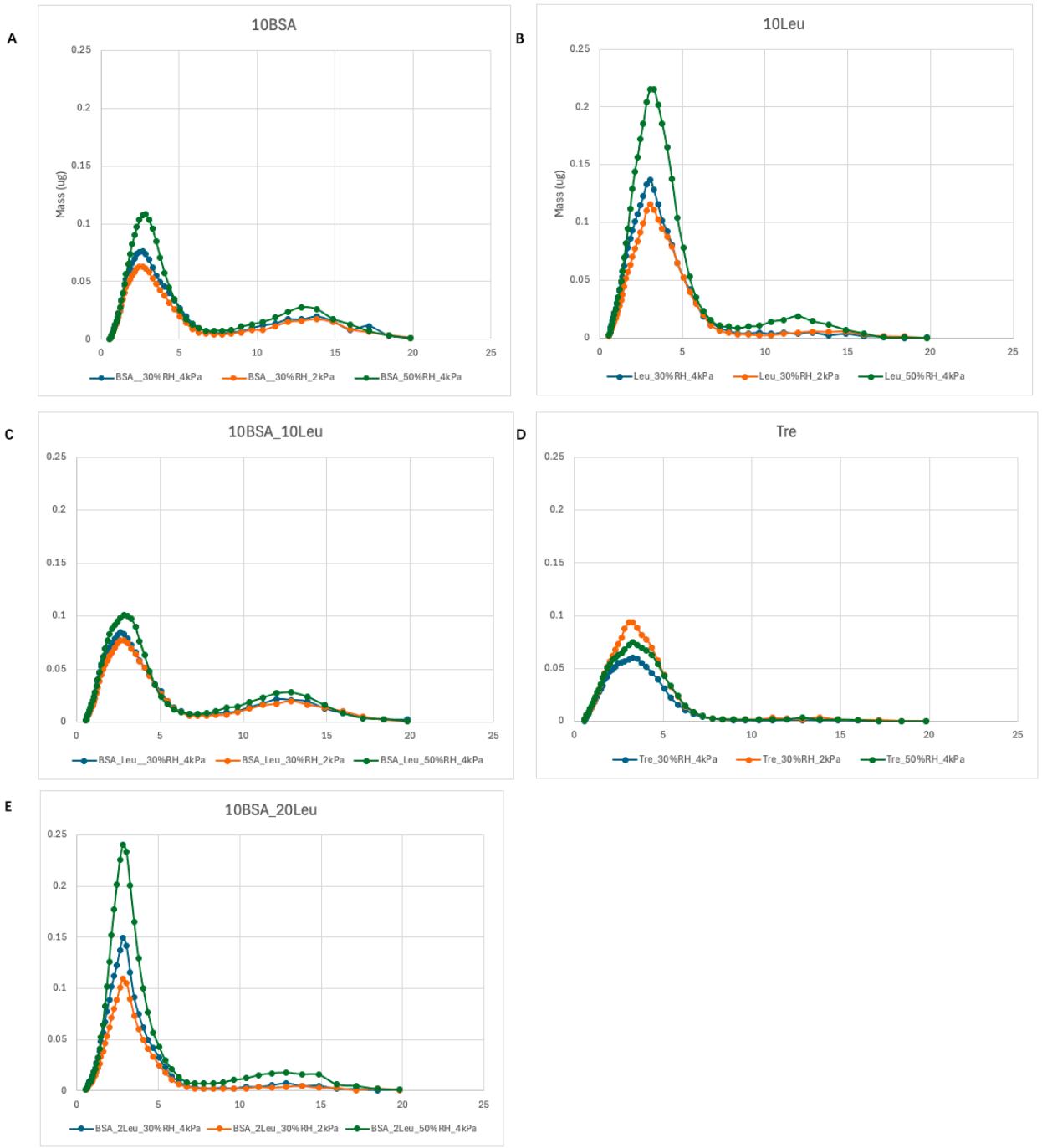

Figure 6.5.3: Unnormalized APS particle size distribution of aerodynamic diameters for different spray-dried powder formulations under varying relative humidity (RH) and pressure conditions. (A) 10BSA; (B) 10Leu; (C) 10BSA_10Leu; (D) Tre; (E) 10BSA_20Leu. The x-axis indicates aerodynamic diameter (µm), and the y-axis shows concentration distribution (mg/m³). Different colors and line styles represent data obtained at 30% and 50% RH with pressure of 2 kPa or 4 kPa. The peak positions and distribution patterns illustrate the aerodynamic behavior and deposition characteristics of each formulation

6.5.4 APS Cumulative Relative Particle Size Distributions: Comparison of Formulations

6.5.4.1 Comparison 2 kPa &4 kPa effects on five formulations

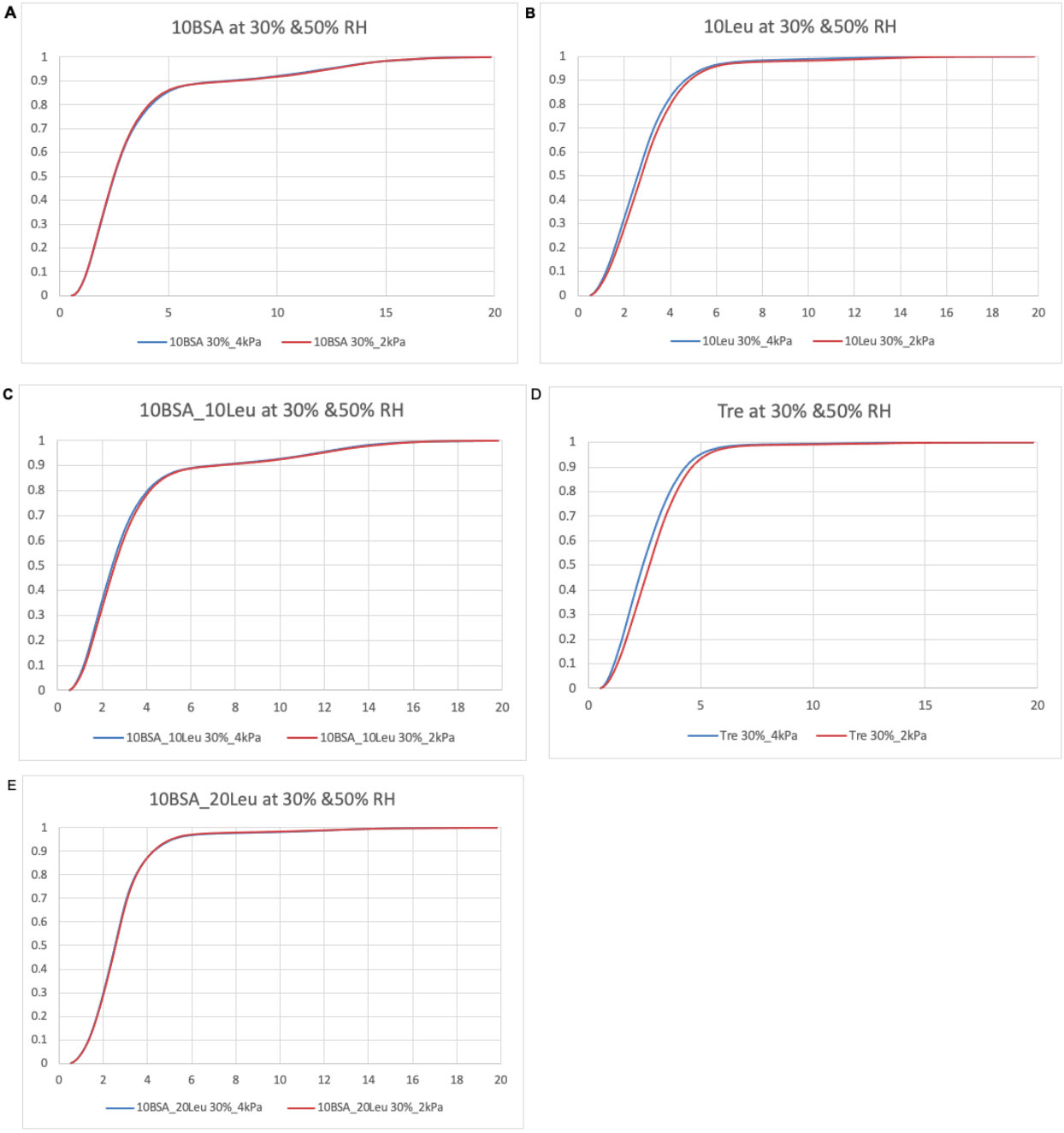

Figure 6.5.4.1: Figures A–E. Cumulative particle size distribution curves of each formulation at 30%RH under different pressure conditions. (A) 10BSA; (B) 10Leu; (C) 10BSA_10Leu; (D) Tre; (E) 10BSA_20Leu. The blue curve represents the data at 4kPa, and the red curve represents the data at 2kPa.

6.5.4.2 Comparison of APS Cumulative Relative Particle Size Distributions

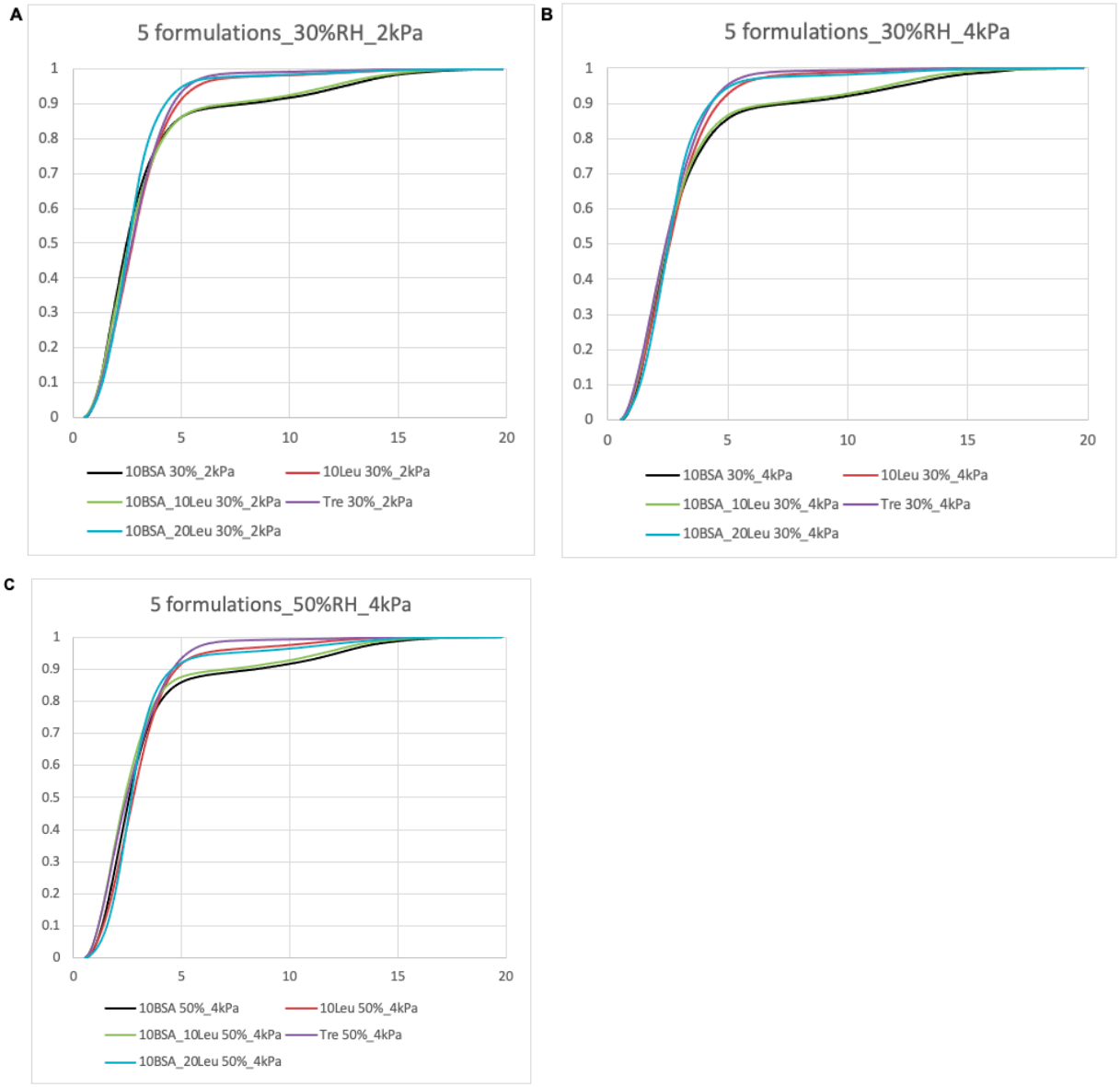

Figure 6.5.4.2: Figures A–C. Cumulative particle size distribution curves of 5 formulation at 4 kPa pressure under different humidity conditions. (A) 30% RH_4kPa; (B) 30% RH_2kPa; (C) 50% RH_4kPa; The figure shows the effect of humidity and pressure on the aerosol particle size distribution of each formulation.

6.5.4.3 Effect of Relative Humidity on APS Cumulative Relative Particle Size Distributions at 4 kPa

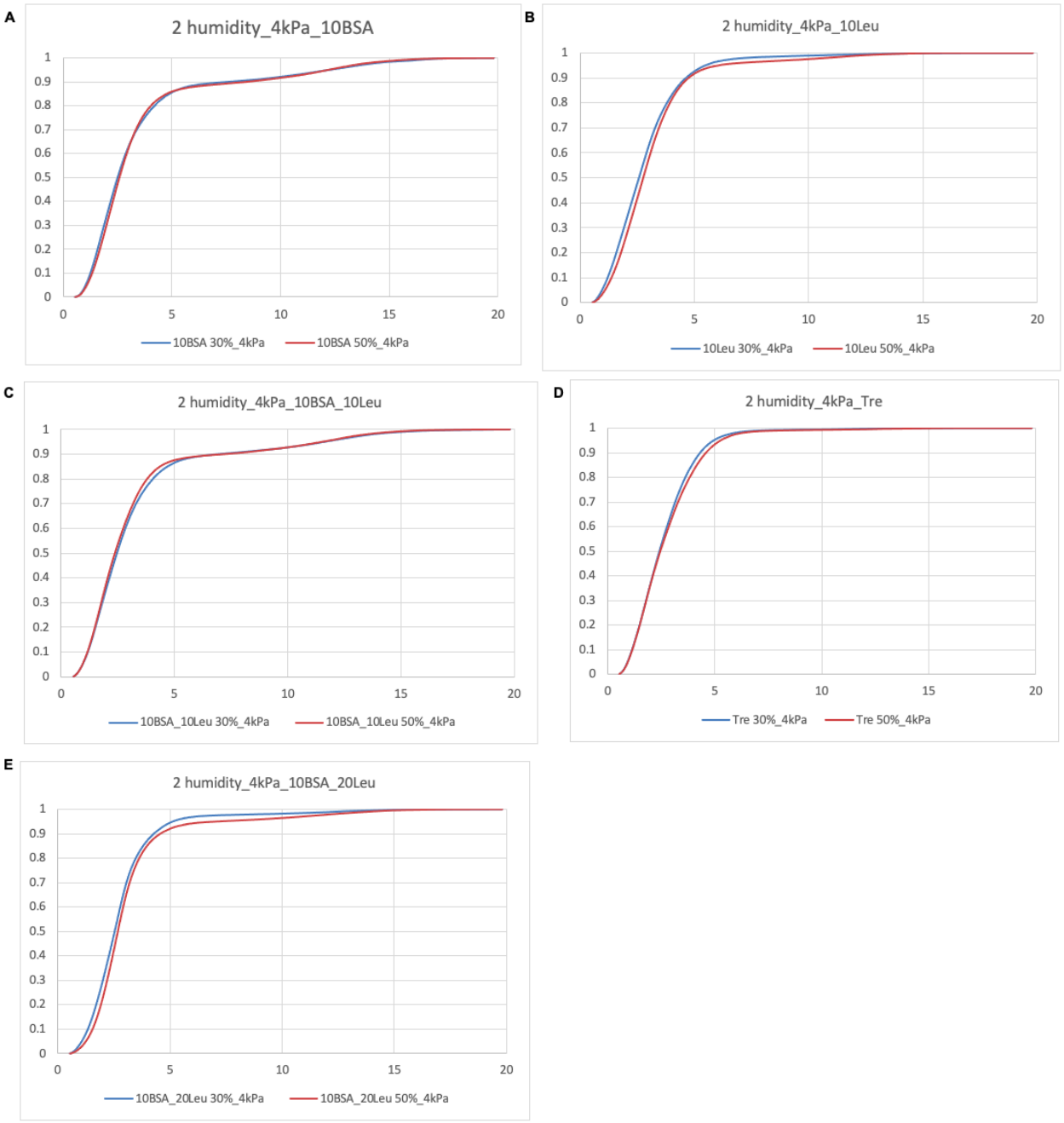

Figure 6.5.4.3: Figures A–E. Cumulative particle size distribution curves of each formulation at 4 kPa pressure under different humidity conditions. (A) 10BSA; (B) 10Leu; (C) 10BSA_10Leu; (D) Tre; (E) 10BSA_20Leu. The blue curve represents the data at 30% relative humidity, and the red curve represents the data at 50% relative humidity. All samples were tested at 4 kPa. The figure shows the effect of humidity on the aerosol particle size distribution of each formulation.